Summer 8-15-2019

The impact of mRNA structure on tRNA selection and ribosome rescue

Erica Nicole Thomas
Washington University in St. Louis

WASHINGTON UNIVERSITY IN ST. LOUIS

Division of Biology and Biomedical Sciences
Plant and Microbial Biosciences

Dissertation Examination Committee:
Hani Zaher, Chair
Doug Chalker
Robert Kranz
Nima Mosammaparast
Dmitri Nusinow

The Impact of mRNA Structural Alterations on tRNA Selection and Ribosome Rescue

by
Erica N. Thomas

A dissertation presented to
The Graduate School
of Washington University in
partial fulfillment of the
requirements for the degree
of Doctor of Philosophy

August 2019
St. Louis, Missouri

Table of Contents

List of Figures

Chapter 1

Chapter 2

Chapter 3

Chapter 4

List of Tables

Acknowledgments

The work described in this dissertation was supported by funding from the Bayer Graduate Research Fellowship (to E.N.T.) and the National Institutes of Health (R01GM112641 to H.S.Z.).

Erica N. Thomas

Washington University in St. Louis

August 2019

Dedicated to my future husband, William, and the countless others who have helped me along the way.

ABSTRACT OF THE DISSERTATION

The impact of mRNA structure on tRNA selection and ribosome rescue

by

Erica N. Thomas

Doctor of Philosophy in Biology and Biomedical Sciences

Plant and Microbial Biosciences

Washington University in St. Louis, 2019

Professor Hani S. Zaher, Chair

The faithful and rapid translation of proteins from genetic information is an essential feature of the ribosome. The general process of tRNA selection is governed by the ability of the ribosome to select for the aminoacylated tRNA (aa-tRNA) that matches the codon in its A-site. The efficiency and accuracy of this selection depends on the ability of nucleotides to form proper hydrogen bonds. While much is known about how chemical alterations of tRNA and rRNA can impact the fidelity of translation, less is known about how similar changes to mRNA affect decoding. In this work, we describe several studies aimed at investigating the impact of mRNA structural alterations on translation. We examine the impact of alkylative damage of mRNA both *in vitro* and *in vivo* and show that the accumulation of these adducts increases ribosomal stalling and subsequent rescue by the trans-translation pathway in bacteria. Additionally, we characterize the base pairing preferences of the most common oxidative damage adduct of mRNA, 8-oxoguanosine, on the ribosome. Finally, we show that the kink structure adopted by the phosphodiester backbone of mRNA on the ribosome impacts translation under sub-optimal base

pairing conditions. Together, this works offers novel insight into the importance of mRNA structure in maintaining the speed and fidelity of translation.

Chapter 1

Alterations and disruption of tRNA selection in bacteria

Erica N. Thomas and Hani S. Zaher

ABSTRACT

Translation is a fundamental step of the central dogma, during which the ribosome decodes an mRNA transcript to produce protein. During the elongation phase, multiple mechanisms work to ensure that the mRNA codon pairs with the proper aminoacyl-tRNA (aa-tRNA). The speed and accuracy of this process can be altered through various means, such as addition of aminoglycoside antibiotics, introduction of ribosomal mutations, and alterations to tRNA modifications. However, fewer studies have focused on how changes to mRNA structure impact tRNA selection. Here, we discuss what is known about tRNA selection, how it could be altered, and the consequences of ribosome stalling in bacteria.

INTRODUCTION

The accuracy and efficiency of translation is vital to the production of functional proteins in all living organisms. On average, translation proceeds with only one misincorporation per 10^3 to 10^4 events (1–3). The accuracy of this template-driven process depends on the ability of the ribosome to properly select the aminoacyl-tRNA (aa-tRNA) that is the correct match for the mRNA codon in the A site. Proper decoding relies on Watson-Crick hydrogen bonding between nucleotides at all three positions of the codon, with the exception of some permissible wobble hydrogen bonding in the third position (4). Interestingly, the energetics of the hydrogen bonding alone cannot explain the observed accuracy of decoding (5, 6). During the process of tRNA selection, the ribosome plays an active role in correctly recognizing the specific geometry of Watson-Crick base pairs before proceeding with peptidyl transfer (7, 8). This intricate process allows for the ribosome to discriminate between substrates with very small differences in the free energy of binding (9).

The bacterial ribosome is composed of two main subunits: the small subunit, or the 30S, and the large subunit, known as the 50S. These two subunits come together during initiation to form the 70S ribosome. Throughout translation, the ribosome utilizes three different tRNA binding sites: 1) the A site, or the aminoacyl-tRNA site, 2) the P site, or the peptidyl-tRNA site, and 3) the E site, or the exit site. During elongation, a ternary complex composed of an aa-tRNA, elongation factor-Tu (EF-Tu), and GTP is delivered to the A site. Several downstream reactions occur, resulting ultimately in the reaction of the newly delivered amino acid with the peptidyl-tRNA in the P site. To complete the cycle, translocation occurs, which is a reaction catalyzed by EF-G that uses the energy of GTP hydrolysis to promote the movement of peptidyl-tRNA into the P site, and the deacylated tRNA into the E site. Translation termination in bacteria begins

when stop codons enter the A site and are recognized by either release factor 1 or 2 (RF1 and RF2) which hydrolyze the peptidyl-tRNA and release the peptide chain (10).

Translation Elongation and tRNA Selection

During tRNA selection, the ribosome must distinguish between the aa-tRNAs that match the codon in the A site, known as cognate aa-tRNAs, and near-cognate aa-tRNAs, which have one mismatch between the codon and anticodon. In order to select the cognate over the near-cognate aa-tRNA, the ribosome recognizes the small energetic differences between them multiple times through mechanisms known as kinetic proofreading and induced fit (11, 12). This repeated exploitation of free energy ($\Delta\Delta G$) separated by a functionally irreversible reaction compounds the effects, resulting in the observed high accuracy of tRNA selection. Kinetic proofreading during this process is possible because the aa-tRNA is delivered to the A site in a complex with GTP and EF-Tu, and the hydrolysis of GTP by EF-Tu serves as the functionally irreversible reaction that separates the two independent interactions between the aa-tRNA and the ribosome. The first utilization of the $\Delta\Delta G$ of binding between the cognate and non-cognate aa-tRNAs occurs during the initial encounter between the ribosome and the GTP form of the ternary complex. The second utilization of the $\Delta\Delta G$ of binding occurs during the association of the ribosome with either the GDP state of the ternary complex or free form the of tRNA after dissociation of EF-Tu. These independent steps of evaluation between the aa-tRNA and the ribosome can lead to greater discrimination, particularly if equilibrium is rapidly attained during the steps before the relatively slow steps of GTPase activation and accommodation (9).

The initial step of tRNA selection is a codon-independent interaction between the ribosome and the ternary complex (Figure 1). This interaction is governed by rate constants k_1

and k_{-1}, and these rates are similar between cognate (no mismatch), near-cognate (one mismatch), and non-cognate (greater than one mismatch) aa-tRNAs (13, 14). The rate of binding between the ribosome and ternary complex is high and has been shown to be dependent on EF-Tu. It is hypothesized that the positive charge and the large size of the L7/L12 stalk of the ribosome interacts with EF-Tu, thus explaining the fast rate of binding between the two (15). The next step is codon recognition (k_2), which is similar for cognate and near-cognates, but is very slow for non-cognates (14). The first step that distinguishes between cognates and near-cognates is dissociation during initial codon recognition (k_{-2}) (16). On average, the rate of dissociation for near-cognates compared to cognates is about one thousand-fold faster under high-fidelity conditions, which is a larger difference than is expected when only considering the free energy differences of tRNA-mRNA binding between cognates and near-cognates (16). This observation suggests that the ribosome plays an active role in stabilizing the cognate interaction through induced fit.

The next steps of tRNA selection are dependent on the GTPase activity of EF-Tu. During GTPase activation (k_3), which is the rate-limiting step of GTP hydrolysis (k_{GTP}), the active site of EF-Tu undergoes a conformational change (17). The forward rate of GTPase activation depends on the properties of the decoding helix, i.e. the pairing interaction between the codon and the anticodon. Therefore, the rate of GTPase activation is faster for cognate aa-tRNAs than for near-cognate aa-tRNAs (16, 18, 19). The inorganic phosphate is released (k_{pi}) after GTP hydrolysis, and EF-Tu is rearranged to its GDP-bound state before dissociating from the aa-tRNA (k_6) (19). This irreversible reaction is followed by a kinetic partitioning that occurs during the second encounter between the ribosome and the aa-tRNA. During this stage, which is known as proofreading, the aa-tRNA either moves completely into the A site during accommodation (k_5)

or dissociates from the ribosome during rejection (k_7). The rate of accommodation is accelerated for cognate aa-tRNAs, while the rate of rejection is accelerated for near-cognate aa-tRNAs in order to maintain the accuracy of translation. If the aa-tRNA is accommodated, it will proceed with peptidyl transfer (k_{pep}) in the large ribosomal subunit where it gets incorporated into the growing peptide chain. (19–21).

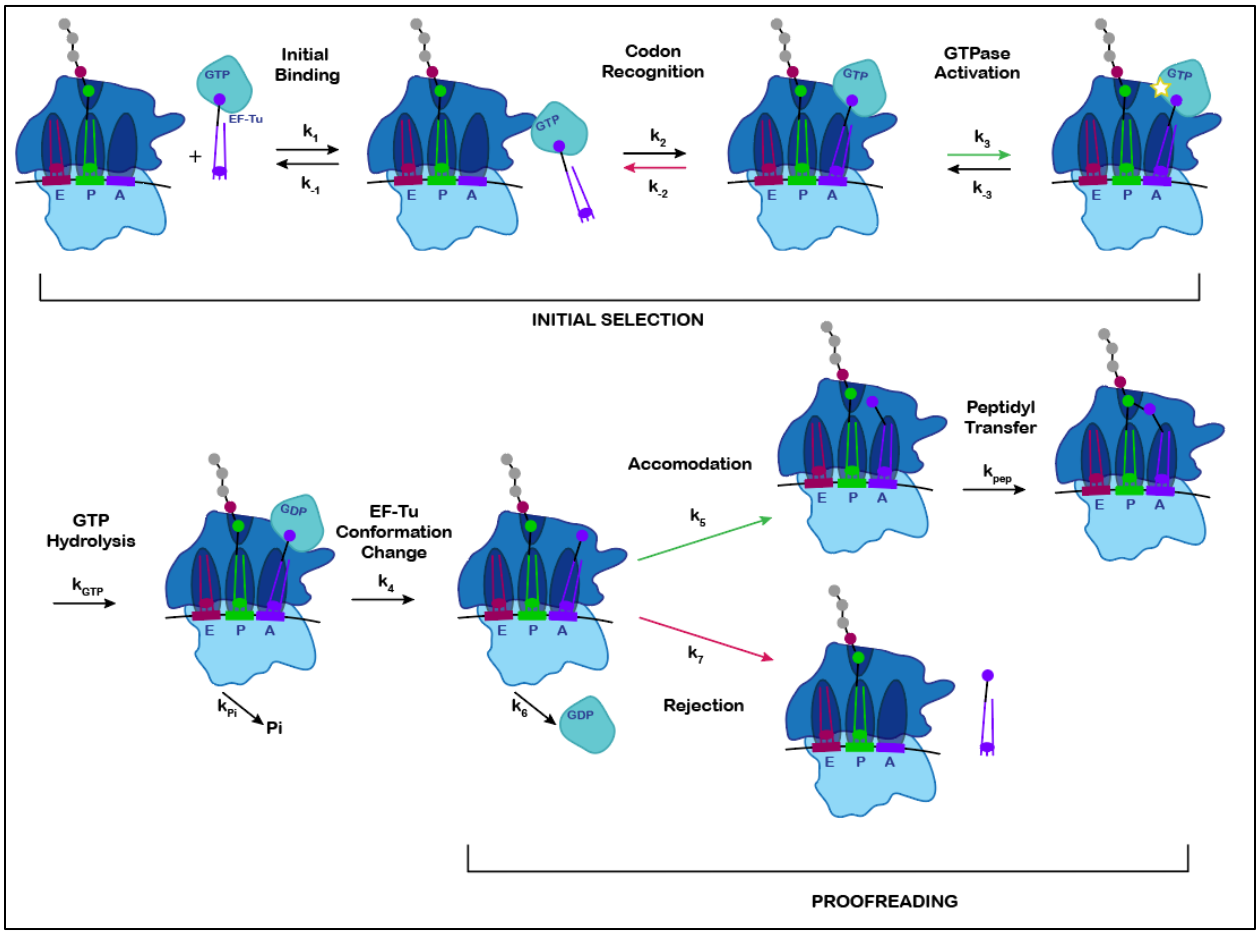

Figure 1.1: Schematic of tRNA selection (10). Green arrows indicate reactions that are accelerated for cognate aa-tRNAs, while red arrows indicate reactions that are accelerated for near-cognate aa-tRNAs. Selection begins with codon-independent initial binding of the ternary complex to the ribosome, governed by k_1 and k_{-1}. Codon recognition is codon dependent and is governed by k_2 and k_{-2}. GTPase activation follows, during which EF-Tu undergoes a conformational change governed by k_3 and k_{-3}. The next step is the irreversible hydrolysis of GTP (k_{GTP}). The dissociation of EF-Tu leads into the proofreading stage, where the kinetic partitioning between accommodation (k_5) and rejection (k_7) occurs. Peptidyl transfer (k_{pep}) follows accommodation.

Peptide Release

Termination of translation occurs when one of the nearly universal stop codons, including UAA, UAG, and UGA, enters the A site. Unlike tRNA selection, which depends on RNA-RNA interactions, peptide release is dependent on protein-RNA interactions. In bacteria, stop codons are recognized by protein factors known as class I release factors (RFs) that subsequently trigger the release of the elongating peptide. RF1 decodes UAG while RF2 decodes UGA, and both of the factors decode UAA (22). Bacteria also depend on RF3, which is a GTPase class II release factor that helps to complete termination. This likely occurs via downstream reactions through coupling the energy of GTP hydrolysis to the removal of the class I RF after peptide release (23). The RFs cannot utilize Watson-Crick base pairing, so they rely on RNA-protein interactions to achieve their low error-frequency of approximately 1 in 10^5 events (24).

Class I release factors share several functional similarities to aa-tRNAs. Both class I RFs and aa-tRNAs have a domain for recognizing the appropriate codons with high specificity in the small subunit of the ribosome. For aa-tRNAs and RFs, these regions are the anticodon and domain 2, respectively. Additionally, they each have another domain involved in promoting catalysis in the peptidyl transfer center (PTC) of the large subunit. For aa-tRNAs and RFs, these regions are the acceptor stem and domain 3, respectively (10). Although these bifunctional species share similarities, they work through fundamentally different mechanisms. For one, instead of Watson-Crick RNA-RNA base pairs, RNA-protein interactions are utilized during peptide release. “Tripeptide anticodons” were identified as the region of RFs that are critical for stop codon recognition (25). These motifs are proline-any amino acid-threonine (PxT) for RF1 and serine-proline-phenylalanine (SPF) for RF2. Several structural studies provide clear evidence that these regions occupy the decoding center near the mRNA in the A site (26–31).

RFs also work through different mechanisms than aa-tRNAs to achieve their specificity. Because RF3 cannot provide the irreversible step necessary for kinetic proofreading, class I RFs derive specificity from relatively large apparent binding (*K*m) contribution for stop codons over sense codons (32). This indicates that all sense codons trigger decreased class I RF binding. Contributions to specificity are also derived from k_{cat} effects that range from 2- to 1000-fold depending on the sense codon and RF, suggesting that class I RFs bind in a qualitatively different fashion to stop and sense codons (32). These binding strategies may be exploited for specificity by RFs because of the inherently larger differences in ΔΔG of binding available for protein-RNA interactions relative to RNA-RNA interactions or because proofreading mechanisms do not exist for RFs (10).

Structural Determinants of tRNA Selection

Several ribosomal proteins and nucleotides have been shown to play vital roles in monitoring the interaction between the anticodon and codon in the decoding center, which encompasses functionally important residues of the 16S rRNA, including nucleotides 1400-1500 of helix 44, 1050-1200 of helix 43, and the 530 loop of helix 18 (33, 34). The specific residues that are critical for tRNA binding to the A-site include G529, G530, A1492, and A1493 (35, 36). Residues A1492 and A1493 monitor the geometry of the codon-anticodon helix in the first two positions, while C518, G530, and portions of ribosomal protein S12 monitor the second and third positions (4, 37). The Watson-Crick geometries of the first two positions are more strictly monitored than the third position, which allows for certain wobble base pair geometries (Figure 2).

In the apo-structure of the ribosome, A1492, A1493, and G530 exist in a conformation where their hydrogen bonding interfaces are facing out of the A-site. Upon binding of the aa-tRNA to the codon, A1492 and A1493 move from an intrahelical position in helix 44 to an extrahelical position while G530 flips from a *syn* to an *anti*-conformation. These nucleotides congregate together to inspect the minor groove of the decoding helix and increase the specificity for Watson-Crick base pairs (4). This active monitoring of the codon-anticodon helix by the ribosome explains the level of tRNA selection accuracy that cannot be achieved by hydrogen bonding between codons and anticodons alone. Once the proper codon-anticodon interaction is detected by the ribosome, downstream signals trigger large conformational changes of the ribosome in a process known as domain closure (38). These movements include the rotation of the head towards the shoulder domain of the 30S subunit as well as the rotation of the shoulder domain towards the inter-subunit space. This brings the shoulder domain close to EF-Tu, which in turn positions the catalytically important His84 of EF-Tu for GTP hydrolysis so tRNA selection can continue into the proofreading phase (39).

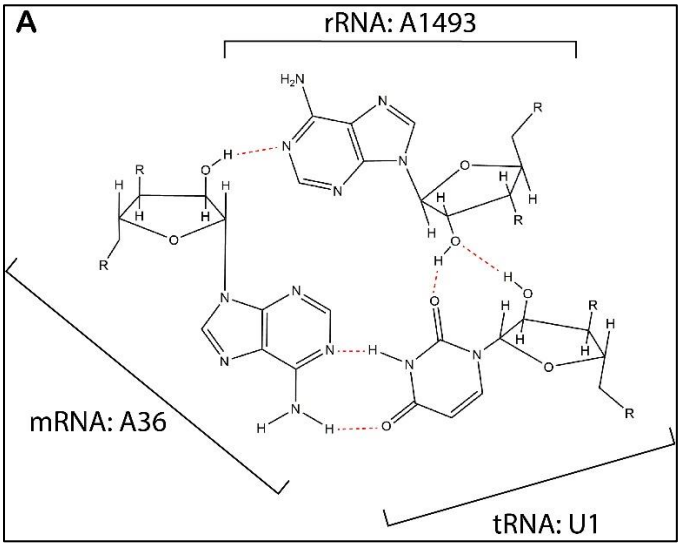

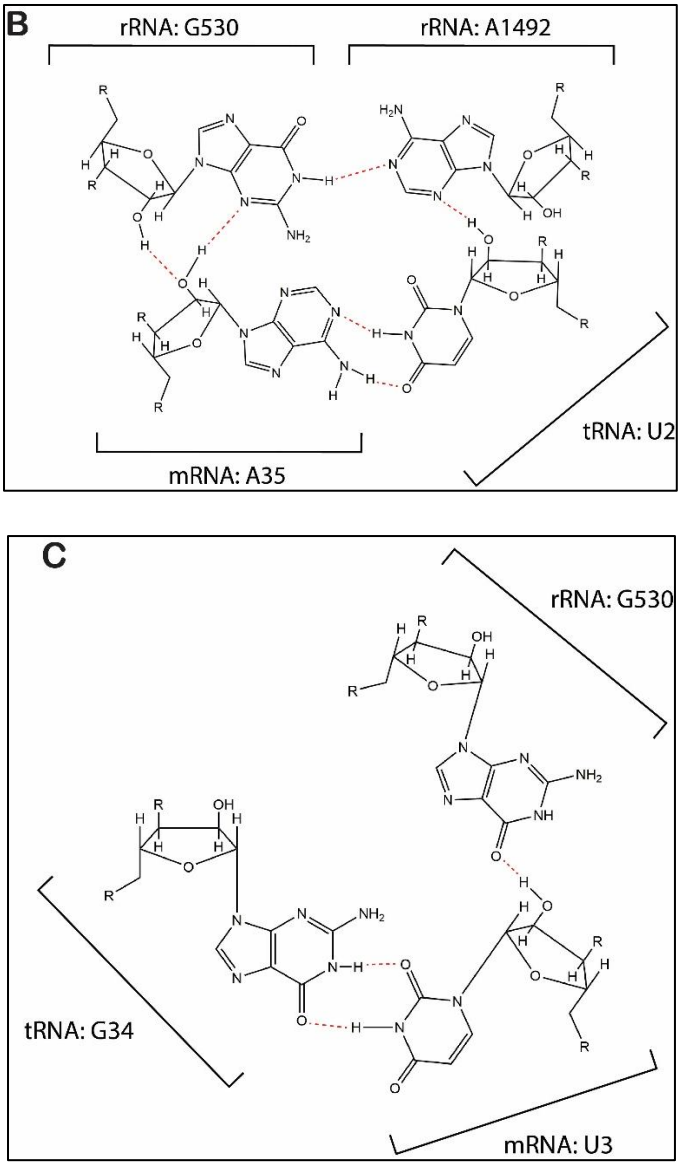

Figure 1.2: Active monitoring of tRNA-mRNA interactions by rRNA residues. A) First-position monitoring of the codon-anticodon interaction by A1493. B) Second-position monitoring by G530 and A1492. C) Third-position monitoring by G530. Note that this figure depicts accurate hydrogen bonds, but the exact stereochemistry of the nucleotides is not represented here (40).

Altering the Accuracy of tRNA Selection

Aminoglycoside Antibiotics

Several mechanisms exist to either restrict or relax the accuracy of tRNA selection. A particular class of antibiotics, known as the aminoglycosides, relax tRNA selection conditions and increase the rate of ribosomal miscoding (41). This class encompasses a large range of molecules including paromomycin, streptomycin, neomycin, kanamycin, and gentamycin that can induce a wide array of miscoding events by working through distinct mechanisms. Paromomycin and streptomycin have been particularly instrumental in helping to elucidate structural changes that occur during tRNA selection (10). Paromomycin accelerates both of the forward reaction rates in tRNA selection, GTPase activation (k_3) and accommodation (k_5), while reducing the rate of near-cognate tRNA dissociation from the A site during codon recognition (k_{-2}) and rejection (k_7) (42, 43). Specifically, paromomycin pushes A1492 and A1493 into an intermediate position where they are able to engage the minor groove of the codon-anticodon helix (44). This conformation looks very similar to the one that is assumed when a cognate aa-tRNA is bound to the A-site codon (45). In this way, it switches the ribosome into a highly activated state regardless of the codon-anticodon interaction in the A site and k_{pep} increases for both near-cognate and cognate aa-tRNAs (43, 46).

Streptomycin also increases miscoding on the ribosome, but through a mechanism independent of paromomycin. The antibiotic has been shown to substantially reduce the forward rates of GTPase activation (k_3) for cognate tRNAs while only slightly stimulating these values for near-cognate tRNAs (47). Structural studies show that streptomycin generates these kinetic changes by inducing a lateral shift of helix 44 (h44), which contains A1492 and A1493. This lateral shift appears to be sufficient to stabilize near-cognate tRNAs. Additionally, this shift

increases the energetic barriers associated with domain closure for cognate tRNAs, resulting in an overall increase in miscoding (48).

Ribosomal Mutations

Several ribosomal mutants in *E. coli* cause tRNA selection to become either more restrictive or promiscuous. The mutations that cause tRNA selection to be more restrictive were discovered in auxotrophic mutants that displayed a dependency on streptomycin (7). Several of these mutations mapped to the gene encoding the small ribosomal protein S12 (rpsL), specifically at the contact points between S12 and the 16S RNA helix 44 and helix 27 that are important for domain closure (49, 50). The mutations disrupt these interactions, thereby destabilizing the closed conformation and increasing accuracy during tRNA selection. Ribosomal ambiguity (ram) mutants are those that increase ribosomal promiscuity and miscoding (51). These mutations frequently alter the small ribosomal subunit proteins S4 (rpsD) and S5 (rpsE). The two proteins form an interface that is disrupted during domain closure. The mutations reduce the number of bonds that must be broken, thereby lowering the energetic barrier necessary for this disruption to occur and increasing ribosomal miscoding (52, 53).

tRNA Modifications

The energetics of hydrogen bonding as well as the active monitoring of the codon-anticodon helix by the ribosome cannot still not fully explain the ability of the ribosome to discriminate between closely related codons. In these cases, accurate decoding relies on the chemical modifications of anticodons to fine-tune their base-pairing properties (54, 55). Modifications can either expand or restrict the decoding capacity of anticodons, and the

expression levels of hundreds of proteins can be altered by variations in these modifications. Specifically, base modifications are common at positions 34 and 37 of the tRNA (56). Position 34 of the tRNA base pairs with the third position wobble base of the codon and allows for it to have an expanded decoding capacity (57, 58). For example, to avoid mispairing with the AUG Met codon, the AUA Ile tRNA utilizes a C that is modified to lysidine (^{k2}C) in position 34 of the anticodon. In this way, the Ile tRNA avoids a U•G wobble with the AUG Met codon at the third position and instead forms a ^{k2}C•A base pair with the AUA codon (59). Position 37 of the anticodon is adjacent to the 3' site of the anticodon and modifications at this site play a critical role in the stabilization of the first base pair of the codon-anticodon helix. For example, modified m^1G_{37} in the anticodons of bacteria prevents frameshifting, whereby the mRNA slips during translation by one or more base pairs in either the 5' (-1) or 3' (+1) direction (60). In this way, modifications of tRNA are critical for accurate decoding.

mRNA Modifications and Structure

While much is known about how tRNA modifications modulate tRNA selection, less is known about how modifications and structural alterations to mRNA can impact translation. More than 100 distinct chemical modifications of RNA are known; however, it remains unclear which chemical modifications are intentional, and which are the result of nucleic acid damage (61). Nucleic acids are susceptible to multiple types of chemical damage, including alkylation, deamination, oxidation, and depurination. Sources of damage include reactive oxygen species, UV radiation, ionizing radiation, alkylating agents, and possibly even the aberrant activity of tRNA modifying enzymes. If these damage-induced adducts interfere with the ability of the nucleotide to form proper base pairs, they can have a negative impact on the speed and accuracy

of translation. Intentional modifications can also be the result of alkylating enzymes; therefore, it is difficult to distinguish between alkylative damage and intentional modifications (62, 63).

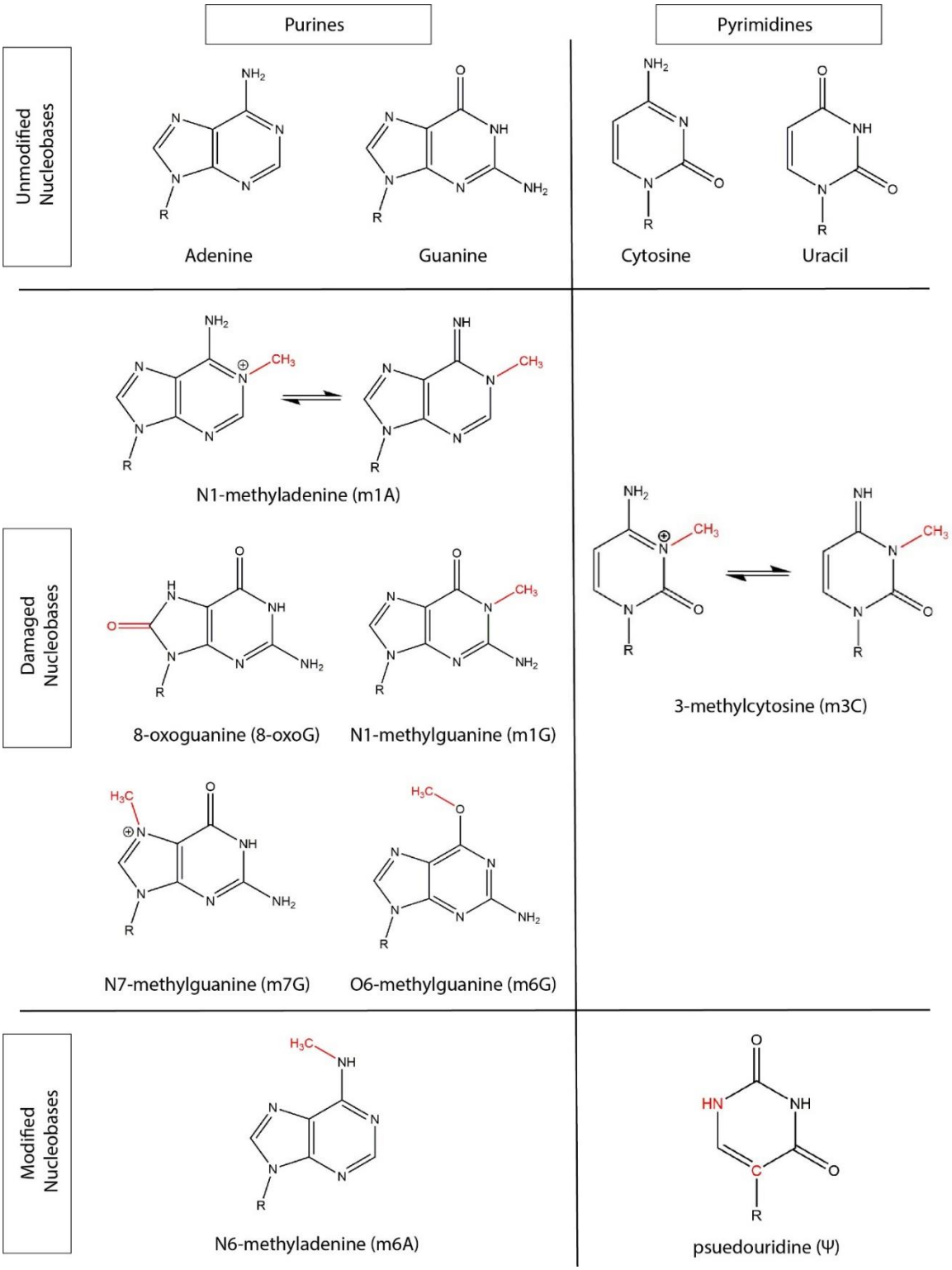

Figure 1.3: Structures of modified nucleobases discussed in this thesis. Altered residues are indicated in red. Damaged nucleobases are those that are generated from exogenous and endogenous chemical damage, while modified nucleotides are intentional regulatory marks introduced by the cell. Resonance structures are indicated for m^1A and m^3C.

Nucleobase Modifications and Adducts

There are several indications that certain mRNA modifications are intentional and dynamic regulatory marks. One indication is that the modification has specific proteins serving as its readers, writers, and erasers that can act on mRNA. For example, N6-methyladenosine (m^6A), which is the most abundant internal modification in eukaryotic mRNA and is also found in bacterial mRNA, is a reversible modification (64). It has dedicated methyltransferases, including methyltransferase-like 3 and 14 (METTL3 and METTL14) as well as Wilms tumor 1-associated protein (WTAP) (65–69). Importantly, it also has dedicated demethylases, including fat mass and obesity associated protein (FTO) and AlkB homologue 5 (ALKBH5) to remove the modification (70, 71). Through these writers and erasers, the levels of m^6A on mRNA can be modulated. Additionally, m^6A possess multiple readers including YTHDF1, YTHDF2, YTHDF3, and YTHDC1 that can recognize this modification and perform downstream functions (72–74). Another indication that a modification is intentional is its specific enrichment in certain regions of mRNA. For example, m^6A is found in over 25% of human transcripts with enrichment in long exons, 3'UTRs, and near stop codons (73). This targeted enrichment suggests that the modification could be serving a function in some aspect of mRNA metabolism (64).

While m^6A serves as an intriguing candidate for an intentional mRNA modification to regulate translation elongation, previous work has shown that it does not significantly interfere with the tRNA selection process (75, 76). This is expected, as the methylated nitrogen still retains one hydrogen to participate in proper base pairing; therefore, it is not likely to be intentionally utilized to modulate the speed or accuracy of tRNA selection. Previous studies have instead suggested that m^6A in mRNA may play a role in a wide variety of processes related to

mRNA metabolism, including the enhancement of nuclear processing and export, the promotion of translation, and mRNA maturation (64).

There are many more mRNA adducts that are the result of nucleotide damage compared to those that serve as intentional modifications (63). These adducts can directly impact the WC interface between nucleotides, generate new hydrogen bonding interfaces, or cause internal rearrangements of atoms such that the original WC interface is altered. Two of the most common types of nucleotide damage that impact base pairing are oxidative and alkylative damage. Oxidative damage is generated from both endogenous and exogenous processes. For example, cellular respiration produces superoxide radical O^{2-} during electron transport through the reduction of molecular oxygen by components of the electron transport chain (77, 78). Additionally, O^{2-} is intentionally produced to kill invading microbes by immune cells using the enzyme NADPH oxidase (79). In order to control cellular levels of O^{2-}, superoxide dismutase catalyzes the metal-dependent dismutation of superoxide into O^2 and H_2O_2 (80). Because H_2O_2 can react with intracellular iron through Fenton and Haber-Weiss chemistry to form highly reactive hydroxyl radicals, it is enzymatically reduced to water and molecular oxygen (81). Additionally, several exogenous sources of oxidative damage include ionizing and UV radiation, as well as toxic compounds (82). Less is known about the accumulation of alkylative damage; however, it is known that several chemotherapeutic agents are alkylating agents that may rely on RNA damage for their efficacy (83). Additionally, several known sources of endogenous alkylative damage are the aberrant activity of the universal methyl donor S-adenosyl methionine (SAM) and nitrosated bile adducts (84).

Oxidative damage can cause myriad damage adducts, but one of the most abundant oxidative damage adducts of mRNA is 8-oxoguanosine (8-oxoG). Under normal conditions, 8-

oxoG is present at approximately 1 in 10^5 residues in total RNA and can increase as much as 10-fold under oxidative stress conditions (85, 86). Previous work has shown that when 8-oxoG is present in mRNA, it decreases the rate of peptidyl transfer in the presence of 8-oxoG•C base pairs while increasing the rate of miscoding in the presence of 8-oxoG•A base pairs (87). From structural studies performed using the DNA modification 8-oxodG, it was shown that the introduction of the O8 to the guanosine causes a steric clash of the nucleobase with the phosphate backbone of the nucleotide. As a result, the nucleobase changes conformation from its normal *anti* conformation to a *syn* conformation to relieve this steric hindrance. This opens a new hydrogen bonding interface and allows for 8-oxoG to mispair with adenosine (88).

Due to the susceptibility of oxygen and nitrogen to alkylative damage, there exists an extensive list of possible alkylative modifications to nucleotides. Several of the modifications can directly interfere with the WC interface between nucleotides, resulting in a decrease in the rate of decoding and in some cases even miscoding. For example, the introduction of a methyl group to the O6 of guanosine causes an internal rearrangement of electrons such that N1 is no longer covalently bound to the hydrogen used to base pair at the WC interface. This results in a significant reduction in the rate of peptidyl transfer in the presence of an O6-methylguanosine (m^6G)•C base pair (75). Additionally, the alteration of N1 from a hydrogen bond donor to a hydrogen acceptor allows for m^6G to base pair in the Watson-Crick conformation with uridine, resulting in an increase in the rate of miscoding in the presence of an m^6G•U base pair (75, 76).

Another alkylative damage adduct of interest in N1-methyladenosine (m^1A). In theory, this adduct should be disruptive to template-driven processes, as it directly interferes with the ability of N1 to form hydrogen bonds as well as introduces a resonance structure with a positive charge. Indeed, one study shows that the introduction of m^1A into an mRNA increases ribosome

stalling at this lesion (76). Interestingly, several reports have implicated that m^1A may serve as an intentional regulatory modification in mRNA (89). The modification is enriched around the start site of transcripts, upstream of the first splice site on highly translated transcripts (90, 91). The observation that m^1A may serve as an intentional modification to promote translation (90) is difficult to reconcile if m^1A does indeed increase ribosome stalling. Additionally, m^1A lacks several of the characteristics of an intentional modification. For example, no readers, writers, or erasers specific to m^1A in mRNA have been identified (89). Controversy also exists around the abundance of m^1A in human cells, as several reports identified hundreds of sites in the transcriptome (90, 91) while another identified only nine (92). More evidence is needed to conclusively state that m^1A serves as an intentional modification of mRNA.

Sugar and Backbone Structure and Modifications

In contrast to the nucleobase, the other two components of an RNA nucleotide, including the ribose sugar and phosphate backbone, have fewer potential modifications and damage adducts. The only common modification of the 2'hydroxyl ribose moiety of all four nucleotides is 2'-O-methylation (2'OMe) (93, 94). While its function remains unclear, it can inhibit adenosine to inosine RNA editing *in vitro* as well as drastically increase ribosome stalling in a position-dependent manner (95, 96). The importance of the 2'OH of the ribose sugar in decoding has also been investigated. The ribosomal RNA residues that monitor the interaction between the codon and anticodon in the A site not only interact with the O2 of the purine base and the N4 of the pyrimidine base, but they also hydrogen bond with the 2'OH of the ribose (4). Interestingly, substitutions of this moiety with deoxy or fluoro groups had minimal impact on tRNA selection but showed that it is required for the remodeling of mRNA during translocation (97).

Even less is known about the structural importance of the phosphate backbone during decoding. In the ribosome, mRNA displays a kink-like structure that is stabilized by electrostatic interactions and it is speculated that this structure prevents slippage and is therefore critical for frame maintenance (98, 99). No information was previously known about if and how this structure of the phosphate backbone contributed to tRNA selection.

Ribosomal Rescue in Bacteria: *Trans*-Translation

When translation elongation is disrupted, eukaryotes have three main cytoplasmic mRNA-surveillance processes that are utilized: 1) nonsense-mediated decay, 2) no-go decay, and 3) non-stop decay (100). The pathway that is utilized to rescue ribosomes and degrade the faulty mRNA and incomplete peptide depends on the context of the disruption. For example, nonsense-mediated decay recognizes premature stop codons (101) and non-stop decay is utilized when transcripts do not contain stop codons (102). No-go decay functions to rescue ribosomes stalled by physical blocks, including chemical damage and structural impediments such as pseudoknots and hairpins (103). Bacteria, on the other hand, utilize at least one quality control pathway, known as *trans*-translation, that can rescue ribosomes that have stalled at the 3' end of a truncated transcript (104). In theory, the *trans*-translation pathway can rescue ribosomes under almost any circumstance, as truncated mRNAs are produced through a variety of processes, including endonucleolytic cleavage, ribosome stalling, chemical insults, and premature transcriptional termination (100). However, it has not been explicitly shown that that this pathway rescues ribosomes stalled by damaged transcripts.

Through the process of *trans*-translation, one molecule known as transfer-messenger RNA (tmRNA), which is encoded by the highly conserved ssrA gene, acts as both a tRNA and

mRNA to ensure that stalled ribosomes complete the translation cycle and are recycled (105). Though some details of the process remain to be elucidated, we do know that tmRNA, which is aminoacylated by alanine (106), binds to the A site of the stalled ribosome (107). At this point, the nascent peptide is then transferred to tmRNA (108), and translation then switches from the 3' end of the defective mRNA to the portion of tmRNA that contains an ssrA-coding sequence (105, 109), which resembles the degradation signal utilized by bacterial proteases (110). This sequence tags the C-terminus of the incomplete protein and signals for its degradation. Like aa-tRNAs, tmRNA binds EF-Tu (111, 112) while also requiring another protein partner known as SmpB (113). The tmRNA molecule binds the A site in a quaternary complex with EF-Tu, SmpB, and GTP.

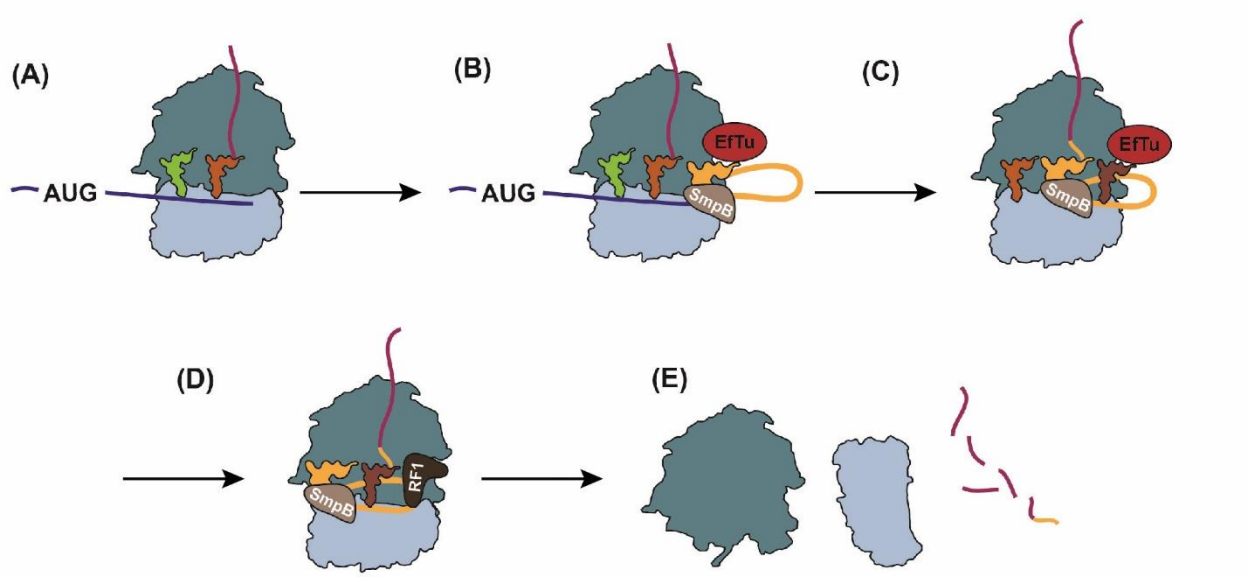

Figure 1.4: Schematic depicting *trans*-translation. A) The ribosome reaches the 3' end of a transcript lacking a stop codon. B) The tmRNA-SmpB-EF-Tu-GTP complex recognizes the stalled ribosome. C) The nascent peptide is transferred to tmRNA. Translation then resumes of the open reading frame (ORF) of ssrA which tags the incomplete peptide at its 3' end. The mRNA is then released and degraded. D) Termination occurs when a release factor recognizes the stop codon in the ssrA ORF. E) The ribosome dissociates and the incomplete peptide is degraded (100).

One of the main questions with regards to *trans*-translation is how the selectivity of this process is governed. As is previously discussed, the specificity of peptidyl transfer is achieved by cognate codon-anticodon interactions between mRNA and tRNA during translation elongation, and these interactions are required to initiate conformational changes in the decoding center (10). Interestingly, tmRNA lacks an anticodon stem loop; therefore, it cannot form the same type of interactions as aa-tRNAs (114). However, crystal structures of the tRNA-like domain of tmRNA in complex with SmpB shows that the protein occupies the decoding center and that the complex adopts a structure which is similar to tRNA, with the N-terminal domain of the protein in place of the anticodon stem loop (115). These structural as well as biochemical studies suggest that SmpB is likely to interact with A1492, A1493, and G530 residues of the decoding center (116, 117); however, the A-minor interactions that these residues have with aa-tRNA and mRNA cannot occur with the protein. Additionally, mutating any of the decoding center residues has no impact on tmRNA activity in a reconstituted system (118). One recent crystal structure of a *T. thermophilus* tmRNA-SmpB-EF-Tu complex shows that the decoding center adopts a conformation that is similar, but not identical to, that observed with normal elongation complexes (119). This supports the idea that SmpB induces rearrangement of A1492 and A1493, but their identities are not critical to the stabilization of the induced state of the ribosome.

Another question with regards to the selectivity of trans-translation is how the process avoids targeting actively translating ribosomes. One common feature of tmRNA targets is that there is little-to-no mRNA downstream of the P site. *In vitro* studies have shown that complexes with greater than six nucleotides downstream of the P site are poorly recognized by tmRNA (120, 121). In solution, the C-terminal domain of SmpB is unstructured (122, 123), but in complex with the ribosome it forms a helical structure (119). This structure extends from the A

site towards the mRNA-entry tunnel where it makes contacts with the 16S rRNA, and early mutational analysis revealed that the ability of this region to form this structure is critical for ssrA tagging (118, 124). Overall, SmpB cannot bind the ribosome unless it has reached the 3'-end of the mRNA because the C-terminus of the protein occupies the site that is normally occupied by the mRNA during translation elongation. This structural clash between SmpB and the mRNA ensures that the tmRNA does not bind the A site of the actively translating ribosome, and hence avoids prematurely terminating protein synthesis.

While much is known about how the initial steps of *trans*-translation occur, more is yet to be uncovered about the process. For example, after the first peptidyl transfer reaction, translocation must occur to bring the tmRNA open reading frame (ORF) into the A site of the ribosome. The new ORF has to occupy the mRNA entry tunnel where SmpB initially binds; as a result, SmpB is predicted to change conformation to allow for template switching (125). This process, by which the resume codon of the tmRNA is positioned into the A-site, is still not well understood, but appears to be dependent on key interactions between SmpB and sequence elements upstream of the ORF (126).

CONCLUSION

While much is known about how changes to the ribosome and tRNA can impact tRNA selection, less is known about how structural changes to mRNA can alter this process. Studies have been performed to investigate the impact of several nucleobase adducts that impact hydrogen bonding, as well as those that serve as intentional modifications; however, several open questions remain. For example, it is known from previous studies in DNA that the frequency at which 8-oxodG base pairs with A or C depends on the fidelity of the polymerase decoding the lesion (127–130). Previous work from our group shows that 8-oxoG in mRNA stalls the ribosome, but the conformation of 8-oxoG within the ribosome remained unclear (87). Additionally, previous work has shown that several alkylative damage adducts can increase ribosomal stalling, bypass, and/or miscoding (75, 76). The molecular pathways in eukaryotes to rescue stalled ribosomes is well characterized (100). In contrast, the bacterial system used to rescue stalled ribosomes from damaged transcripts was still unknown. Finally, the importance of the kink structure in the phosphate backbone of mRNA in the context of the ribosome remained uninvestigated. Addressing these and other questions will help to elucidate the importance of mRNA structure in translation.

QUESTIONS ADDRESSED BY THIS THESIS WORK

Although our understanding of how mRNA structure can impact translation has greatly increased in the last decade, there still exist significant gaps in knowledge of how the ribosome deals with alterations in mRNA structure. Broadly, my thesis work has focused on understanding how modifications to mRNA impact tRNA selection. My research focused around four questions:

- Does 8-oxoG in mRNA prefer to base pair in the *syn* or *anti* conformation in the context of the A-site of the ribosome?
- Does the presence of m^1A in mRNA cause ribosome stalling and/or specific miscoding events?
- How do bacteria rescue ribosomes stalled by alkylative damage?
- Is the kink-structure of the mRNA phosphate backbone in the ribosome important for tRNA selection?

REFERENCES

1. Bouadloun,F., Donner,D. and Kurland,C.G. (1983) Codon-specific missense in vivo. *Embo J*, **2**, 1351–1356.

2. Edelmann,P. and Gallant,J. (1977) Mistranslation in E. coli. *Cell*, **10**, 131–137.

3. E.B.,K. and P.J.,F. (2007) The frequency of translational misreading errors in E. coli is largely determined by tRNA competition. *Rna*, **13**, 87–96.

4. Ogle,J.M., Brodersen,D.E., Jr,W.M.C., Tarry,M.J., Carter,A.P., Ramakrishnan,V., Ogle,J.M., Brodersen,D.E., Jr,W.M.C., Tarry,M.J., *et al.* (2002) Recognition of Cognate Transfer RNA by the 30S Ribosomal Subunit Published by : American Association for the Advancement of Science Stable URL : http://www.jstor.org/stable/3083592 Recognition of Cognate Transfer RNA by the 30S Ribosomal Subunit. **292**, 897–902.

5. Lipsett,M.N., Heppel,L.A. and Bradley,D.F. (1960) Complex formation between adenine oligonucleotides and polyuridylic acid. *BBA - Biochim. Biophys. Acta*, **41**, 175–177.

6. McLaughlin,C.S., Dondon,J., Grunberg-Manago,M., Michelson,A.M. and Saunders,G. (1968) Stability of the messenger RNA-transfer RNA-ribosome complex. *J. Mol. Biol.*, **32**, 521–542.

7. Gorini,L. and Kataja,E. (1964) Phenotypic Repair By Streptomycin of Defective Genotypes in E. Coli. *Proc. Natl. Acad. Sci.*, **51**, 487–493.

8. Davies,J., Gilbert,W. and Gorini,L. (1964) Streptomycin, Suppression, and the Code. *Proc. Natl. Acad. Sci.*, **51**, 883–890.

9. Cochella,L. and Green,R. (2005) Fidelity in protein synthesis. *Curr. Biol.*, **15**, R536–R540.

10. Zaher,H.S. and Green,R. (2009) Fidelity at the Molecular Level: Lessons from Protein Synthesis. *Cell*, **136**, 746–762.

11. Hopfield,J.J. (1974) Kinetic proofreading: a new mechanism for reducing errors in biosynthetic processes requiring high specificity. *Proc. Natl. Acad. Sci. U. S. A.*, **71**, 4135–9.

12. Ninio,J. (1975) Kinetic amplification of enzyme discrimination. *Biochimie*, **57**, 587–595.

13. Rodnina,M. V., Fricke,R. and Wintermeyer,W. (1994) Transient Conformational States of Aminoacyl-tRNA during Ribosome Binding Catalyzed by Elongation Factor Tu. *Biochemistry*, **33**, 12267–12275.

14. Pape,T., Wintermeyer,W. and Rodnina,M. V (1998) Complete Kinetic Mechanism of elongation factor Tu-dependent binding of aminoacyl-tRNA to the A site of the E. coli ribosome. *EMBO J.*, **17**, 1–8.

15. Diaconu,M., Kothe,U., Schlünzen,F., Fischer,N., Harms,J.M., Tonevitsky,A.G., Stark,H., Rodnina,M. V. and Wahl,M.C. (2005) Structural basis for the function of the ribosomal L7/12 stalk in factor binding and GTpase activation. *Cell*, **121**, 991–1004.

16. Gromadski,K.B. and Rodnina,M. V. (2004) Kinetic Determinants of High-Fidelity tRNA

Discrimination on the Ribosome. *Mol. Cell*, **13**, 191–200.

17. Rodnina,M. V, Fricke,R., Kuhn,L. and Wintermeyer,W. (1995) Codon-dependent conformational change of elongation factor Tu preceding GTP hydrolysis on the ribosome. *EMBO J.*, **14**, 2613–9.

18. Gromadski,K.B., Daviter,T. and Rodnina,M. V. (2006) A uniform response to mismatches in codon-anticodon complexes ensures ribosomal fidelity. *Mol. Cell*, **21**, 369–377.

19. Pape,T., Wintermeyer,W. and Rodnina,M. (1999) Induced fit in initial selection and proofreading of aminoacyl-tRNA on the ribosome. *EMBO J.*, **18**, 3800–3807.

20. Kothe,U. and Rodnina,M. V. (2007) Codon Reading by tRNAAla with Modified Uridine in the Wobble Position. *Mol. Cell*, **25**, 167–174.

21. Ledoux,S. and Uhlenbeck,O.C. (2008) Different aa-tRNAs Are Selected Uniformly on the Ribosome. *Mol. Cell*, **31**, 114–123.

22. Youngman,E.M., McDonald,M.E. and Green,R. (2008) Peptide Release on the Ribosome: Mechanism and Implications for Translational Control. *Annu. Rev. Microbiol.*, **62**, 353–373.

23. Freistroffer,D. V., Pavlov,M.Y., MacDougall,J., Buckingham,R.H. and Ehrenberg,M. (1997) Release factor RF3 in E. coli accelerates the dissociation of release factors RF1 and RF2 from the ribosome in a GTP-dependent manner. *EMBO J.*, **16**, 4126–4133.

24. Jorgensen,F., Adamski,F.M., Tate,W.P. and Kurland,C.G. (1992) Release factor dependent false stops are infrequent in ecoli.pdf. *J. Mol. Biol.*

25. Anderson,K., Bhat,M., Kiehart,D., Fehon,R., Cavener,D., Oda,H. and Petitt,M. (2000) A tripeptide ` anticodon ’ deciphers stop codons in messenger RNA. **403**.

26. Klaholz,B.P., Pape,T. and Zavialov,A. V (2003) Structure of the Escherichia coli ribosomal termination complex with release factor 2. **421**, 90–94.

27. Petry,S., Brodersen,D.E., Iv,F.V.M., Dunham,C.M., Selmer,M., Tarry,M.J., Kelley,A.C. and Ramakrishnan,V. (2005) Crystal Structures of the Ribosome in Complex with Release Factors RF1 and RF2 Bound to a Cognate Stop Codon. 10.1016/j.cell.2005.09.039.

28. Rawat,U.B.S., Zavialov,A. V and Sengupta,J. (2003) A cryo-electron microscopic study of ribosome-bound termination factor RF2. **890**, 2001–2004.

29. Korostelev,A., Asahara,H., Lancaster,L., Laurberg,M. and Hirschi,A. (2008) Crystal structure of a translation termination complex formed with release factor RF2.

30. Laurberg,M., Asahara,H., Korostelev,A., Zhu,J., Trakhanov,S. and Noller,H.F. (2008) Structural basis for translation termination on the 70S ribosome. **454**, 852–857.

31. Weixlbaumer,A., Jin,H., Neubauer,C., Voorhees,R.M., Petry,S., Kelley,A.C. and Ramakrishnan,V. (2009) Insights into translational termination from the structure of RF2 bound to the ribosome. *Science (80-.).*, **322**, 953–956.

32. Freistroffer,D. V., Kwiatkowski,M., Buckingham,R.H. and Ehrenberg,M. (2000) The accuracy of codon recognition by polypeptide release factors. *Proc. Natl. Acad. Sci.*, **97**,

2046–2051.

33. Moazad,D. and Noller,H.F. (1987) Interaction of antibiotics with functional sites in 16S ribosomal RNA. *Nature*.

34. Moazed,D. and Noller,H.F. (1990) Binding of tRNA to the ribosomal A and P sites protects two distinct sets of nucleotides in 16 S rRNA. *J. Mol. Biol.*, **211**, 135–145.

35. Powers,T. and Noller,H.F. (1990) Dominant lethal mutations in a conserved loop in 16S rRNA (site-directed mutageliesis/rRNA mutations/A PL promoter/ribosomal A site). *Biochemistry*, **87**, 1042–1046.

36. Powers,T. and Noller,H.F. (1994) Selective perturbation of G530 of 16 S rRNA by translational miscoding agents and a streptomycin-dependence mutation in protein S12. *J. Mol. Biol.*, **235**, 156–172.

37. Yoshizawa,S., Fourmy,D. and Puglisi,J.D. (1999) Recognition of the codon-anticodon helix by ribosomal RNA. *Science (80-.).*, **285**, 1722–1725.

38. Ogle,J.M., Murphy IV,F. V., Tarry,M.J. and Ramakrishnan,V. (2002) Selection of tRNA by the ribosome requires a transition from an open to a closed form. *Cell*, **111**, 721–732.

39. Voorhees,R.M., Schmeing,T.M., Kelley,A.C. and Ramakrishnan,V. (2010) The mechanism for activation of GTP hydrolysis on the ribosome. *Science (80-.).*, **330**, 835–838.

40. Ramakrishnan,V. (2002) Ribosome structure and the mechanism of translation. *Cell*, **108**, 557–72.

41. Davies,J. and Davis,B.D. (1968) Misreading of Ribonucleic Acid Code Words Induced by Aminoglycoside Antibiotics. *J. Biol. Chem.*

42. Karimi,R. and Ehrenberg,M. (1994) Dissociation Rate of Cognate Peptidyl-tRNA from the A-Site of Hyper-Accurate and Error-Prone Ribosomes. *Eur. J. Biochem.*, **226**, 355–360.

43. Pape,T., Wintermeyer,W. and Rodnina,M. V. (2000) Conformational switch in the decoding region of 16S rRNA during aminoacyl-tRNA selection on the ribosome. *Nat. Struct. Biol.*, **7**, 104–107.

44. Fourmy,D., Yoshizawa,S. and Puglisi,J.D. (1998) Paromomycin binding induces a local conformational change in the A-site of 16 S rRNA. *J. Mol. Biol.*, **277**, 333–345.

45. Fourmy,D., Recht,M.I., Blanchard,S.C. and Puglisi,J.D. (2009) Structure of the A Site of Escherichia coli 16S Ribosomal RNA Complexed with an Aminoglycoside Antibiotic Published by : American Association for the Advancement of Science Stable URL : http://www.jstor.org/stable/2892058. *Adv. Sci.*, **274**, 1367–1371.

46. Ramakrishnan,V., Carter,A.P., Clemons,W.M., Brodersen,D.E., Morgan-Warren,R.J. and Wimberly,B.T. (2000) Functional insights from the structure of the 30S ribosomal subunit and its interactions with antibiotics. *Nature*, **407**, 340–348.

47. Gromadski,K.B. and Rodnina,M. V. (2004) Streptomycin interferes with conformational coupling between codon recognition and GTPase activation on the ribosome. *Nat. Struct. Mol. Biol.*, **11**, 316–322.

48. Demirci,H., Iv,F.M., Murphy,E., Gregory,S.T. and Albert,E. (2013) A structural basis for streptomycin-induced misreading of the genetic code. *Nat. Commun.*, 10.1038/ncomms2346.A.

49. Anderson,W.F., Gorini,L. and Breckenridge,L. (2006) Role of ribosomes in streptomycin-activated suppression. *Proc. Natl. Acad. Sci.*, **54**, 1076–1083.

50. Ozaki,M., Mizushima,S. and Nomura,M. (1969) Identification and functional characterization of the protein controlled by the streptomycin-resistant locus in E. coli. *Nature*, **222**, 333–9.

51. Rosset,R. and Gorini,L. (1969) A ribosomal ambiguity mutation. *J. Mol. Biol.*, **39**, 95–112.

52. Andersson,D.I. and Kurland,C.G. (1983) Ram ribosomes are defective proofreaders. *MGG Mol. Gen. Genet.*, **191**, 378–381.

53. Zaher,H.S. and Green,R. (2010) Hyperaccurate and Error-Prone Ribosomes Exploit Distinct Mechanisms during tRNA Selection. *Mol. Cell*, **39**, 110–120.

54. Murphy,F. V., Ramakrishnan,V., Malkiewicz,A. and Agris,P.F. (2004) The role of modifications in codon discrimination by tRNALysUUU. *Nat. Struct. Mol. Biol.*, **11**, 1186–1191.

55. Olejniczak,M., Dale,T., Fahlman,R.P. and Uhlenbeck,O.C. (2005) Idiosyncratic tuning of tRNAs to achieve uniform ribosome binding. *Nat. Struct. Mol. Biol.*, **12**, 788–793.

56. Agris,P.F. (2008) Bringing order to translation: The contributions of transfer RNA anticodon-domain modifications. *EMBO Rep.*, **9**, 629–635.

57. Lorenz,C., Lünse,C.E. and Mörl,M. (2017) Trna modifications: Impact on structure and thermal adaptation. *Biomolecules*, **7**.

58. Crick,F.H.C. (1966) Codon—anticodon pairing: The wobble hypothesis. *J. Mol. Biol.*, **19**, 548–555.

59. Ortiz-meoz,R.F. and Green,R. (2011) Helix 69 Is Key for Uniformity during Substrate Selection on. **286**, 25604–25610.

60. Maehigashi,T., Dunkle,J.A., Miles,S.J. and Dunham,C.M. (2014) Structural insights into +1 frameshifting promoted by expanded or modification-deficient anticodon stem loops. *Proc. Natl. Acad. Sci.*, **111**, 12740–12745.

61. Machnicka,M.A., Milanowska,K., Oglou,O.O., Purta,E., Kurkowska,M., Olchowik,A., Januszewski,W., Kalinowski,S., Dunin-Horkawicz,S., Rother,K.M., *et al.* (2013) MODOMICS: A database of RNA modification pathways - 2013 update. *Nucleic Acids Res.*, **41**, 262–267.

62. Wurtmann,E.J. and Wolin,S.L. (2009) RNA under attack: Cellular handling of RNA damage RNA under attack: Cellular handling of RNA damage E. J. Wurtmann et.al. *Crit. Rev. Biochem. Mol. Biol.*, **44**, 34–49.

63. Simms,C.L. and Zaher,H.S. (2016) Quality control of chemically damaged RNA. *Cell. Mol. Life Sci.*, **73**, 3639–3653.

64. Meyer,K.D. and Jaffrey,S.R. (2014) The dynamic epitranscriptome: N6-methyladenosine and gene expression control. *Nat. Rev. Mol. Cell Biol.*, **15**, 313–326.

65. Harper,J.E., Miceli,S.M., Roberts,R.J. and Manley,J.L. (1990) Sequence specificity of the human mRNA N6-adenosine methylase in vitro. *Nucleic Acids Res.*, **18**, 5735–5741.

66. Bokar,J.A., Shambaugh,M.E., Polayes,D., Matera,A.G. and Rottman,F.M. (1997) Purification and cDNA cloning of the AdoMet-binding subunit of the human mRNA (N6-adenosine)-methyltransferase. *RNA*, **3**, 1233–47.

67. Ping,X.L., Sun,B.F., Wang,L., Xiao,W., Yang,X., Wang,W.J., Adhikari,S., Shi,Y., Lv,Y., Chen,Y.S., *et al.* (2014) Mammalian WTAP is a regulatory subunit of the RNA N6-methyladenosine methyltransferase. *Cell Res.*, **24**, 177–189.

68. Liu,J., Yue,Y., Han,D., Wang,X., Fu,Y., Zhang,L., Jia,G., Yu,M., Lu,Z., Deng,X., *et al.* (2014) A METTLE3-METTL14 complex mediates mammalian nuclear RNA N6-adenosine methylation. *Nat. Chem. Biol.*, **10**, 93–95.

69. Riaz,N., Wolden,S.L., Gelblum,D.Y. and Eric,J. (2016) N6-methyladenosine modification destabilizes developmental regulators in embryonic stem cells. *Nat. Cell. Biol.*, **118**, 6072–6078.

70. Gerken,T., Girard,C.A., Tung,Y.C.L., Webby,C.J., Saudek,V., Hewitson,K.S., Yeo,G.S.H., McDonough,M.A., Cunliffe,S., McNeill,L.A., *et al.* (2007) The obesity-associated FTO gene encodes a 2-oxoglutarate-dependent nucleic acid demethylase. *Science (80-.).*, **318**, 1469–1472.

71. Zheng,G., Dahl,J.A., Niu,Y., Fedorcsak,P., Huang,C.M., Li,C.J., Vågbø,C.B., Shi,Y., Wang,W.L., Song,S.H., *et al.* (2013) ALKBH5 Is a Mammalian RNA Demethylase that Impacts RNA Metabolism and Mouse Fertility. *Mol. Cell*, **49**, 18–29.

72. Xiao Wang1 Adrian Gomez1, Gary C. Hon2, Yanan Yue1, Dali Han1, Ye Fu1, Marc Parisien3, Qing Dai1, Guifang Jia1, 4, Bing Ren2, Tao Pan3, and Chuan He1,Z.L. (2014) m6A-dependent regulation of messenger RNA stability. *Nature*, **505**, 1–20.

73. Dominissini,D., Moshitch-Moshkovitz,S., Schwartz,S., Salmon-Divon,M., Ungar,L., Osenberg,S., Cesarkas,K., Jacob-Hirsch,J., Amariglio,N., Kupiec,M., *et al.* (2012) Topology of the human and mouse m6A RNA methylomes revealed by m6A-seq. *Nature*, **485**, 201–206.

74. Schwartz,S., Agarwala,S.D., Mumbach,M.R., Jovanovic,M., Mertins,P., Shishkin,A., Tabach,Y., Mikkelsen,T.S., Satija,R., Ruvkun,G., *et al.* (2013) High-Resolution mapping reveals a conserved, widespread, dynamic mRNA methylation program in yeast meiosis. *Cell*, **155**, 1409–1421.

75. Hudson,B.H. and Zaher,H.S. (2015) O6-Methylguanosine leads to position-dependent effects on ribosome speed and fidelity. *Rna*, **21**, 1648–1659.

76. You,C., Dai,X. and Wang,Y. (2017) Position-dependent effects of regioisomeric methylated adenine and guanine ribonucleosides on translation. *Nucleic Acids Res.*, **45**, 9059–9067.

77. Balaban,R.S., Nemoto,S. and Finkel,T. (2005) Mitochondria, oxidants, and aging. *Cell*, **120**,

483–495.

78. Finkel,T. and Holbrook,N.J. (2000) Oxidants, oxidative stress and the biology of ageing. *Nature*, **408**, 239–47.

79. Babior,B.M., Kipnes,R.S. and Curnutte,J.T. (1973) Biological Defense Mechanisms. The Production by Leukocytes of Superoxide, A Potential Bactericidal Agent. *Concise Publ.*, **52**, 741–744.

80. Pick,M., Rabani,J., Yost,F. and Fridovich,I. (1974) The Catalytic Mechanism of the Manganese-Containing Superoxide Dismutase of Escherichia coli Studied by Pulse Radiolysis. *J. Am. Chem. Soc.*, **96**, 7329–7333.

81. Koppenol,W.H. (2004) The Haber-Weiss cycle – 70 years later. *Redox Rep.*, **6**, 229–234.

82. Ravanat,J., Douki,T. and Cadet,J. (2001) Direct and indirect effects of UV radiation on DNA and its components. **63**, 88–102.

83. Bellacosa,A. and Moss,E.G. (2003) RNA Repair : Damage Control. **13**, 482–484.

84. Rydberg,B. and Lindahl,T. (1982) Nonenzymatic methylation of DNA by the intracellular methyl group S-adenosyl_L-methionine is a potentially mutagenic reaction. *EMBO J.*, **1**, 211–216.

85. Hofer,T., Badouard,C., Cotgreave,I.A. and Nucle,A. (2005) Hydrogen peroxide causes greater oxidation in cellular RNA than in DNA. **386**, 333–337.

86. Shen,Z., Wu,W. and Hazen,S.L. (2000) Activated Leukocytes Oxidatively Damage DNA , RNA , and the Nucleotide Pool through Halide-Dependent Formation of Hydroxyl Radical †. 10.1021/bi992809y.

87. Simms,C.L., Hudson,B.H., Mosior,J.W., Rangwala,A.S. and Zaher,H.S. (2014) An Active Role for the Ribosome in Determining the Fate of Oxidized mRNA. *Cell Rep.*, **9**, 1256–1264.

88. Cheng,X., Kelso,C., Hornak,V., de los Santos,C., Grollman,A.P. and Simmerling,C. (2005) Dynamic behavior of DNA base pairs containing 8-oxoguanine. *J. Am. Chem. Soc.*, **127**, 13906–18.

89. Zhang,C. and Jia,G. (2018) Reversible RNA Modification N1-methyladenosine (m1A) in mRNA and tRNA. *Genomics, Proteomics Bioinforma.*, **16**, 155–161.

90. Dominissini,D., Nachtergaele,S., Moshitch-moshkovitz,S., Peer,E., Kol,N., Ben-haim,M.S., Dai,Q., Segni,A. Di, Clark,W.C., Zheng,G., *et al.* (2016) The dynamic N 1 -methyladenosine methylome in eukaryotic messenger RNA. *Nature*, **530**, 441–446.

91. Li,X., Xiong,X., Wang,K., Wang,L., Shu,X., Ma,S. and Yi,C. (2016) Transcriptome-wide mapping reveals reversible and dynamic N 1 -methyladenosine methylome. *Nat. Publ. Gr.*, **12**, 311–316.

92. Safra,M., Sas-chen,A., Nir,R., Winkler,R., Nachshon,A., Bar-yaacov,D., Erlacher,M., Rossmanith,W., Stern-ginossar,N. and Schwartz,S. (2017) The m1A landscape on cytosolic and mitochondrial mRNA at single-base resolution. *Nat. Publ. Gr.*, **551**, 251–255.

93. Dai,Q., Moshitch-moshkovitz,S., Han,D., Kol,N., Amariglio,N., Rechavi,G. and Dominissini,D. (2017) Nm-seq maps 2 ′ - O - methylation sites in human mRNA with base precision. *Nat. Publ. Gr.*, **14**.

94. Decatur,W.A. and Fournier,M.J. (2002) rRNA modifications and ribosome function. **27**, 344–351.

95. Choi,J., Indrisiunaite,G., HDemirci,H., Ieong,K.W., Wang,J., Petrov,A., Prabhakar,A., Rechavi,G., Dominissini,D., He,C., *et al.* (2018) 2'O-methylation in mRNA disrupts tRNA decoding during translation elongation. *Nat. Struct. Mol. Biol.*, **25**.

96. Yi-brunozzi,H.Y., Easterwood,L.M., Kamilar,G.M. and Beal,P.A. (1999) Synthetic substrate analogs for the RNA-editing adenosine deaminase ADAR-2. **27**, 2912–2917.

97. Khade,P.K. and Joseph,S. (2011) Messenger RNA interactions in the decoding center control the rate of translocation. *Nat. Publ. Gr.*, **18**, 1300–1302.

98. Demeshkina,N., Jenner,L., Westhof,E., Yusupov,M. and Yusupova,G. (2012) A new understanding of the decoding principle on the ribosome. *Nature*, **484**, 256–259.

99. Selmer,M., Dunham,C.M., Murphy,F. V, Weixlbaumer,A., Petry,S., Kelley,A.C., Weir,J.R. and Ramakrishnan,V. (2006) Structure of the 70S ribosome complexed with mRNA and tRNA. *Science*, **313**, 1935–42.

100. Simms,C.L., Thomas,E.N. and Zaher,H.S. (2017) Ribosome-based quality control of mRNA and nascent peptides. *Wiley Interdiscip. Rev. RNA*, **8**, 1–27.

101. Lykke-Andersen,S. and Jensen,T.H. (2015) Nonsense-mediated mRNA decay: An intricate machinery that shapes transcriptomes. *Nat. Rev. Mol. Cell Biol.*, **16**, 665–677.

102. Klauer,A.A. and van Hoof,A. (2013) Degradation of mRNAs that lack a stop codon: A decade of nonstop progress. *Wiley Interdiscip. Rev. RNA*, **3**, 649–660.

103. Harigaya,Y. and Parker,R. (2010) No-go decay: a quality control mechanism for RNA in translation. *Wiley Interdiscip. Rev. RNA*, **1**, 132–141.

104. Keiler,K.C., Waller,P.R.H. and Sauer,R.T. (1996) Role of a Peptide Tagging System in Degradation of Proteins Synthesized from Damaged Messenger RNA. *Science (80-.).*, **271**, 990–993.

105. Moore,S.D. and Sauer,R.T. (2007) The tmRNA System for Translational Surveillance and Ribosome Rescue. *Annu. Rev. Biochem.*, **76**, 101–124.

106. Nishikawa,K., Inokuchi,H., Kitabatake,M., Yokogawa,T. and Komine,Y. (2006) A tRNA-like structure is present in 10Sa RNA, a small stable RNA from Escherichia coli. *Proc. Natl. Acad. Sci.*, **91**, 9223–9227.

107. Valle,M., Gillet,R., Kaur,S., Henne,A., Ramakrishnan,V. and Frank,J. (2003) Visualizing tmRNA Entry into a Stalled Ribosome. *Science (80-.).*, **300**, 127–130.

108. Hallier,M., Ivanova,N., Rametti,A., Pavlov,M., Ehrenberg,M. and Felden,B. (2004) Pre-binding of small protein B to a stalled ribosome triggers trans-translation. *J. Biol. Chem.*, **279**, 25978–25985.

109. Gottesman,S., Roche,E., Zhou,Y.N. and Sauer,R.T. (1998) The ClpXP and ClpAP proteases degrade proteins with carboxy-terminal peptide tails added by the SsrA-tagging system. *Genes Dev.*, **12**, 1338–1347.

110. Keiler,K.C. and Sauer,R.T. (1996) Sequence determinants of C-terminal substrate recognition by the Tsp protease. *J. Biol. Chem.*, **271**, 2589–2593.

111. Rudinger-Thirion,J., Giege,R. and Felden,B. (1999) Aminoacylated tmRNA from Escherichia coli interacts with prokaryotic elongation factor Tu. *Rna*, **5**, 989–992.

112. Barends,S., Karzai,A.W., Sauer,R.T., Wower,J. and Kraal,B. (2001) Simultaneous and functional binding of SmpB and EF-Tu·GTP to the alanyl acceptor arm of tmRNA. *J. Mol. Biol.*, **314**, 9–21.

113. Wali Karzai,A., Susskind,M.M. and Sauer,R.T. (1999) SmpB, a unique RNA-binding protein essential for the peptide-tagging activity of SsrA (tmRNA). *EMBO J.*, **18**, 3793–3799.

114. Gutmann,S., Haebel,P.W., Metzinger,L., Sutter,M., Felden,B. and Ban,N. (2003) Crystal structure of the transfer-RNA domain of transfer-messenger RNA in complex with SmpB. *Nature*, **424**, 699–703.

115. Bessho,Y., Shibata,R., Sekine,S. -i., Murayama,K., Higashijima,K., Hori-Takemoto,C., Shirouzu,M., Kuramitsu,S. and Yokoyama,S. (2007) Structural basis for functional mimicry of long-variable-arm tRNA by transfer-messenger RNA. *Proc. Natl. Acad. Sci.*, **104**, 8293–8298.

116. Kaur,S., Gillet,R., Li,W., Gursky,R. and Frank,J. (2006) Cryo-EM visualization of transfer messenger RNA with two SmpBs in a stalled ribosome. *Proc. Natl. Acad. Sci.*, **103**, 16484–16489.

117. Kurita,D., Sasaki,R., Muto,A. and Himeno,H. (2007) Interaction of SmpB with ribosome from directed hydroxyl radical probing. *Nucleic Acids Res.*, **35**, 7248–7255.

118. Miller,M.R., Liu,Z., Cazier,D.J., Gebhard,G.M., Herron,S.R., Zaher,H.S., Green,R. and Buskirk,A.R. (2011) The role of SmpB and the ribosomal decoding center in licensing tmRNA entry into stalled ribosomes. *Rna*, **17**, 1727–1736.

119. Neubauer,C., Gillet,R., Kelley, a. C. and Ramakrishnan,V. (2012) Decoding in the Absence of a Codon by tmRNA and SmpB in the Ribosome (Supporting online material). *Science (80-.).*, **335**, 1366–1369.

120. Ivanova,N., Pavlov,M.Y. and Ehrenberg,M. (2005) tmRNA-induced release of messenger RNA from stalled ribosomes. *J. Mol. Biol.*, **350**, 897–905.

121. Ivanova,N., Pavlov,M.Y., Felden,B. and Ehrenberg,M. (2004) Ribosome rescue by tmRNA requires truncated mRNAs. *J. Mol. Biol.*, **338**, 33–41.

122. Dong,G., Nowakowski,J. and Hoffman,D.W. (2002) Structure of small protein B : the protein component of the tmRNA ± SmpB system for ribosome rescue. **21**, 1845–1854.

123. Someya,T., Nameki,N., Hosoi,H., Suzuki,S., Hatanaka,H., Fujii,M., Terada,T., Shirouzu,M.

and Inoue,Y. (2003) Solution structure of a tmRNA-binding protein , SmpB , from Thermus thermophilus. **535**, 94–100.

124. Kurita,D., Muto,A. and Himeno,H. (2010) Role of the C-terminal tail of SmpB in the early stage of trans -translation. 10.1261/rna.1916610.2002.

125. Fu,J., Hashem,Y., Wower,I., Lei,J., Liao,H.Y., Zwieb,C., Wower,J. and Frank,J. (2010) Visualizing the transfer-messenger RNA as the ribosome resumes translation. *EMBO J.*, **29**, 3819–3825.

126. Bron,P., Giudice,E., Rolland,J., Thomas,D., Felden,B. and Gillet,R. (2010) tmRNA – SmpB : a journey to the centre of the bacterial ribosome. **29**, 3810–3818.

127. Mcculloch,S.D., Kokoska,R.J., Garg,P., Burgers,P.M. and Kunkel,T.A. (2009) The efficiency and fidelity of 8-oxo-guanine bypass by DNA polymerases δ and η. *Nucleic Acids Res.*, **37**, 2830–2840.

128. Freudenthal,B.D., Beard,W.A. and Wilson,S.H. (2013) DNA polymerase minor groove interactions modulate mutagenic bypass of a templating 8-oxoguanine lesion. *Nucleic Acids Res.*, **41**, 1848–1858.

129. Vasquez-Del Carpio,R., Silverstein,T.D., Lone,S., Swan,M.K., Choudhury,J.R., Johnson,R.E., Prakash,S., Prakash,L. and Aggarwal,A.K. (2009) Structure of human DNA polymerase κ inserting dATP opposite an 8-OxoG DNA lesion. *PLoS One*, **4**.

130. Brieba,L.G., Eichman,B.F., Kokoska,R.J., Doublié,S., Kunkel,T.A. and Ellenberger,T. (2004) Structural basis for the dual coding potential of 8-oxoguanosine by a high-fidelity DNA polymerase. *EMBO J.*, **23**, 3452–3461.

Chapter 2

Alkylative damage of mRNA leads to ribosome stalling and rescue by *trans*-translation in bacteria

Erica N. Thomas, Emily P. McHugh, Thomas Marcinkiewicz, and Hani S. Zaher

ABSTRACT

The highly efficient and accurate process of translation can be disrupted by damage to nucleic acids. Several endogenous and exogenous damaging agents can cause the accumulation of alkylative adducts, which can disrupt the normal hydrogen bonding between nucleotides. Multiple alkylative adducts of nucleotides have been shown to impact the speed and/or accuracy of the decoding process *in vitro*, and several adducts are able to stall the ribosome. However, little is known about the cellular response to ribosome stalling by alkylative damage *in vivo*. In order to investigate the impact of alkylative damage of RNA on ribosome rescue, we treat *E. coli* with two common alkylating agents, methyl methanesulfonate (MMS) and methylnitronitrosoguanidine (MNNG), and observe the accumulation of several disruptive adducts, including N(1)-methyladenosine (m^1A). Using a well-defined bacterial translation system, we confirm that m^1A stalls ribosomes *in vitro*. In bacteria, ribosomal stalling is primarily relieved by *trans*-translation, which utilizes transfer-messenger RNA (tmRNA) to release the ribosome and tag the incomplete peptide for degradation. To assess if ribosomes use *trans*-translation to rescue ribosomes stalled by alkylative damage *in vivo*, we utilize a previously generated mutant transfer-messenger RNA (tmRNA) that encodes a His_6 tag in place of its peptide degradation signal. When *E. coli* expressing tmRNA- His_6 are treated with alkylating agents, we observe an increase in tmRNA activity. These data demonstrate that alkylative damage to RNA in bacteria leads to ribosome stalling and rescue by the *trans*-translation pathway.

INTRODUCTION

Nucleic acids are consistently experiencing damage from numerous endogenous and exogenous insults, including reactive oxygen species, ultraviolet radiation, and alkylating agents (1, 2). In particular, the oxygen and nitrogen atoms of nucleobases are readily modified by alkylating agents. RNA is more susceptible to chemical insults than DNA, likely due to its exposed Watson-Crick (WC) hydrogen bonding interface (3, 4). Alkylation of the WC interface of mRNA is particularly disruptive during the process of decoding on the ribosome (5). The initial stage of tRNA selection, known as codon recognition, depends on the ability of the mRNA codon and the anticodon of the amino acyl tRNA (aa-tRNA) to form proper hydrogen bonds (6, 7). Watson-Crick-base-pair conformations are accepted at all three positions of the codon-anticodon, while certain wobble conformations are also tolerated at the third position (8, 9). The introduction of alkylative damage to this interface is known to disrupt hydrogen bonding interactions and as a result, is highly likely to reduce translational speed and fidelity (10).

Several alkylative damage adducts of mRNA have either been predicted or shown to be detrimental to the decoding process. For example, O6-methylguanosine (m^6G), N1-methylguanosine (m^1G), 3-methylcytidine (m^3C), and N1-methyladenosine (m^1A) are of interest due to their potential to interfere with normal WC interfaces (10). Prior work has shown the presence of m^6G in mRNA interferes with the speed and accuracy of decoding (11, 12). The introduction of a methyl group to the O6 of guanosine causes an internal rearrangement of electrons such that N1 is no longer covalently bound to the hydrogen used to base pair at the WC interface. This results in a significant reduction in the rate of peptidyl transfer in the presence of an m^6G•C base pair (11). Additionally, the alteration of N1 from a hydrogen bond donor to a hydrogen acceptor allows for m^6G to base pair in the Watson-Crick conformation with uridine,

resulting in an increase in the rate of miscoding in the presence of an m^6G•U base pair (11). Due to the difficulty of incorporating the adduct into a synthesized transcript, the impact of m^3C on decoding fidelity has remained elusive. However, we predict that this lesion causes ribosomal stalling, as it disrupts the N3 position that is directly involved in hydrogen bonding with guanosine.

Recently, N1-methyladenosine has been the focus of several studies due to its potential role as a regulatory modification on mRNA (13). Depending on the m^1A-seq technique used, N1-methyladenosine abundance has been found on human transcripts ranging from 20% of the transcriptome (14, 15) to only nine sites in mRNA (16). The adduct has been shown to be enriched around the start codon of transcripts, upstream of the 1st splice site. Over half of the identified m^1A adducts have been mapped to the coding region of transcripts (14, 15). A specific regulatory role of this modification has not been identified; on the contrary, studies generally support the hypothesis that m^1A exists primarily as a damage adduct. For example, one study using crude *E. coli* translation extracts showed that m^1A significantly increased ribosome stalling when it was present at any of the three positions in the codon (12). This effect on translation is anticipated, considering that m^1A is particularly disruptive to the hydrogen bonding interface, as it interferes with the ability of the N1 to hydrogen bond and introduces a resonance structure with a positive charge to the nucleotide (Figure 2A). Additionally, m^1A can lead to local duplex melting in RNA which could impede the codon-anticodon helix (17).

We hypothesize that an increase in the abundance of chemical damage that disrupts the hydrogen boding interface between mRNA and tRNA, such as alkylation, will result in increased ribosomal stalling *in vivo*. Eukaryotes have several mRNA-surveillance pathways to rescue stalled ribosomes from a variety of scenarios, including premature stop codons (nonsense-mediated decay) (18), transcripts lacking stop codons (non-stop decay) (19), and physical blocks (no-go

decay) (20). Bacteria, on the other hand, utilize at least one quality-control pathway, known as *trans*-translation, to rescue ribosomes stalled at the 3' end of a truncated transcript (21, 22). During this process, one molecule known as transfer-messenger RNA (tmRNA), which is encoded by the highly conserved ssrA gene, acts as both a tRNA and mRNA to rescue stalled ribosomes and ensure that the incomplete peptide is tagged for degradation (22). The tmRNA molecule, in complex with EF-Tu and another protein partner known as SmpB, recognizes the stalled ribosome and binds to the A site (23), at which point the nascent peptide is transferred to tmRNA (24). Translation is then switched from the 3' end of the defective mRNA to the portion of tmRNA that contains the ssrA-coding sequence (22, 25). This sequence codes for a tag that resembles the degradation signal utilized by bacterial proteases (26), and signals for the incomplete peptide to be degraded. The ssrA sequence also contains a stop codon which is recognized by release factors so the ribosome can complete the translation cycle and be recycled. Additionally, there is evidence to suggest that the tmRNA-SmpB complex recruits RNase R to degrade the damaged mRNA (27, 28).

In theory, the *trans*-translation pathway can rescue ribosomes stalled from a variety of obstacles, as truncated mRNAs are produced during several processes, including endonucleolytic cleavage, ribosome stalling, chemical insults, and premature transcriptional termination (1). However, *trans*-translation has not been specifically shown to rescue ribosomes stalled from chemically damaged transcripts. Here, we introduce alkylative damage to *E. coli* RNA and subsequently observe the activity of *trans*-translation. We first demonstrate that treating *E. coli* with common alkylating agents increases the levels of several disruptive alkylative adducts, including m^1A. As previous data was generated using crude extracts to demonstrate that m^1A resulted in ribosome stalling (12), we utilized our well-characterized reconstituted *in vitro*

translation system to obtain quantitative data with regards to the effect of m^1A on peptidyl-transfer (29). Additionally, when we treat *E. coli* with alkylating agents, we observe increased levels of tmRNA activity, suggesting that *trans*-translation is responsible for rescuing ribosomes from damaged transcripts in bacteria. Furthermore, when we treat *E. coli* lacking functional tmRNA with alkylating agents, they exhibit delayed recovery compared to wild-type (WT) cells, supporting the hypothesis that alkylative damage results in defects in translation.

RESULTS

Treatment of *E. coli* with MMS or MNNG causes significant increases in alkylative damage of RNA

In order to investigate the impact of alkylative damage on ribosomal rescue in bacteria, we first established a method to introduce alkylative damage to RNA in *E coli*. We chose to treat cells with either methyl methanesulfonate (MMS) or methylnitronitrosoguanidine (MNNG), two agents that work through different nucleophilic substitution mechanisms to alkylate nucleotides. MMS alkylates its target through an SN2-type mechanism, while MNNG reacts through an SN1-type one (4); therefore, we expected to observe differences in the types and levels of adduct that each agent generated. After treatment with the alkylating agents, RNA was extracted, digested with P1 nuclease into individual nucleotides, and subsequently treated with calf-intestinal phosphatase (CIP) to generate nucleosides which were analyzed by liquid chromatography – mass spectrometry (LC-MS). We generated standard curves for each of the unmodified nucleosides, as well as for N1-methyladenosine (m^1A), N6-methyladenosine (m^6A), N1-methylguanosine (m^1G), O6-methylguanosine (m^6G), and N3-methylcytidine (m^3C) in order to directly quantify the modified nucleosides within each condition (Supplemental Figure S1).

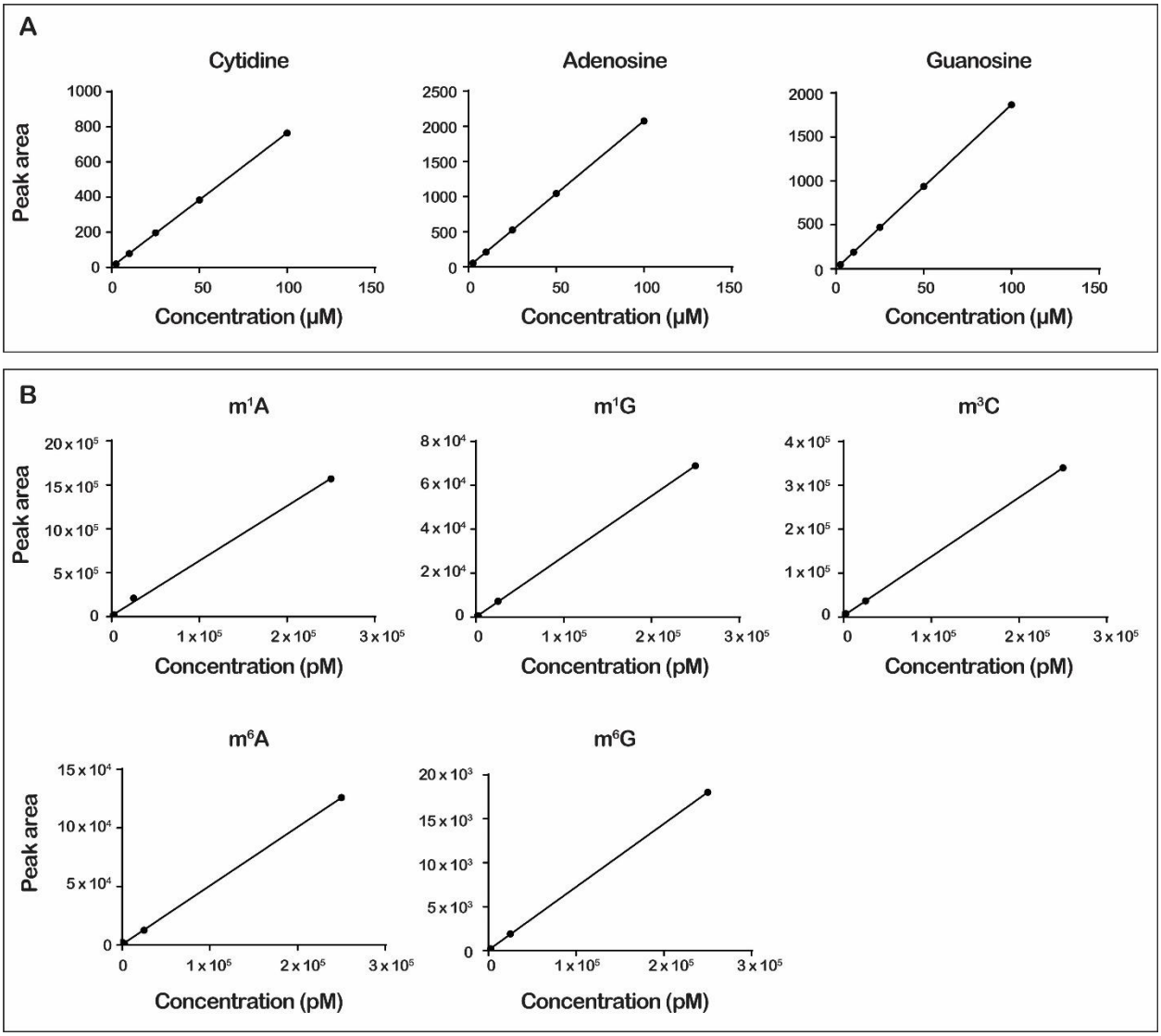

Supplementary Figure 2.S1: LC-MS calibration curves for modified and unmodified nucleosides

A) The integrated peak area for absorbance at 260 nm was recorded for known micromolar concentrations of unmodified nucleoside standards. Peak area versus concentration was plotted and fit to a linear equation, which was used to calculate sample concentrations. B) The integrated peak area for cps intensity was recorded for known picomolar concentrations of modified nucleoside standards. Peak area versus concentration was plotted and fit to a linear equation, which was used to calculate sample concentrations.

One previous study measured endogenous m^6A/A levels of 0.3% in *E. coli* (30). In agreement with these experiments, we observe approximately 0.6% m^6A/A in untreated RNA (Figure 1A). We did not measure an increase in m^6A levels after treatment with either alkylating

agent (Figure 1A). This result was expected, as neither MMS nor MNNG alkylate the N6 position of adenosine (4). Additionally, MMS and MNNG have been shown to cause low levels of m^1G accumulation in DNA (4); however, we do not measure significant increases in the levels of this modification (Figure 1B). This is likely because m^1G is an intentional modification of *E. coli* tRNA and rRNA (31), so when the cells are treated with MMS and MNNG we do not detect substantial accumulation of this adduct over background. Indeed, the base level of m^1G was at least 200-fold higher than m^1A (Figure 1).

Contrary to m^6A and m^1G levels, we measure 10 to 200-fold increases in m^3C and m^1A when we treat cells with MMS or MNNG (Figures 1C and 1D), and at least a 12-fold increase in m^6G in those treated with MNNG (Figure 1E). This is consistent with previous studies which show that the O6 position of guanosine is primarily targeted by MNNG but not MMS, and that m^3C and m^1A are minor alkylative adducts in double-stranded DNA (32) but are substantially more reactive as nucleophiles in the absence of hydrogen bonding (33). This same increase in reactivity for m^1G in single-stranded RNA is not observed because it is a secondary amine with an adjacent carbonyl group which is less reactive than m^1A and m^3C, both of which have the higher reactivity profiles of amidine groups (4).

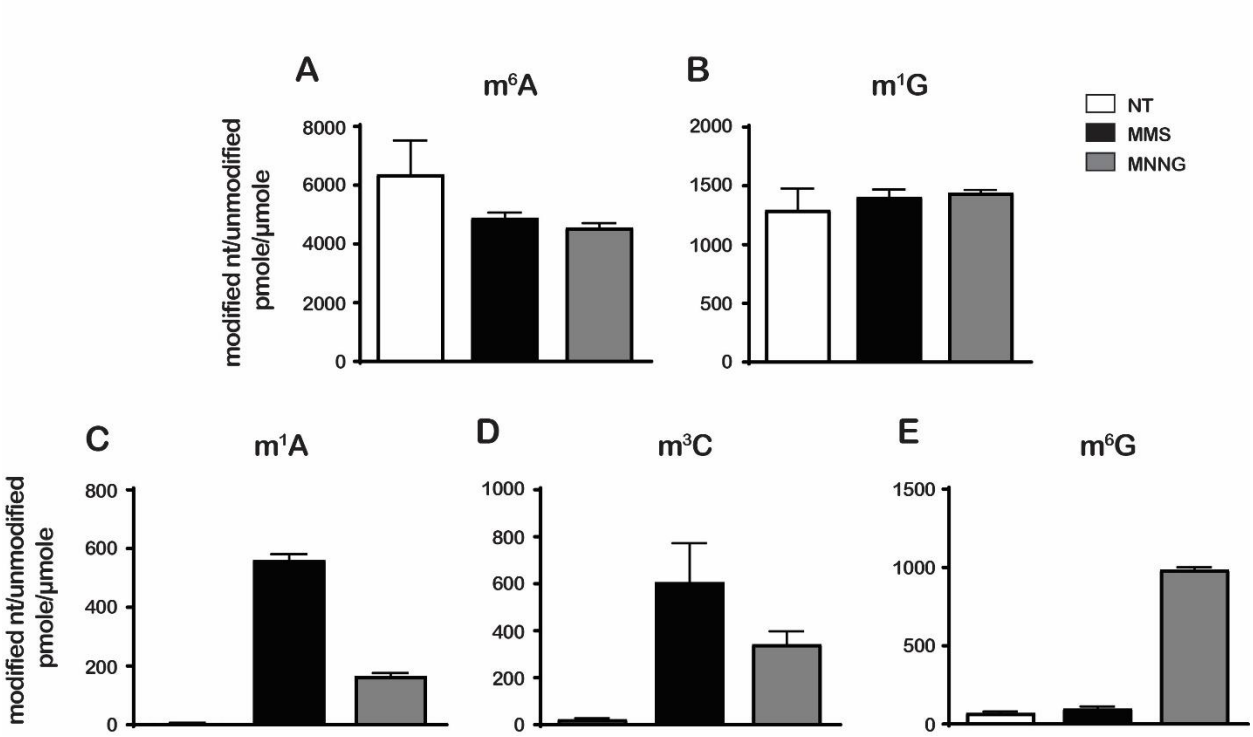

Figure 2.1: Treatment of *E. coli* with MMS and MNNG results in significant accumulation of detrimental alkylative damage adducts in RNA
A-E) Quantification of the integrated peak area of modified nucleosides in picomolar concentrations normalized to the integrated peak areas of absorbance at 260nm for their corresponding unmodified nucleosides in micromolar concentrations. Nucleosides were quantified from untreated cells (white), MMS-treated cells (black), and MNNG-treated cells (gray). The quantified nucleoside for each plot is indicted above.

N1-methyladenosine stalls ribosomes and behaves as a non-cognate codon *in vitro*

Having established a method of increasing the levels of alkylative adducts in *E. coli* mRNA, we next used our well-defined reconstituted bacterial translation system to quantify changes in peptidyl-transfer introduced by the presence of m^1A in mRNA (29). Using this system, incorporation efficiency of any single amino acid can be measured. We generated ribosomal initiation complexes carrying f-[^{35}S]-Met-$tRNA^{fMet}$ in the P site and displaying either an intact GAA codon, or an m^1A adduct at the second position ($G^{m1}AA$) in the A site (Figure 2B). The intact GAA codon is normally decoded by Glu-$tRNA^{Glu}$. Since m^1A inhibits the ability of the N3 on

adenosine to form hydrogen bonds as well as introduces a positive charge in the hydrogen bonding interface, normal Watson-Crick interactions would be disrupted, and we predicted that this would lead to a reduction in the rate of translation and potentially miscoding events (Figure 2A).

We reacted the intact and m^1A-containing initiation complexes with cognate Glu-$tRNA^{Glu}$ ternary complexes at multiple timepoints and visualized the dipeptide products using an electrophoretic thin-layer chromatography (TLC) system. The points were fitted to a first-order rate equation, and the rate of each reaction was calculated. We found that the presence of m^1A resulted in a 250-fold decrease in the rate of translation, as well as an almost 90% decrease in the endpoint (Figure 2C). These results demonstrate that m^1A is highly detrimental to the decoding process in the presence of cognate tRNAs and is likely disruptive enough to result in ribosomal stalling.

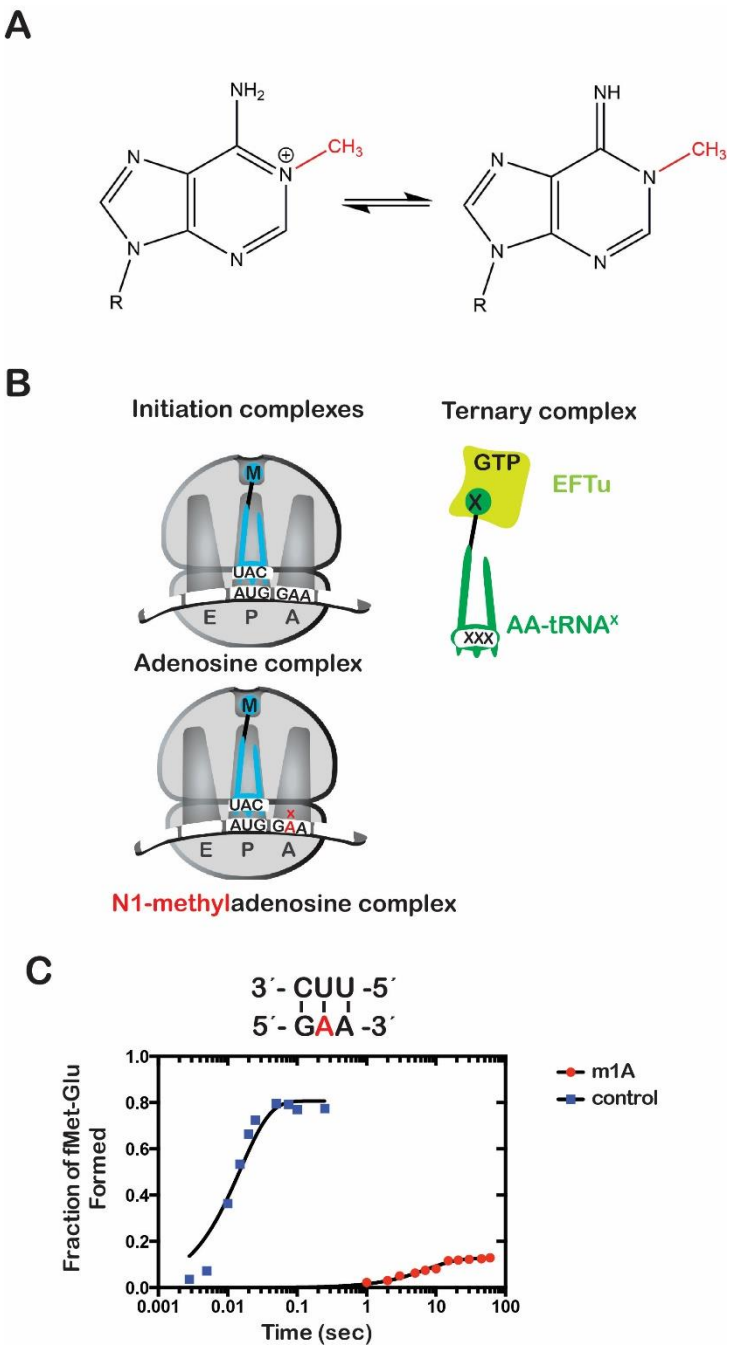

Figure 2.2: N(1)-methyladenosine (m^1A) in mRNA significantly decreases the rate and endpoint of translation *in vitro*

A) Chemical structure of m^1A. The N1-methyl group is highlighted in red, and the resonance structure of the molecule is represented. B) Schematic representation of adenosine and m^1A initiation complexes encoding for the dipeptide Met-Glu. Both complexes contain the initiator fMet-$tRNA^{fMet}$ in the P site; the A complex displays a GAA codon, while the m^1A complex displays a $G^{m1}AA$ codon in the A site. C) Represented time-courses of duplicate peptide-bond formation reactions between initiation complexes either containing (red) or lacking (blue) m^1A and Glu-$tRNA^{Glu}$ cognate ternary complexes.

Having established that m^1A disrupts the ability of the codon to form a cognate interaction, we next tested if the presence of m^1A causes the codon to behave as a near-cognate codon, which harbors a single mismatch. When a cognate tRNA pairs with a corresponding undamaged codon, a series of local conformational changes occur so that specific residues of the ribosome make contacts with the codon-anticodon complex. These local rearrangements lead to global changes, resulting in the shift of the ribosome from an open to a closed conformation, a process known as 'domain closure', thus allowing the complex to proceed through the remainder of tRNA selection (34). This process is altered by the addition of the aminoglycoside antibiotic paromomycin, which forces the ribosomal residues involved in the conformational changes into an intermediate position between the open and closed conformations. This reduces the energic barriers necessary for the ribosome to undergo domain closure in the presence of near-cognate amino acyl-tRNAs (aa-tRNAs), thus resulting in an increase in the rate of miscoding (35, 36). If m^1A causes the codon to behave like a near-cognate instead of a cognate codon in the presence of the cognate ternary complex, we expect that the addition of paromomycin to this reaction would increase the rate of peptide bond formation.

We reacted the m^1A -containing initiation complex described earlier with cognate Glu-$tRNA^{Glu}$ ternary complexes in the presence and absence of paromomycin. We observed no significant difference between these reactions, demonstrating that paromomycin does not rescue the effect of m^1A on peptide-bond formation (Figure 3). Since near-cognate interactions are rescued in the presence of antibiotics, this suggests that m^1A disrupts the ability of the codon to form base-pairing interactions with the cognate anticodon so drastically it acts as a non-cognate. From these results, we predict that m^1A is not only disrupting the ability of the A to form a

hydrogen bond, but also distorting the codon-anticodon helix significantly enough to disrupt the hydrogen bonds of its neighboring nucleotides.

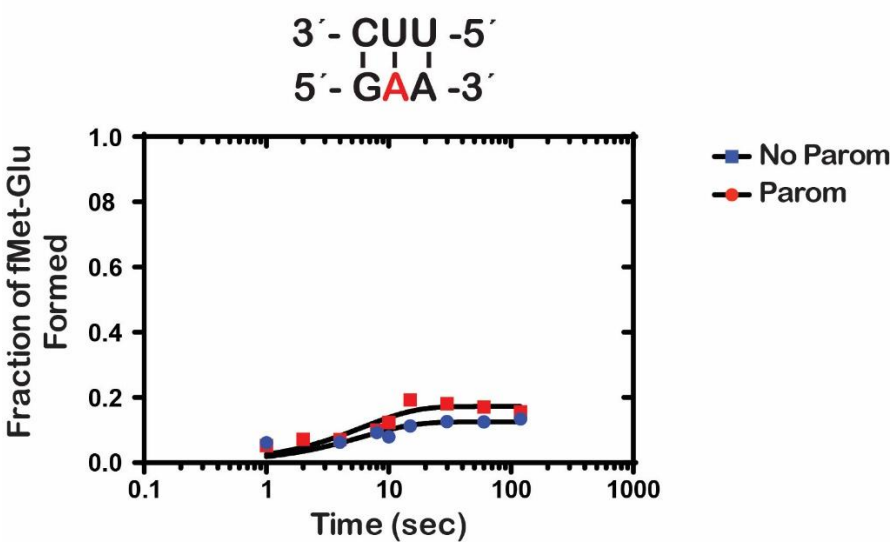

Figure 2.3: Paromomycin does not rescue the impact of m^1A on peptide bond formation Representative time-course of duplicate peptide-bond formation reactions between initiation complexes containing m^1A and Glu-$tRNA^{Glu}$ cognate ternary complexes. Reactions were performed either in the presence (red) or absence (blue) of the aminoglycoside antibiotic paromomycin.

To provide further evidence to support the observation that m^1A causes the codon to behave as a non-cognate, we investigated if m^1A altered miscoding in the presence of near- and non-cognate tRNAs. We performed a tRNA survey, in which we reacted the previously described m^1A-containing and lacking initiation complexes with all possible ternary complexes for two minutes, which is sufficient time to reach the endpoint of significant reactions (Figure 4). As anticipated for the codon containing the unmodified adenosine, we observed no significant dipeptide accumulation except for the reaction in the presence of the cognate ternary complex (Figure 4). For the codon containing m^1A, no significant dipeptide accumulation occurred in the presence of any aa-tRNA, supporting the hypothesis that m^1A causes the codon to behave as a non-cognate.

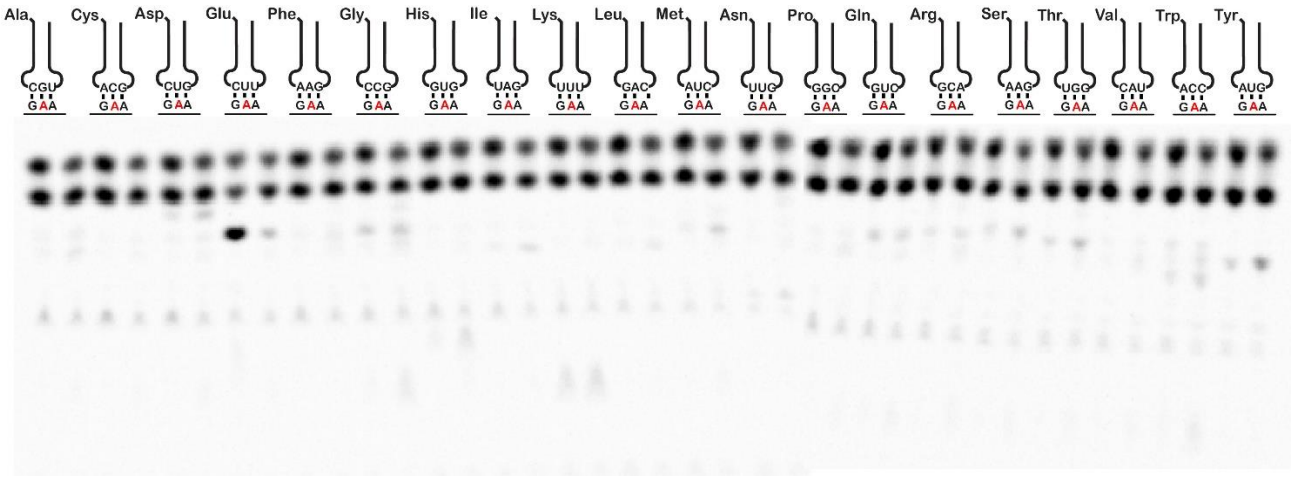

Figure 2.4: Specific miscoding events are not observed for a codon containing m^1A
Phosphorimager scan of electrophoretic TLCs used to follow dipeptide-formation reactions (two-minute incubation time). TCs are indicated above and within each set, the reaction on the left was performed using an IC displaying an unmodified GAA codon while the reaction on the right was performed using an IC displaying a modified G^{m1}AA codon.

N1-methyladenosine does not interfere with *trans*-translation *in vitro*

The results thus far show that m^1A is highly disruptive to peptidyl transfer *in vitro*. From this data, we hypothesized that alkylative damage to *E. coli* would cause ribosomal stalling *in vivo*. We predicted that the main ribosomal rescue system in bacteria, the *trans*-translation pathway, would be responsible for releasing stalled ribosomes from these damaged transcripts (21). However, if the presence of m^1A in the A site disrupts the interaction between the codon and the anticodon of the ternary complex, it is possible that it interferes with the ability of tmRNA or SmpB to bind the A site and begin *trans*-translation. In this case, the ribosome would be unable to be rescued by *trans*-translation from transcripts damaged by m^1A *in vivo*.

To test if m^1A in the A site interferes with the binding of tmRNA or SmpB, we performed *in vitro* peptidyl transfer reactions in the presence of either a codon containing m^1A or a codon with an unmodified A, and an *in vitro* reconstituted quaternary complex containing SmpB, tmRNA, EF-Tu, and GTP. Similar to tmRNA *in vivo*, the tmRNA used in this experiment

was amino-acylated with alanine (37). We utilized the same mRNA constructs that were used in the *in vitro* peptidyl transfer assays, as we had shown that the transcript containing m^1A significantly interfered with peptidyl transfer. These transcripts are not ideal substrates for *trans*-translation, as they contain twelve nucleotides downstream of the P site instead of seven, which has previously been shown to be the maximum number of downstream nucleotides for sufficient activation of *trans*-translation (38, 39). Even using sub-optimal substrates, we observe similar rates and endpoints of peptidyl transfer for codons containing either A or m^1A (Figures 5A and 5B). This data suggests that m^1A does not significantly interfere with the binding of SmpB or tmRNA to the A site; therefore, the possibility remains that m^1A leads to ribosomal stalling *in vivo* that is subsequently rescued by *trans*-translation.

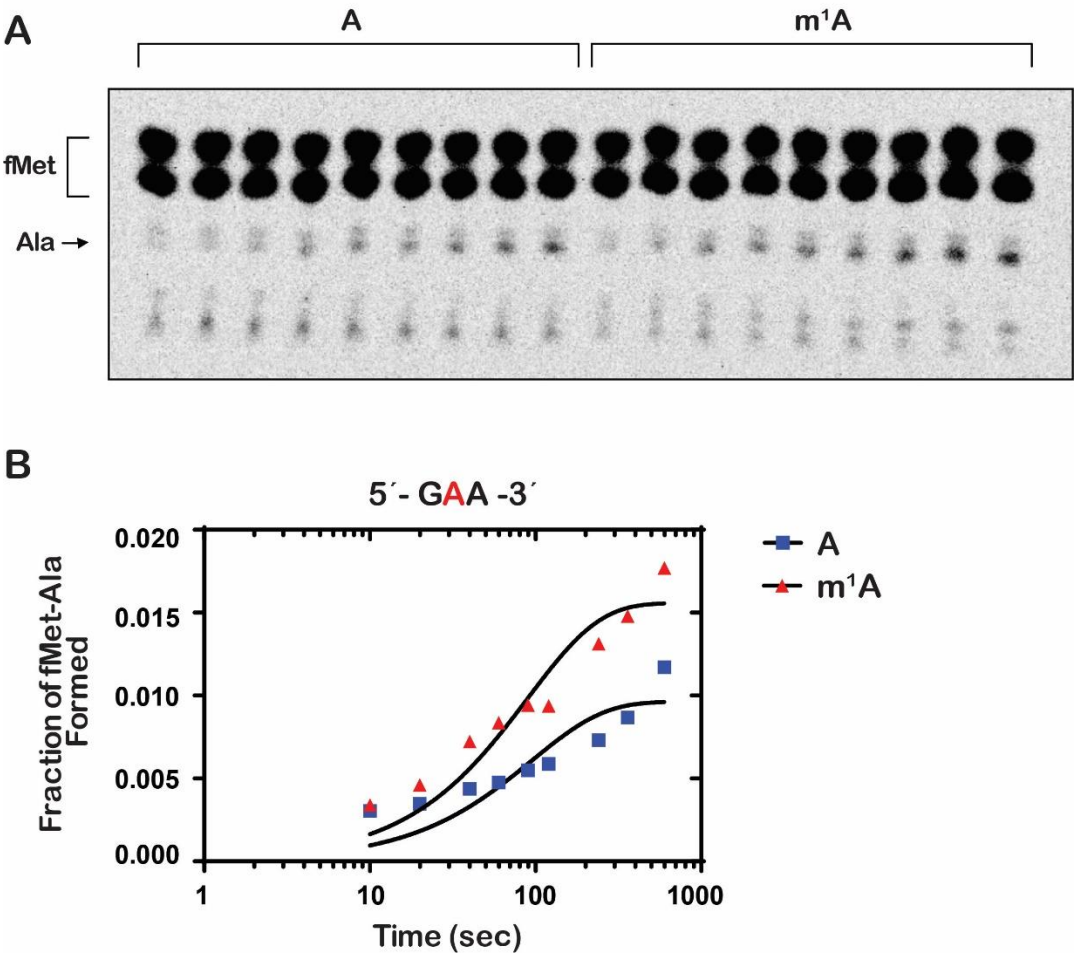

Figure 2.5: m^1A does not significantly interfere with the recognition of initiation complexes by *trans*-translation *in vitro*
A) Phosphorimager scan of an electrophoretic TLC used to follow dipeptide-formation reactions. The timecourse on the left was performed using ICs displaying an unmodified GAA codon and *trans*-translation quaternary complexes. The timecourse on the right was performed using ICs displaying a modified $G^{m1}AA$ codon and *trans*-translation quaternary complexes. B) Quantification of the timecourses performed in A.

Alkylative damage of RNA increases tmRNA activity *in vivo*

Having established a method to introduce alkylative damage adducts to *E. coli* RNA through treatment with MMS or MNNG, we took advantage of a previously generated tmRNA construct which contains an altered native degradation peptide tag sequence; specifically, the six C-terminal residues are substituted for an HHHHHH (His_6) tag (tmRNA-H_6), in order to assess the activity of tmRNA (40). Using this system, if ribosomes stall *in vivo* and tmRNA is activated, His_6 tagging of incomplete peptides will increase.

We treated *E. coli* expressing tmRNA-H_6 with either 0.1% MMS or 5 μg/mL MNNG and performed a western blot to analyze the resulting total protein. As predicted, we observed approximately 2 to 3-fold increases in His_6-tagging levels (Figures 6A and 6B). To show that the treatments were causing significant alkylative damage, we also probed for the activation of Ada, which is an enzyme that is involved in the adaptive response (41). Ada is normally present at very low levels in the cell, and it induces its own expression as well as the expression of other proteins involved in the adaptive response upon alkylative damage (42, 43). Indeed, we observe significant increases in Ada activation when we treat with MMS or MNNG, and along with the LC-MS data, demonstrates that we are introducing significant alkylative damage.

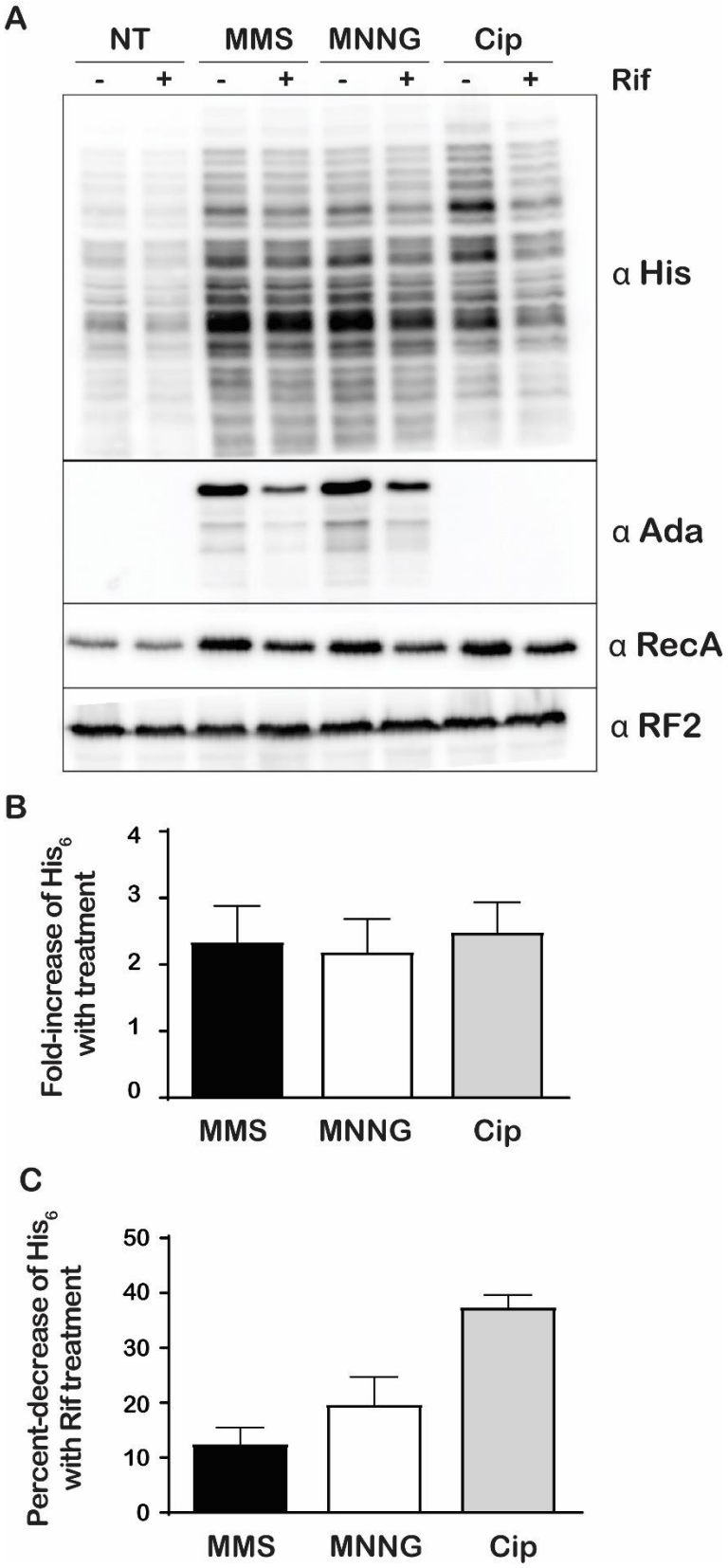
A
NT
MMS
MNNG
Cip
- + - + - + - +
Rif
α His
α Ada
α RecA
α RF2
B
Fold-increase of His6 with treatment
4
3
2
1
0
MMS
MNNG
Cip
C
Percent-decrease of His6 with Rif treatment
50
40
30
20
10
0
MMS
MNNG
Cip

Figure 2.6: Alkylative damage of RNA in *E. coli* induces ribosome rescue through the *trans*-translation pathway
A) Western blot displaying total protein collected from *E. coli* expressing tmRNA-His_6. Cells were either untreated or treated with MMS, MNNG, or ciprofloxacin. Additionally, cells either received (+) or did not receive (-) a pre-treatment with rifampicin before treatment with the indicated damaging agent. Blots were probed with α His, α Ada, α RecA, and α RF2. B) Quantification of the increase in His_6 levels for each no rifampicin pre-treatment condition. His_6 samples were first normalized to their corresponding RF2 loading control, and then fold-increases in His_6 levels were calculated by dividing the treated samples by the untreated samples. Quantification was performed in triplicate ± SD. C) Quantification of the fold-decrease of His_6 levels upon pre-treatment with rifampicin. His_6 samples were first normalized to their corresponding RF2 loading control. Fold-decreases in His_6 levels were calculated by dividing the rif pre-treatment condition for each sample with its corresponding no-rif pre-treatment condition and subtracting this value from 1. Quantification was performed in triplicate ± SD.

In order to show that the increase in tmRNA activity was due to alkylative damage rather than other potential effects from cell death, we treated *E. coli* with 0.1% MMS and performed a spot assay with the treated cells and do not observe significant death at this concentration (Supplemental Figure S2A and S2B). Additionally, a previous report has shown that when the ClpAP, ClpXP, and Lon proteases are inactive, the levels of his-tagging by the tmRNA system increase, as the incomplete peptide products are able to further accumulate (40). When *E. coli* with null alleles of *clpP*, *clpX*, and *lon* genes are treated with the alkylating agents, we observe even more extensive his-tagging as the incomplete peptides generated from alkylative damage accumulate (Supplemental Figure S3).

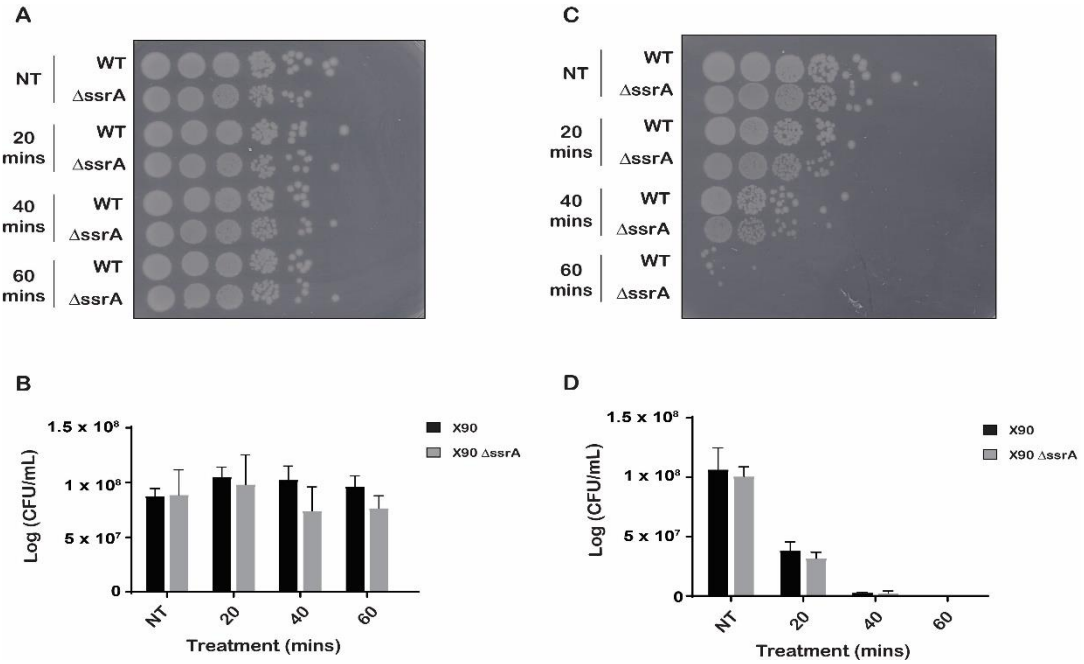

Supplementary Figure 2.S2: WT and Δ*ssrA E. coli* exhibit similar survival phenotypes after treatment with MMS

A) Spot assay of WT and Δ*ssrA* cells either after no treatment or treatment with 0.1% MMS for the indicated amount of time. B) Quantification of colony forming units in (A) performed in at least duplicates. C) Spot assay of WT and Δ*ssrA* cells either after no treatment or treatment with 0.5% MMS for the indicated amount of time. D) Quantification of colony forming units in (C) performed in at least duplicates.

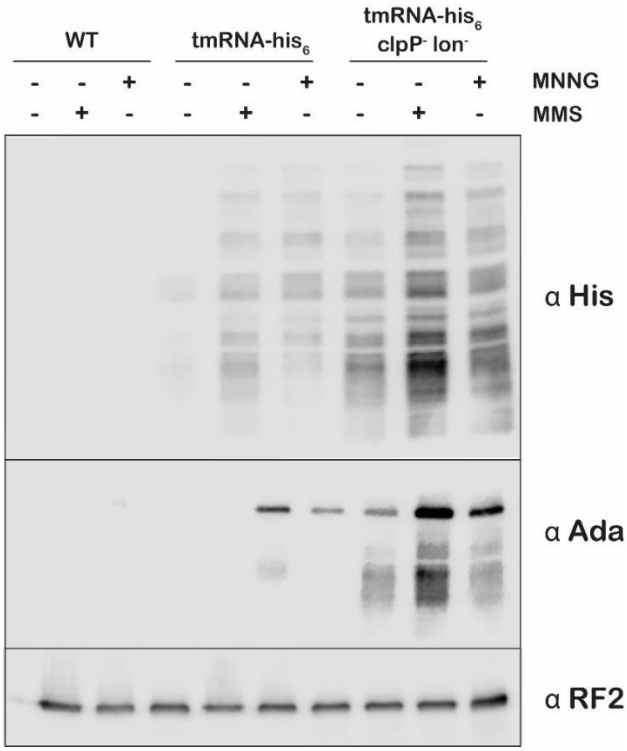

Supplementary Figure 2.S3: Deletion of ClpAP, ClpXP, and Lon proteases results in further accumulation of His_6 after alkylative damage
Western blot displaying total protein collected from either WT *E. coli,* strains expressing tmRNA-His_6, or strains expressing tmRNA-His_6 with null alleles of clpP, clpX, and lon genes. Cells were either untreated or treated with MMS or MNNG. The blot was probed with α His, α Ada, and α RF2.

As has been noted in a previous study, the his-tagging patterns between each of the samples appear almost identical (40). This was a surprising observation, as we expected the alkylative damage to be randomly located throughout the transcriptome, thereby causing a more uniform streak of his-tagging or banding patterns that varied from sample to sample. In order to investigate if this consistent banding pattern was an artifact of the His antibody we were using, we probed a western blot with His antibodies from three different manufacturers. Each antibody had a distinct His-tagging pattern (Supplemental Figure S4). This data suggests that the consistent His-tagging pattern is likely more due to an artifact of the His antibodies than a particular pattern of proteins that are preferentially His-tagged.

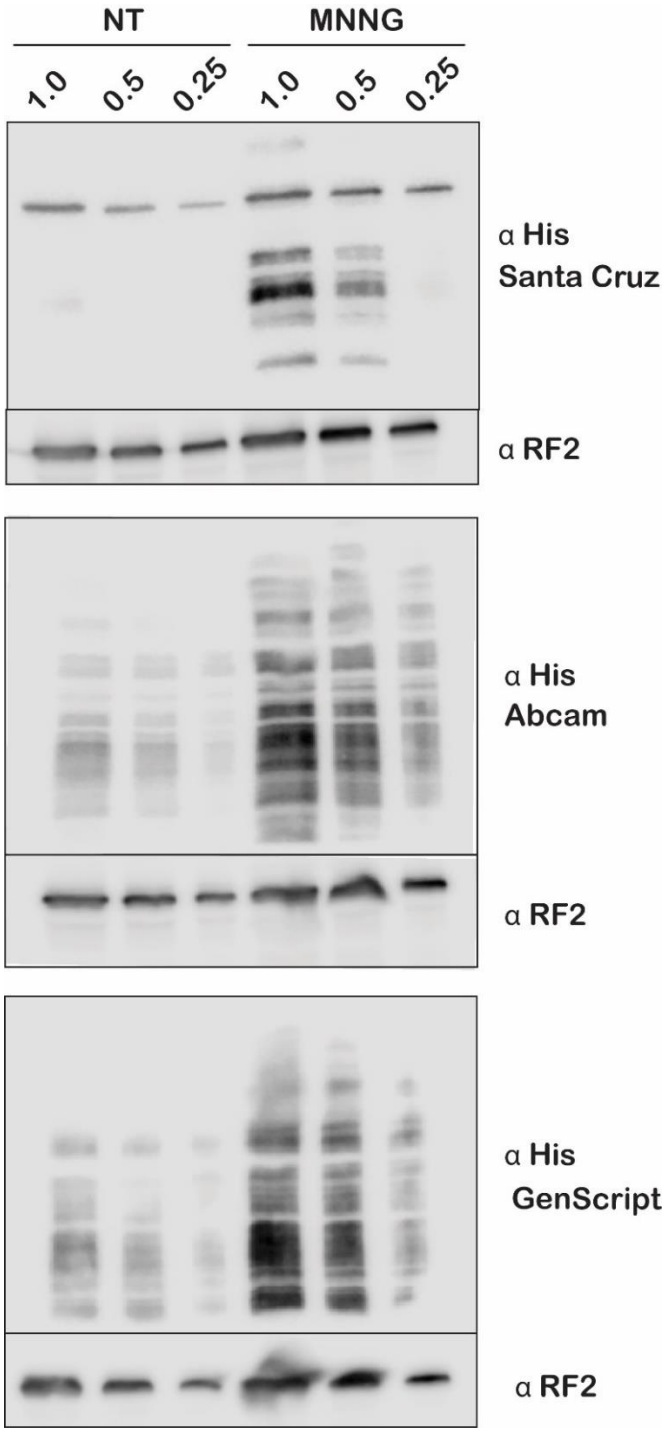

Supplementary Figure 2.S4: Different His antibodies display unique banding patterns on western blots

Western blots displaying total protein collected from *E. coli* expressing tmRNA-His_6. Cells were either untreated or treated with MNNG. Each treatment set contains a dilution series (1.0, 0.5, and 0.25) of total protein. Western blots were probed with three His antibodies from different manufacturers, including Santa Cruz Biotechnology, Abcam, or GenScript. α RF2 was used as a loading control.

The accumulation of His-tagged peptide products suggests that alkylative damage of RNA is stalling ribosomes *in vivo* and activating tmRNA. However, the alkylative damage from MMS and MNNG damages DNA as well as RNA (4). This is supported by the increase in RecA, which is a protein that is essential for the maintenance and repair of DNA (44), that we observe increasing via western blot when we treat with these alkylating agents (Figure 6A). Therefore, it was also possible that the resulting increase in His-tagging was primarily due to the production of truncated transcripts from damaged DNA. These truncated transcripts lack a stop codon; therefore, ribosomes will stall at the 3' end of the transcript with an empty A site and this has been previously shown to activate the response of tmRNA (22). To ensure that the observed His -tagging was due to RNA damage rather than truncated RNA produced from damaged DNA, we pre-treated the cells with a rifampicin (Rif) approximately forty seconds before treating with damaging agents. Rif is an inhibitor of RNA polymerase initiation; therefore, the pretreatment with rif halts transcriptional initiation and allows us to separate the effects of DNA damage from RNA damage (45). In addition to MMS and MNNG, we also treated the cells with ciprofloxacin (cip) and mitomycin C (MMC). Cip is an antibiotic that inhibits the ligation activity of DNA gyrase and topoisomerase IV but not the cleavage activity, thereby causing the topoisomerases to create double stranded breaks in DNA (46). MMC causes intra- and inter-strand DNA crosslinks that can block the activities of DNA polymerase and RNA polymerase (47). We predict that these two agents, which specifically cause DNA damage, will produce truncated transcripts and cause His-tagging by tmRNA. We also expect to observe a decrease in His-tagging generated by DNA damaging agents, but not for the alkylating agents, after pre-treatment with rif if the tmRNA activity is due primarily to alkylative damage of RNA rather than truncated transcripts.

When we pre-treat *E. coli* expressing tmRNA-H_6 with rif and then with MMS, we observe a slight (10%) decrease in His-tagging levels compared to the no pre-treatment condition, suggesting that the His-tagging in this condition is primarily due to RNA damage (Figure 6C). When we treat the cells with MNNG, we do observe a slightly higher decrease (20%) in the amount of His-tagging for the rif pre-treatment condition compared to no pre-treatment (Figure 6C). This suggests that a portion of the His-tagging is due to truncated transcripts produced from DNA damage; however, the levels of His-tagging in the rif pre-treatment condition are still significantly higher than the samples with no alkylative damage. When we treat cells with cip, we observe significant His-tagging in the no rif pre-treatment condition, approximately the same fold-increase as MNNG and MMS (Figure 6B). This observation supports our initial hypothesis that DNA damage generates truncated transcripts that cause ribosomal stalling and activate tmRNA. However, when we pre-treat the cells with rif and then with cip, we observe a 40% decrease in His-tagging (Figure 6C). When we treated cells with MMC, we did observe increases in RecA activation but no significant increases in levels of His-tagging, demonstrating that the DNA crosslinking damage induced by MMC does not activate the tmRNA system (Supplemental Figure S4). While little is known about how RNA polymerase stalling is resolved from double-stranded breaks, from this data we predict that double-stranded breaks produce more truncated mRNA transcripts than crosslinking. Overall, we conclude that while truncated transcripts produced from damaged DNA do activate tmRNA, the predominate source of tmRNA activation in MMS- and MNNG- treated samples is the alkylative damage of RNA.

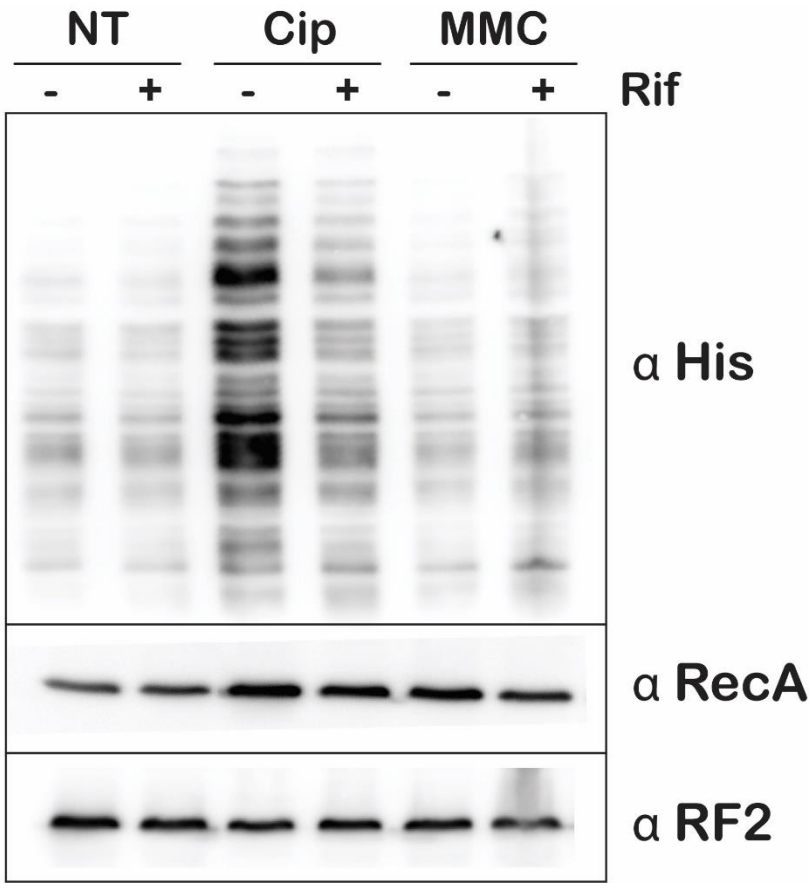

Supplementary Figure 2.S5: Ciprofloxacin, but not mitomycin C, increases His_6 levels
Western blot displaying total protein collected from *E. coli* expressing tmRNA-His_6. Cells were either untreated or treated with ciprofloxacin (cip) or mitomycin C (MMC). Additionally, cells either received (+) or did not receive (-) a pre-treatment with rifampicin before treatment with the indicated damaging agent. The blot was probed with α His, α RecA, and α RF2.

The ability to rescue stalled ribosomes is important for cellular recovery after alkylative damage

Even though the ssrA gene that encodes tmRNA is highly conserved in bacteria, previous studies have shown that Δ*ssrA E. coli* show no appreciable growth phenotype under standard laboratory conditions but do exhibit delayed growth under certain stress conditions (37, 48). Since we observed that tmRNA is utilized to rescue ribosomes stalled due to damaged RNA, we hypothesized that the ability for cells to rescue stalled ribosomes is important for cellular recovery upon treatment with alkylating agents. To test this, we treated Δ*ssrA* and WT cells with

either 0.5% MMS or 20 μg/mL MNNG, washed the cells to remove the alkylating agent, and allowed them to recover while monitoring growth. If *trans*-translation is responsible for rescuing ribosomes stalled by alkylative damage, we expect to observe a lag in the recovery time for Δ*ssrA* cells compared to WT after treatment with alkylating agents.

As expected, in the absence of any pretreatment, Δ*ssrA* and WT cells recover at approximately the same rate. However, after treatment with MMS or MNNG, Δ*ssrA* cells have an approximately 1.5-hour lag in their recovery compared to WT cells (Figure 7). This data demonstrates that cells lacking tmRNA are more sensitive to alkylative damage. To rule out cellular death as a cause for the observed lag, we treated both Δ*ssrA* and WT cells with 0.5% MMS for 20, 40, and 60 minutes, washed the cells to remove the alkylating agents, and performed spot assays to quantify cell death. We observe similar rates of cell death for Δ*ssrA* and WT cells, suggesting that the previously observed lag in recovery time is not due to a difference in the number of cells killed, but rather the ability of the cells to quickly recover after treatment with alkylating agents (Supplementary Figure S2C and S2D). This data suggests that the ability for cells to efficiently recover post-alkylative damage depends on their ability to rescue stalled ribosomes from damage RNA using tmRNA.

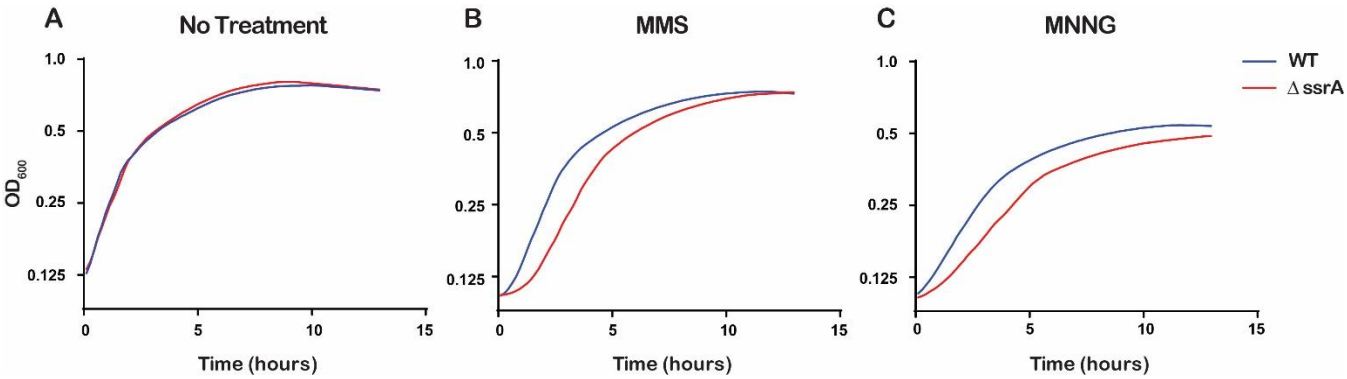

Figure 2.7: Ribosome rescue by tmRNA is important for cellular recovery after treatment with alkylating agents

Average of three replicate growth assays plotting the recovery of *E. coli* post-alkylative damage. WT (blue) and Δ*ssrA* (red) cells either received no treatment or treatment with MMS or MNNG. The alkylating agents were washed from the samples and the OD_{600} of the cells was recorded during the recovery period.

DISCUSSION

Several recent reports have shown that mRNA can be intentionally modified to control its function (49). For example, m^6A is a reversible modification of mRNA that appears to play a role in the regulation of gene expression (50). Additionally, mRNA containing pseudouridine (Ψ) has been shown to produce significantly higher levels of functional protein than its unmodified counterpart (51). Although much has been revealed about the role that intentional modifications serve in regulating various aspects of mRNA metabolism, most chemical modifications of mRNA are disruptive damage adducts (10). Previous work had shown that several alkylative damage adducts, including m^1A and m^6G, drastically slow translation and cause increases in miscoding events *in vitro* (11, 12). However, little was known about how alkylative damage of mRNA elicits cellular responses *in vivo.* Additionally, the quantitative effects of m^1A on the speed and accuracy of translation remained unknown. Here, we introduce alkylative damage to bacterial RNA and monitored cellular responses to translation. A priori, we hypothesized that the main ribosome rescue system in bacteria, the *trans*-translation pathway, works to release stalled ribosomes from transcripts containing alkylative damage. Indeed, we find that upon treatment of *E. coli* with alkylating agents, *trans*-translation activity significantly increased (Figure 5). Furthermore, we show that when cells lack functional *trans*-translation, they do not recover as efficiently after treatment with alkylating agents (Figure 6).

In order to assess the cellular response of bacteria to alkylative damage, we first established a method to reliably introduce alkylative damage adducts to *E. coli in vivo*. We chose two common alkylating agents, MMS and MNNG, which work through an SN2- and SN1-type nucleophilic substitution mechanism, respectively (4). We measured the levels of several modifications via LC-MS with and without treatment, and each of the observed changes is

supported by existing literature (4). As a negative control, we chose to measure changes in m^6A levels, as exocyclic amino groups of guanine, cytosine, and adenine are known to be poor nucleophiles in methylation reactions. Indeed, we do not observe significant changes in m^6A levels upon treatment with the agents (Figure 1A). We do observe increases in levels of m^1A and m^3C which are known targets of MMS and MNNG in single-stranded DNA and RNA (Figures 1C and 1D) (4, 32). Additionally, we observe increases in m^6G levels only in MNNG-treated samples (Figure 1E). This is consistent with studies showing that MNNG produces a greater percentage of O-methyl adducts (4).

Our group had previously utilized an *in vitro* reconstituted bacterial translation system to investigate the impact of m^6G on decoding (11); however, we had not analyzed the effects of m^1A. We hypothesized that the positively charged resonance structure of m^1A would not only disrupt its ability to base pair but would also distort the codon-anticodon helix significantly enough to disrupt the ability of its neighboring nucleotides to base pair. Structural studies of the A site show that the first and second position of the codon-anticodon helix are strictly monitored by rRNA residues as well as ribosomal proteins to ensure that only Watson-Crick base pairs are recognized as acceptable interactions (34, 52, 53). We chose to analyze m^1A in the second position of the codon rather than the first because if our hypothesis held true, first position m^1A may interfere with the ability of the nucleotide immediately 5' of the transcript to base pair. In this experimental setup, the upstream codon is the start codon, so in theory this could reduce the efficiency of translation initiation, which was not the focus of this study.

The rate and endpoint of peptide-bond formation in the presence of m^1A was substantially less than those measured for the unmodified control (Figure 2C). This is supported by a previous study showing that m^1A in mRNA increases ribosome stalling in crude extracts

(Figure 2C) (12). Furthermore, the addition of paromomycin to this reaction does not suppress the effect of m^1A on peptide-bond formation (Figure 3) and the tRNA survey between the m^1A-containin codon and all potential near- and non-cognate aa-tRNAs shows no substantial reactivity (Figure 4), suggesting that the adduct causes the codon to behave like a non-cognate. Overall, the disruptive nature of m^1A in the coding region does not support the idea that it is an intentional modification that promotes translation (14), but rather that it is a highly detrimental adduct of mRNA.

Having confirmed that m^1A is a disruptive adduct of mRNA *in vitro*, we then sought to investigate the cellular response to alkylative damage *in vivo*. We first demonstrated *in vitro* that m^1A does not significantly interfere with the recognition of the IC by the *trans*-translation quaternary complex (Figure 5), suggesting that translating ribosomes stalled by alkylative lesions such as m^1A can be targeted by *trans*-translation. Using a tmRNA modified to His-tag incomplete peptides from stalled translation complexes (40), we observe increased *trans*-translation activity upon cellular treatment with alkylating agents (Figure 6A). This suggests that alkylative damage of RNA causes ribosomal stalling that is severe enough to elicit responses from ribosome rescue pathways. Because bacterial mRNAs do not contain poly-A tails like eukaryotic transcripts, it is difficult to purify bacterial mRNA from rRNA and tRNA; therefore, we cannot be certain that the observed effects on translation are due to mRNA damage exclusively. However, there exist several compelling reasons to support the hypothesis that the tmRNA response is primarily due to mRNA damage. For one, the complex folding of rRNA as well as its association with ribosomal proteins is thought to make it a poor target for alkylative damage (10). Specifically, the rRNA residues responsible for monitoring the base pairing in the decoding center are not exposed to the cytoplasm in translating ribosomes; therefore, it is

unlikely that they are damaged by the agents (54). Additionally, tRNA are susceptible to alkylative damage, but only 3 out of an average of 76 nucleotides directly participate in base pairing with the codon. This reduces the probability that damaged nucleotides in tRNA cause the observed ribosomal stalling. The secondary structure of tRNA does not protect it from damage, as it has been shown that tRNA accumulate damage to the same extent when they are folded as when they are denatured (55). However, the CCA enzyme in *E. coli*, which attaches the conserved CCA sequence at the 3' end of all mature tRNAs, has been shown to have an innate ability to discriminate against tRNA backbone damage (56). Because the CCA sequence serves as the site of amino acid attachment for tRNAs, this suggests that damaged tRNAs would not be aminoacylated, thereby also reducing the probability that damaged tRNAs are utilized during translation.

We also confirm that the majority of tmRNA activity is due to RNA damage rather than truncated transcripts produced by damaged DNA. One intriguing observation from these experiments is that ciprofloxacin, but not MMC, increases tmRNA activity in the no-rifampicin pre-treatment condition (Supplementary Figure S5). These DNA damaging agents work through independent mechanisms – ciprofloxacin produces double-strand breaks (46) while MMC generates crosslinks (47). When RNA polymerase encounters a DNA crosslink, it can change conformation and backtrack on the DNA which extrudes the 3' end of the mRNA (57, 58). These backtracked polymerases are arrested, and their active sites no longer align with the 3' hydroxyl end of the mRNA (58). They then can become targets for several pathways which work to restore transcription and repair the DNA (59, 60). The RNA and stalled RNA polymerase are only released after multiple attempts at restoring transcription (61). This repair of DNA and restoration of transcription in the presence of crosslinks could explain why we do not observe

significant tmRNA activity, as the production of a truncated transcript from this scenario could be rare. Contrary to stalling on a crosslink, little is known about the fate of bacterial RNA polymerase when it encounters a double-stranded break. Based on our observation that ciprofloxacin significantly increases tmRNA activity, we hypothesize that double-stranded breaks are more likely to result in the production of truncated transcripts than DNA crosslinks.

Several studies have shown that bacteria lacking a functional *trans*-translation pathway do not recover as efficiency after cellular stress, including nutrient and oxidative stress (37, 48). We observe that alkylative stress also causes a delayed recovery period in cells lacking tmRNA, likely because they are unable to efficiency rescue stalled ribosomes and resume growth (Figure 7). The Δ*ssrA* cells are likely still able to eventually resume growth after alkylative damage because of the existence of several alternative ribosome-rescue factors. One factor, known as alternative ribosome-rescue factor A (ArfA) works by recruiting RF2 to hydrolyze the peptidyl-tRNA and release the ribosome (62, 63). This factor acts as a backup for *trans*-translation, as its expression increases when tmRNA activity is limited (64, 65). Additionally, it is not as ideal of a system as *trans*-translation, as it does not tag the incomplete peptide for degradation. Another factor that can release stalled ribosomes is ArfB, although it does not appear to function solely as a backup for tmRNA and its physiological function remains to be elucidated (66, 67). Regardless, these alternative ribosome rescue factors in *E. coli* are likely responsible for the eventual recovery we observe.

Our hypothesis that alkylative damage is detrimental enough to decoding to cause ribosomal stalling and rescue *in vivo* is also supported by the observation that bacteria contain at least one protein that can repair alkylative lesions of mRNA. For example, AlkB is an alpha-ketoglutarate-dependent hydroxylase in *E. coli* that has been shown to repair alkylative lesions of

single-stranded DNA and RNA, including m^1A, m^3C, and m^1G (68). We also predict that the targeting of stalled ribosomes by *trans*-translation results in the degradation of alkylated transcripts, as previous studies have suggested that tmRNA recruits RNaseR to degrade non-stop mRNA (27). Although the accumulation of alkylative damage under physiological conditions or disease states has not been the focus of many studies, our work supports the idea that it is important for cellular viability to rescue and prevent ribosomes from stalling on alkylated transcripts and that *trans*-translation is the main pathway through which bacteria alleviate this disruption to decoding.

EXPERIMENTAL PROCEDURES

Strains

Strains were either derivatives of *E. coli* MG1655 (F- lambda- ilvG- rfb-50 rph-1) or X90 (*ara*Δ(*lac-pro*) *nalA argE*(Am) *rif thi-1/*F*' lacI*^{q} *lac*$^{+}$ *pro*$^{+}$) (69). We received the following strains from the lab of Dr. Sean Moore: SM694 (X90, *ssrA::his*$_{6}$ *- kan*), SM876 (X90, *ssrA::his*$_{6}$ *- kan, clpPX-lon::cam*), and SM20 (X90, Δ*ssrA, cam*) (40). We received the SKEC4 (MG1655, Δ*ssrA,* Δ*smpB, kan*) strain from Dr. Allen Buskirk. P1 transduction was used to introduce kan^{R} - linked tmRNA-H_6 into MG1655.

Western Analysis

To prepare total protein for Western blot analysis, *E. coli* were precipitated, washed with LB, and resuspended in 2xSDS loading dye. The resuspension volume was adjusted to normalize for OD_{600} of the culture at the time of collection. Total protein was separated by SDS-PAGE and transferred to PVDF membrane in 1x Transfer buffer (25 mM Tris, 192 mM glycine, 20% Methanol) in a wet apparatus. After transfer, the membrane was shaken for one hour in PBST (3.2 mM Na2HPO4, 0.5 mM KH2PO4, 1.3 mM KCl, 135 mM NaCl, 0.05% Tween 20, pH 7.4.) with 5% w/v powdered milk. The membrane was then washed with PBST and incubated with primary antibody overnight at 4°C. The following dilutions of primary antibodies were used: 1:2500 anti-His (Abcam unless otherwise specified), 1:500 anti-Ada (Santa Cruz Biotechnologies), 1:10,000 anti-RecA (Abcam), and 1:1,000 anti-RF2 (purified as described in Zaher and Green Cell paper). The blot was then washed three times for 5 minutes, and then incubated with the corresponding HRP-conjugated secondary antibody (1:10,000) in PBST for one hour. After washing three times for 5 minutes, the membrane was treated with an HRP-

reactive chemiluminescent reagent (Pierce ELC Western Blotting Substrate). Quantity One software was utilized to quantify Western blots.

Treatment of *E. coli* with Damaging Agents

For all Western blot analyses, *E. coli* were treated with the following concentrations of damaging agents: 0.1% MMS (Sigma-Aldrich), 5 μg/mL MNNG (TCI Products), 50 μg/mL ciprofloxacin (Sigma-Aldrich), or 6 μg/mL MMC (Sigma-Aldrich). To determine the treatment time that generated significant tmRNA activity and Ada activation, MG1655 cells containing tmRNA-His_6 were grown from OD 0.05 to mid-log phase (OD 0.3-0.4) and treated with MMS for several timepoints. The resulting total protein was analyzed via western blot (Supplemental Figure S6). We observed significant tmRNA activity and Ada activation after a 20-minute treatment, which is the treatment time we utilized for the remaining samples analyzed via Western blot.

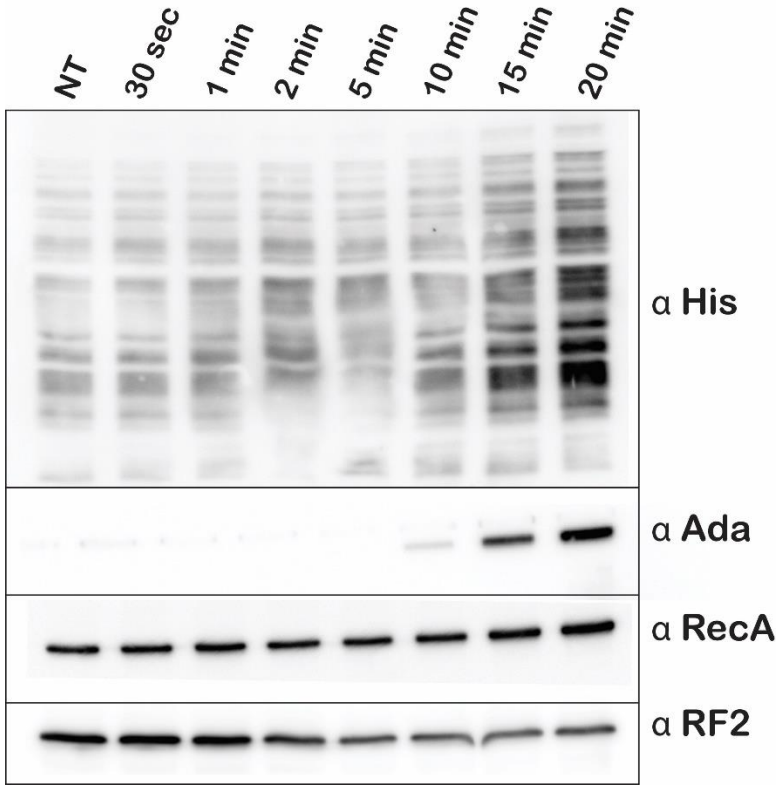

Supplementary Figure 2.S6: Optimal His_6, Ada, and RecA levels are achieved after 20 minutes of MMS treatment
Western blot displaying total protein collected from *E. coli* expressing tmRNA-His_6. Cells were either untreated or treated with MMS for various lengths of time. The blot was probed with α His, α Ada, α RecA, and α RF2.

To determine the optimal length of time for rifampicin pre-treatments, we treated MG1655 cells containing tmRNA-His_6 with 6 ug/mL rifampicin for several timepoints followed by 20 min treatments with either MMS or ciprofloxacin. The resulting protein was analyzed via western blot (Supplemental Figure S7). We observed significant decreases in Ada activation in the MMS-treated samples and significant decreases in tmRNA activity and RecA activation in the ciprofloxacin-treated samples after 10 seconds of rifampicin pre-treatment. We utilized a 10 to 45-second rifampicin pre-treatment time for the remaining samples analyzed via western blot.

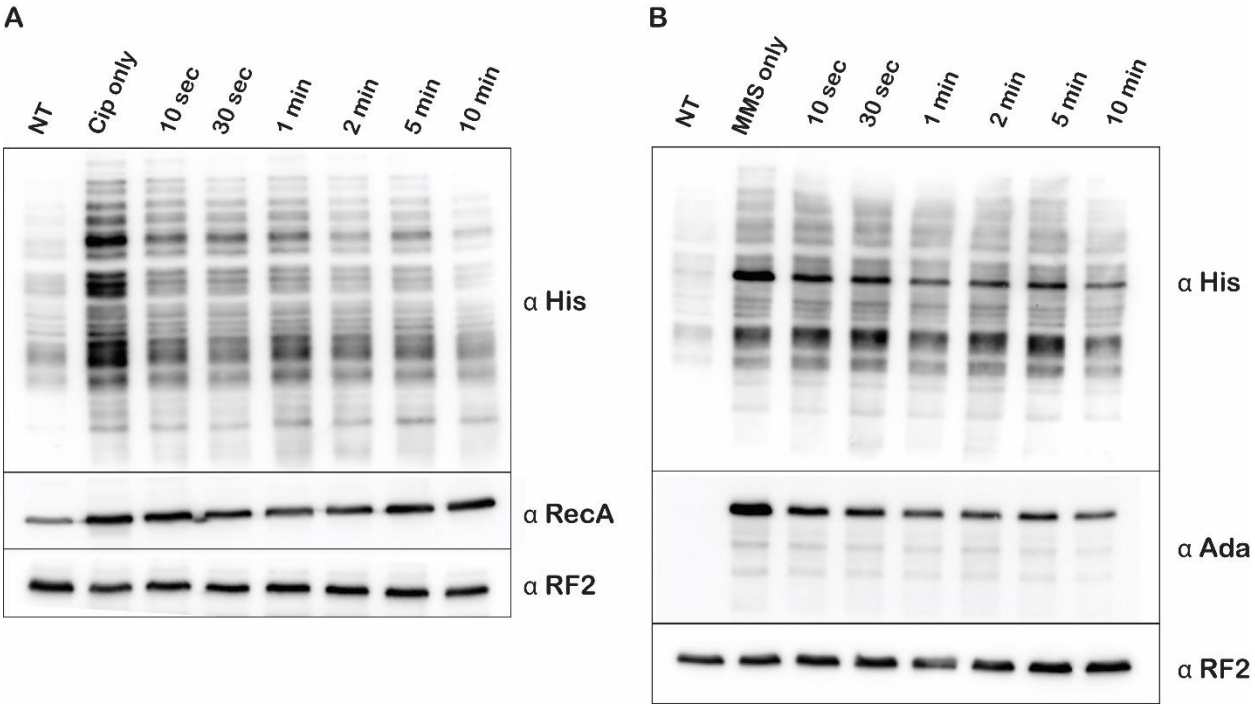

Supplementary Figure 2.S7: Significant transcriptional runoff is achieved after 10 seconds of rifampicin treatment
Western blots displaying total protein collected from *E. coli* expressing tmRNA-His_6. A) Cells were either untreated, treated with only ciprofloxacin, or pre-treated with rifampicin for various

amounts of time before ciprofloxacin treatment. The blot was probed with α His, α RecA, and α RF2. B) Cells were either untreated, treated with only MMS, or pre-treated with rifampicin for various amounts of time before MMS treatment. The blot was probed with α His, α Ada, and α RF2.

Quantification of Nucleosides via Liquid Chromatography – Mass Spectrometry

Overnight cultures of MG1655 *E. coli* were diluted to OD 0.05 in LB and grown to an OD of 0.3-0.4 at 37°C before 20 min treatment with either 0.1% MMS or 5 μg/mL MNNG. RNA was isolated using a hot phenol method as previously described (70). 10 μg of total RNA was digested by P1 nuclease (10 Units) at 50°C overnight. A final concentration of100mM Tris pH 7.5 and 1:100 v/v dilution of calf intestinal phosphatase (CIP) were added to the samples, and the reaction was incubated for 1 hour at 37°C to convert 5'-monophosphates to nucleosides. The samples were diluted to 150 μL and filtered (0.22 μm pore size) before injecting 10 μL into an Agilent 1290 Infinity II UHPLC connected to an Agilent 6470 Triple Quadrupole mass spectrometer. Nucleosides were separated on a Zorbax Eclipse Plus C18 column (2.1 x 50 mm x 1.8 micron) and then analyzed using multiple-reaction monitoring in positive-ion mode. Calibration curves were generated with known concentrations of standards. Unmodified nucleosides were monitored by absorbance at 260 nm. Modified nucleosides were monitored by MRM. The retention times and mass transitions of each nucleoside are listed in Supplemental Table S1. Free unmodified A, G, and C standards were purchased from Acros Organics and U was purchased from TCI Products. Free modified nucleosides m^7G, m^1G, and m^3C were purchased from Carbosynth, m^6G and m^6A were purchased from Berry's Associates, and m^1A was purchased from Cayman Chemical Company. Data was analyzed using Agilent qualitative analysis, Excel, and Graphpad Prism software.

	precursor mass	product ion	retention time	collision energy

A	268.1	136	1.92	18
C	244.1	112	0.48	14
G	284.2	152	2.4	16
U	245.2	152.1	1	14
m1A	282.2	150.1	0.9	16
m6A	282	150	4.08	16
m3C	258.2	126	0.8	8
m7G	298.2	166	1.5	10
m1G	298	166	4.623	4.143
m6G	298	166	4.84	4.84

Supplementary Table 2.S1: Mass transitions, retention times, and collision energies for nucleoside standards

Charging of Aminoacyl-tRNA

[^{35}S]-fMet-tRNA^{fMet} was prepared as previously described (71). The tRNAs were aminoacylated by incubating total tRNA mix (Roche) at 150 μM with the appropriate amino acid (0.4 mM), tRNA synthetase (~5 μM) and ATP (2 mM) in charging buffer composed of 100 mM K-HEPES (pH 7.6), 20 mM MgCl2, 10 mM KCl, 1 mM DTT. After a 30-minute incubation at 37°C, the aa-tRNAs were purified by phenol/chloroform extraction, ethanol precipitated, and resuspended in 20 mM KOAc (pH 5.2) and 1 mM DTT.

Formation of Ribosomal Initiation Complexes

Protocols were performed as previously described (72). All initiation complex (IC) formation and peptidyl transfer reactions were performed in 1x polymix buffer (46 in 8oxoG paper), composed of 95 mM KCl, 5 mM NH_4Cl, 5 mM $Mg(OAc)_2$, 0.5 mM $CaCl_2$, 8 mM putrescine, 1 mM spermidine, 10 mM K_2HPO_4 (pH 7.5), 1 mM DTT. In order to generate ICs, 70S ribosomes (2μM), IF1, IF2, IF3, [^{35}S]-fMet-tRNA^{fMet} (3μM each), mRNA (6μM), and GTP (2 mM) in 1 × polymix buffer were incubated at 37°C for 30 min. The initiation complexes were purified from free tRNAs and initiation factors over a 500 μL sucrose cushion composed of 1.1 M sucrose, 20

mM Tris-HCl pH 7.5, 500 mM NH_4Cl, 0.5 mM EDTA, and 10 mM $MgCl_2$. The mixture was spun for 2 hours at 287,000 × g at 4°C, and the pellet was resuspended in 1 × polymix buffer and stored at -80°C. The fractional radioactivity that pelleted was used to determine the concentration of IC.

Modified mRNAs containing m1A used in the IC formation reaction were purchased from The Midland Certified Reagent Company, and its sequence is as follows: C AGA GGA GGU AAA AAA AUG G(1-methyl-A)A UUG UAC AAA. The unmodified control mRNA was transcribed from a dsDNA template using T7 polymerase and purified via denaturing PAGE (74).

Kinetics of Peptidyl Transfer

In order to exchange bound GDP for GTP, EF-Tu (30 µM final) was initially incubated with GTP (2 mM final) in 1x polymix buffer for 15 mins at 37°C. The mixture was then incubated with aminacyl-tRNAs (~6 µM) for 15 mins at 37°C to form ternary complexes (TC). For reactions performed in the presence of paromomycin, 10 µg/mL final of the antibiotic were added to this mixture. Kinetics assays were also performed using *trans*-translation quaternary complexes (QCs), which were formed by incubating Ala-$tRNA^{Ala}$ with SmpB, EF-Tu, and GTP in 1x polymix for 15 mins at 37°C. The TC or QC mixture was then combined with an equivalent volume of IC at 37°C either using RQF-3 quench-flow instrument or by hand. KOH to a final concentration of 500 mM was used to stop reactions at different time points. Dipeptide products and free fMet were separated using cellulose TLC plates that were electrophoresed in pyridine-acetate at pH 2.8 (50 in 8oxog paper). TLC plates were then exposed to a phosphor screen overnight, after which they were imaged using a Personal Molecular Imager (PMI) system. The images were quantified, and the fraction of dipeptide fMet at each time point was used to determine the rate of peptide bond formation using GraphPad Prism software.

Alkylative Damage Recovery Assays

Overnight cultures of MG1655 and Δ*ssrA* MG1655 cells were diluted to OD_{600} 0.05 and grown to 0.3 – 0.4 at 37°C before treating with either 0.5% MMS or 20 μg/mL MNNG for 20 mins. The OD_{600} of the cells was recorded at the time of collection, and the samples were washed twice with LB and resuspended in an adjusted volume of LB. Cells were diluted to an OD_{600} of 0.005 at 100 μL final volume in a 96-well plate. Plates were shaken at 37°C for 20 hours in a BioTek Eon microtiter plate reader which measured the OD_{600} of each well every 10 mins. OD_{600} data over time was fit to an exponential function in Graphpad Prism to plot the growth curve.

Spot Assays for Viability Analysis

X90 and SM20 E. coli were grown from OD 0.5 to OD 0.3 at 37°C before treating with either 0.1% or 0.5% MMS. At each time point, an aliquot of the culture was removed, washed with LB, and then serially diluted 1:10 eight times. 4 μL of each dilution were spotted on an LB plate. The plates were imaged and colonies were counted using the Colony Counter plugin on ImageJ.

REFERENCES

1. Simms,C.L., Thomas,E.N. and Zaher,H.S. (2017) Ribosome-based quality control of mRNA and nascent peptides. *Wiley Interdiscip. Rev. RNA*, **8**, 1–27.

2. Wurtmann,E.J. and Wolin,S.L. (2009) RNA under attack: Cellular handling of RNA damage RNA under attack: Cellular handling of RNA damage E. J. Wurtmann et.al. *Crit. Rev. Biochem. Mol. Biol.*, **44**, 34–49.

3. Hofer,T., Badouard,C., Bajak,E., Ravanat,J.L., Mattsson,Å. and Cotgreave,I.A. (2005) Hydrogen peroxide causes greater oxidation in cellular RNA than in DNA. *Biol. Chem.*, **386**, 333–337.

4. Wyatt,M.D. and Pittman,D.L. (2008) Methylating agents and DNA repair responses: methylated bases and sources of strand breaks. *Chem Res Toxicol*, **19**, 1580–1594.

5. Ougland,R., Zhang,C.M., Liiv,A., Johansen,R.F., Seeberg,E., Hou,Y.M., Remme,J. and Falnes,P. (2004) AlkB restores the biological function of mRNA and tRNA inactivated by chemical methylation. *Mol. Cell*, **16**, 107–116.

6. Zaher,H.S. and Green,R. (2009) Fidelity at the Molecular Level: Lessons from Protein Synthesis. *Cell*, **136**, 746–762.

7. Voorhees,R.M. and Ramakrishnan,V. (2013) Structural Basis of the Translational Elongation Cycle. *Annu. Rev. Biochem.*, **82**, 203–236.

8. Ogle,J.M., Brodersen,D.E., Jr,W.M.C., Tarry,M.J., Carter,A.P., Ramakrishnan,V., Ogle,J.M., Brodersen,D.E., Jr,W.M.C., Tarry,M.J., *et al.* (2002) Recognition of Cognate Transfer RNA by the 30S Ribosomal Subunit Published by : American Association for the Advancement of Science Stable URL : http://www.jstor.org/stable/3083592 Recognition of Cognate Transfer RNA by the 30S Ribosomal Subunit. **292**, 897–902.

9. Yoshizawa,S., Fourmy,D. and Puglisi,J.D. (1999) Recognition of the codon-anticodon helix by ribosomal RNA. *Science (80-.).*, **285**, 1722–1725.

10. Simms,C.L. and Zaher,H.S. (2016) Quality control of chemically damaged RNA. *Cell. Mol. Life Sci.*, **73**, 3639–3653.

11. Hudson,B.H. and Zaher,H.S. (2015) O6-Methylguanosine leads to position-dependent effects on ribosome speed and fidelity. *Rna*, **21**, 1648–1659.

12. You,C., Dai,X. and Wang,Y. (2017) Position-dependent effects of regioisomeric methylated adenine and guanine ribonucleosides on translation. *Nucleic Acids Res.*, **45**, 9059–9067.

13. Zhang,C. and Jia,G. (2018) Reversible RNA Modification N1-methyladenosine (m1A) in mRNA and tRNA. *Genomics, Proteomics Bioinforma.*, **16**, 155–161.

14. Dominissini,D., Nachtergaele,S., Moshitch-moshkovitz,S., Peer,E., Kol,N., Ben-haim,M.S., Dai,Q., Segni,A. Di, Clark,W.C., Zheng,G., *et al.* (2016) The dynamic N 1 - methyladenosine methylome in eukaryotic messenger RNA. *Nature*, **530**, 441–446.

15. Li,X., Xiong,X., Wang,K., Wang,L., Shu,X., Ma,S. and Yi,C. (2016) Transcriptome-wide

mapping reveals reversible and dynamic N 1 -methyladenosine methylome. *Nat. Publ. Gr.*, **12**, 311–316.

16. Safra,M., Sas-chen,A., Nir,R., Winkler,R., Nachshon,A., Bar-yaacov,D., Erlacher,M., Rossmanith,W., Stern-ginossar,N. and Schwartz,S. (2017) The m1A landscape on cytosolic and mitochondrial mRNA at single-base resolution. *Nat. Publ. Gr.*, **551**, 251–255.

17. Zhou,H., Kimsey,I.J., Nikolova,E.N., Sathyamoorthy,B., Grazioli,G., Mcsally,J., Bai,T., Wunderlich,C.H., Kreutz,C., Andricioaei,I., *et al.* (2016) m 1 A and m 1 G disrupt A-RNA structure through the intrinsic instability of Hoogsteen base pairs. *Nat. Publ. Gr.*, **23**, 803–810.

18. Lykke-Andersen,S. and Jensen,T.H. (2015) Nonsense-mediated mRNA decay: An intricate machinery that shapes transcriptomes. *Nat. Rev. Mol. Cell Biol.*, **16**, 665–677.

19. Klauer,A.A. and van Hoof,A. (2013) Degradation of mRNAs that lack a stop codon: A decade of nonstop progress. *Wiley Interdiscip. Rev. RNA*, **3**, 649–660.

20. Harigaya,Y. and Parker,R. (2010) No-go decay: a quality control mechanism for RNA in translation. *Wiley Interdiscip. Rev. RNA*, **1**, 132–141.

21. Keiler,K.C., Waller,P.R.H. and Sauer,R.T. (1996) Role of a Peptide Tagging System in Degradation of Proteins Synthesized from Damaged Messenger RNA. *Science (80-.).*, **271**, 990–993.

22. Moore,S.D. and Sauer,R.T. (2007) The tmRNA System for Translational Surveillance and Ribosome Rescue. *Annu. Rev. Biochem.*, **76**, 101–124.

23. Valle,M., Gillet,R., Kaur,S., Henne,A., Ramakrishnan,V. and Frank,J. (2003) Visualizing tmRNA Entry into a Stalled Ribosome. *Science (80-.).*, **300**, 127–130.

24. Hallier,M., Ivanova,N., Rametti,A., Pavlov,M., Ehrenberg,M. and Felden,B. (2004) Pre-binding of small protein B to a stalled ribosome triggers trans-translation. *J. Biol. Chem.*, **279**, 25978–25985.

25. Gottesman,S., Roche,E., Zhou,Y.N. and Sauer,R.T. (1998) The ClpXP and ClpAP proteases degrade proteins with carboxy-terminal peptide tails added by the SsrA-tagging system. *Genes Dev.*, **12**, 1338–1347.

26. Keiler,K.C. and Sauer,R.T. (1996) Sequence determinants of C-terminal substrate recognition by the Tsp protease. *J. Biol. Chem.*, **271**, 2589–2593.

27. Richards,J., Mehta,P. and Karzai,A.W. (2006) RNase R degrades non-stop mRNAs selectively in an SmpB-tmRNA-dependent manner. **62**, 1700–1712.

28. Ge,Z., Mehta,P., Richards,J. and Karzai,A.W. (2010) Non-stop mRNA decay initiates at the ribosome. **78**, 1159–1170.

29. Zaher,H.S. and Green,R. (2009) Quality control by the ribosome following peptide bond formation. *Nature*, **457**, 161–166.

30. Deng,X., Chen,K., Luo,G., Weng,X., Ji,Q., Zhou,T. and He,C. (2015) Widespread occurrence of N 6 -methyladenosine in bacterial mRNA. **43**, 6557–6567.

31. Machnicka,M.A., Milanowska,K., Oglou,O.O., Purta,E., Kurkowska,M., Olchowik,A., Januszewski,W., Kalinowski,S., Dunin-Horkawicz,S., Rother,K.M., *et al.* (2013) MODOMICS: A database of RNA modification pathways - 2013 update. *Nucleic Acids Res.*, **41**, 262–267.

32. Beranek,D.T. (1990) Distribution of methyl and ethyl adducts following alkylation with monofunctional alkylating agents. *Mutat. Res.*, **231**, 11–30.

33. Bodell,W.J. and Singer,B. (1979) Influence of Hydrogen Bonding in DNA and Polynucleotides on Reaction of Nitrogens and Oxygens toward Ethylnitrosourea. *Biochemistry*, 10.1021/bi00580a029.

34. Ogle,J.M., Murphy IV,F. V., Tarry,M.J. and Ramakrishnan,V. (2002) Selection of tRNA by the ribosome requires a transition from an open to a closed form. *Cell*, **111**, 721–732.

35. Pape,T., Wintermeyer,W. and Rodnina,M. V. (2000) Conformational switch in the decoding region of 16S rRNA during aminoacyl-tRNA selection on the ribosome. *Nat. Struct. Biol.*, **7**, 104–107.

36. Ramakrishnan,V., Carter,A.P., Clemons,W.M., Brodersen,D.E., Morgan-Warren,R.J. and Wimberly,B.T. (2000) Functional insights from the structure of the 30S ribosomal subunit and its interactions with antibiotics. *Nature*, **407**, 340–348.

37. Nishikawa,K., Inokuchi,H., Kitabatake,M., Yokogawa,T. and Komine,Y. (2006) A tRNA-like structure is present in 10Sa RNA, a small stable RNA from Escherichia coli. *Proc. Natl. Acad. Sci.*, **91**, 9223–9227.

38. Ivanova,N., Pavlov,M.Y. and Ehrenberg,M. (2005) tmRNA-induced release of messenger RNA from stalled ribosomes. *J. Mol. Biol.*, **350**, 897–905.

39. Ivanova,N., Pavlov,M.Y., Felden,B. and Ehrenberg,M. (2004) Ribosome rescue by tmRNA requires truncated mRNAs. *J. Mol. Biol.*, **338**, 33–41.

40. Moore,S.D. and Sauer,R.T. (2005) Ribosome rescue: tmRNA tagging activity and capacity in Escherichia coli. *Mol. Microbiol.*, **58**, 456–466.

41. Jeggot,P. (1979) Isolation and Characterization of Escherichia coli K-12 Mutants Unable to Induce the Adaptive Response to Simple Alkylating Agents. **139**, 783–791.

42. Sakumi,K. and Sekiguchi,M. (1989) Regulation of Expression of the ada Gene Controlling the Adaptive Response. *J. Mol. Biol.*

43. Uphoff,S., Lord,N.D., Okumus,B., Potvin-trottier,L., Sherratt,D.J. and Paulsson,J. (2016) Stochastic activation of a DNA damage response causes cell-to-cell mutation rate variation. **351**, 1094–1098.

44. Cox,M.M. (1991) The RecA protein as a recombinational repair system. **5**, 1295–1299.

45. Wehrli,W. Rifampin: mechanisms of action and resistance. *Rev. Infect. Dis.*, **5 Suppl 3**, S407-11.

46. LeBel,M. (1988) Ciprofloxacin: chemistry, mechanism of action, resistance, antimicrobial spectrum, pharmacokinetics, clinical trials, and adverse reactions. *Pharmacotherapy*, **8**, 3–

33.

47. Verweij,J. and Pinedo,H.M. (1990) Mitomycin C: mechanism of action, usefulness and limitations. *Anticancer. Drugs*, **1**, 5–13.

48. Wali Karzai,A., Susskind,M.M. and Sauer,R.T. (1999) SmpB, a unique RNA-binding protein essential for the peptide-tagging activity of SsrA (tmRNA). *EMBO J.*, **18**, 3793–3799.

49. Peer,E., Rechavi,G. and Dominissini,D. (2017) Epitranscriptomics : regulation of mRNA metabolism through modifications. *Curr. Opin. Chem. Biol.*, **41**, 93–98.

50. Xiao Wang1 Adrian Gomez1, Gary C. Hon2, Yanan Yue1, Dali Han1, Ye Fu1, Marc Parisien3, Qing Dai1, Guifang Jia1, 4, Bing Ren2, Tao Pan3, and Chuan He1,Z.L. (2014) m6A-dependent regulation of messenger RNA stability. *Nature*, **505**, 1–20.

51. Karikó,K., Muramatsu,H., Welsh,F.A., Ludwig,J., Kato,H., Akira,S. and Weissman,D. (2008) Incorporation of pseudouridine into mRNA yields superior nonimmunogenic vector with increased translational capacity and biological stability. *Mol. Ther.*, **16**, 1833–40.

52. Wimberly,B.T., Carter,A.P., Clemons,W.M., Brodersen,D.E., Morgan-Warren,R.J., Ramakrishnan,V., Vonrhein,C. and Hartsch,T. (2000) Structure of the 30S ribosomal subunit. *Nature*, **407**, 327–339.

53. Carter,A.P., Brodersen,D.E., Morgan-warren,R.J., Hartsch,T., Wimberly,B.T. and Ramakrishnan,V. (2001) Crystal Structure of an Initiation Factor Bound to the 30S Ribosomal Subunit. *Science (80-.).*, **291**, 498–501.

54. Clemons,W.M., May,J.L.C., Wimberly,B.T., McCutcheon,J.P., Capel,M.S. and Ramakrishnan,V. (1999) Structure of a bacterial 30S ribosomal subunit at 5.5 Å resolution. *Nature*, **400**, 833–840.

55. Liu,M., Gong,X., Alluri,R.K., Wu,J., Sablo,T. and Li,Z. (2012) Characterization of RNA damage under oxidative stress in Escherichia coli. **393**, 123–132.

56. Hou,Y. (2010) Critical Review CCA Addition to tRNA : Implications for tRNA Quality Control. **62**, 251–260.

57. Saxowsky,T.T. and Doetsch,P.W. (2006) RNA Polymerase Encounters with DNA Damage : Transcription-Coupled Repair or Transcriptional Mutagenesis ? 10.1021/cr040466q.

58. Ashlev,M.I.K. (1997) Transcriptional arrest : Escherichia coli RNA polymerase translocates backward , leaving the 3 ˜end of the RNA intact. **94**, 1755–1760.

59. Roberts,J. and Park,J. (2004) Mfd , the bacterial transcription repair coupling factor : translocation , repair and termination. 10.1016/j.mib.2004.02.014.

60. Borukhov,S., Sagitov,V. and Goldfarb,A. (1993) Transcript cleavage factors from E. coli. *Cell*, **72**, 459–466.

61. Park,J., Marr,M.T. and Roberts,J.W. (2002) E . coli Transcription Repair Coupling Factor (Mfd Protein) Rescues Arrested Complexes by Promoting Forward Translocation. **109**, 757–767.

62. Shimizu,Y. (2012) ArfA Recruits RF2 into Stalled Ribosomes. *J. Mol. Biol.*, **423**, 624–631.

63. Chadani,Y., Ito,K., Kutsukake,K. and Abo,T. (2012) ArfA recruits release factor 2 to rescue stalled ribosomes by peptidyl-tRNA hydrolysis in Escherichia coli. **86**, 37–50.

64. Garza-sánchez,F., Schaub,R.E., Janssen,B.D. and Hayes,C.S. (2011) tmRNA regulates synthesis of the ArfA ribosome rescue factor. **80**, 1204–1219.

65. Chadani,Y., Matsumoto,E., Aso,H. and Wada,T. (2011) trans -translation-mediated tight regulation of the expression of the alternative ribosome-rescue factor ArfA in Escherichia coli.

66. Chadani,Y., Ono,K., Kutsukake,K. and Abo,T. (2011) Escherichia coli YaeJ protein mediates a novel ribosome-rescue pathway distinct from SsrA- and ArfA-mediated pathways. **80**, 772–785.

67. Handa,Y., Inaho,N. and Nameki,N. (2011) YaeJ is a novel ribosome-associated protein in Escherichia coli that can hydrolyze peptidyl – tRNA on stalled ribosomes. **39**, 1739–1748.

68. Trewick,S.C., Henshaw,T.F., Hausinger,R.P., Lindahl,T. and Sedgwick,B. (2002) Oxidative demethylation by Escherichia coli AlkB directly reverts DNA base damage. *Nature*, **419**, 174–178.

69. Parsell,D.A. and Sauer,R.T. (1989) The Structural Stability of a Protein Is an Important Determinant of Its Proteolytic Susceptibility in. **264**, 7590–7595.

70. Simms,C.L., Yan,L.L., Zaher,H.S., Simms,C.L., Yan,L.L. and Zaher,H.S. (2017) Ribosome Collision Is Critical for Quality Control during No-Go Decay Article Ribosome Collision Is Critical for Quality Control during No-Go Decay. *Mol. Cell*, **68**, 361-373.e5.

71. Walker,S.E. and Fredrick,K. (2008) Preparation and evaluation of acylated tRNAs. *Methods*, **377**, 364–377.

72. Pierson,W.E., Hoffer,E.D., Keedy,H.E., Simms,C.L., Dunham,C.M. and Zaher,H.S. (2016) Uniformity of Peptide Release Is Maintained by Methylation of Release Factors. *Cell Rep.*, **17**, 11–18.

73. Jelenc,P.C. (1979) Nucleoside triphosphate regeneration decreases the frequency of. *Proc. Natl. Acad. Sci. U. S. A.*, **76**, 3174–3178.

74. Zaher,H.S. and Unrau,P.J. (2004) T7 RNA Polymerase Mediates Fast Promoter-Independent Extension of Unstable Nucleic Acid Complexes †. *Biochemistry*, **43**, 7873–7880.

75. Youngman,E.M., Brunelle,J.L., Kochaniak,A.B. and Green,R. (2004) The active site of the ribosome is composed of two layers of conserved nucleotides with distinct roles in peptide bond formation and peptide release. *Cell*, **117**, 589–99.

Chapter 3

Insights into the base-pairing preferences of 8-oxoguanosine on the ribosome

This chapter is currently published in Nucleic Acids Research as Erica N. Thomas, Carrie L. Simms, Hannah E. Keedy, and Hani S. Zaher (2019). Insights into the base-pairing preferences of 8-oxoguanosine on the ribosome.

ABSTRACT

Of the four bases, guanine is the most susceptible to oxidation, which results in the formation of 8-oxoguanine (8-oxoGua). In protein-free DNA, 8-oxodG adopts the *syn* conformation more frequently than the *anti* one. In the *syn* conformation, 8-oxodG base pairs with dA. The equilibrium between the *anti* and *syn* conformations of the adduct are known to be altered by the enzyme recognizing 8-oxodG. We previously showed that 8-oxoG in mRNA severely disrupts tRNA selection, but the underlying mechanism for these effects was not addressed. Here, we use miscoding antibiotics and ribosome mutants to probe how 8-oxoG interacts with the tRNA anticodon in the decoding center. Addition of antibiotics and introduction of error-inducing mutations partially suppressed the effects of 8-oxoG. Under these conditions, rates and/or endpoints of peptide-bond formation for the cognate (8-oxoG•C) and near-cognate (8-oxoG•A) aminoacyl-tRNAs increased. In contrast, the antibiotics had little effect on other mismatches, suggesting that the lesion restricts the nucleotide from forming other interactions. Our findings suggest that 8-oxoG predominantly adopts the *syn* conformation in the A site. However, its ability to base pair with adenosine in this conformation is not sufficient to promote the necessary structural changes for tRNA selection to proceed.

KEYWORDS

Ribosome, translation, tRNA selection, 8-oxoguanosine, oxidative damage

INTRODUCTION

Decoding of the genetic information is a remarkably accurate process that ensures the maintenance of faithful protein production. In all domains of life, the ribosome carries out this crucial task by utilizing multiple strategies to select for the aminoacyl-tRNA (aa-tRNA) that corresponds to mRNA in the A site (1, 2). This process of tRNA selection is divided into two phases: initial phase and proofreading, which are separated by the irreversible step of GTP hydrolysis by EF-Tu (3). During the initial selection phase, aa-tRNA binds the A site of the ribosome in a ternary complex with EF-Tu and GTP. During this stage, near-cognate aa-tRNAs, which harbor a single mismatch, are discriminated against due to their inability to fully base pair with the A-site codon. This results in the accelerated dissociation of the ternary complex. After this initial codon-recognition step, EF-Tu undergoes a conformational change before GTP is hydrolyzed (4). This step of GTPase activation is significantly accelerated for cognate aa-tRNAs, thereby contributing to the overall accuracy of the tRNA selection process. After GTP hydrolysis, GDP-bound EF-Tu undergoes additional conformational changes before dissociating from the ribosome (5, 6). During the subsequent proofreading stage, the selection process is partitioned into accommodation and rejection (7, 8). Cognate aa-tRNAs rapidly accommodate to then participate in peptidyl transfer (PT), whereas near-cognate aa-tRNAs are more likely to be rejected (9–11). This multi-step process of tRNA selection results in an overall misincorporation rate of 10^{-4} – 10^{-3} per PT event (12–15)

X-ray crystallography and cryo-EM reconstitution studies of various ribosome complexes have provided some important molecular rationale for the process of tRNA selection, especially during the initial selection stage (16–18). The EF-Tu-bound aa-tRNA binds the A site in a bent state, referred to as the A/T state, where its anticodon can sample the codon (19). Once base pairing

between the codon and the anticodon occurs, the conserved A1492, A1493, and G530 residues of the decoding center change conformation and interact with the minor groove of the codon-anticodon helix in a recently-identified stepwise manner (17). These interactions are only possible if strict Watson-Crick base pairing is maintained at the first two positions of the codon. Additional contacts are made by other ribosomal RNA (rRNA) residues as well as ribosomal protein S12 (20). These local rearrangements in the decoding center trigger a global change in the small ribosomal subunit (30S) (21). This so-called "domain closure" moves the shoulder of the 30S as well as EF-Tu closer to the large subunit (50S). As a result, the GTPase domain of EF-Tu binds the sarcin-ricin loop (SRL), activating the factor for GTP hydrolysis through interactions with the catalytic histidine (22). It has been suggested that if the anticodon of the aa-tRNA is tightly bound in the decoding center following EF-Tu dissociation, accommodation ensues. On the other hand, if the tRNA is loosely bound then it is more likely to dissociate and be rejected (7, 23).

Several antibiotics are known to affect the overall selection process by altering the interactions between the tRNA-mRNA complex and the decoding center. The most studied and well-understood group is the aminoglycoside class of antibiotics. Nearly all bind in the decoding center and reduce the energetics of "domain closure" by driving an "ON"-state of the decoding center nucleotides. For instance, paromomycin binds in a rRNA pocket close to A1492 and A1493 and induces them to adopt a structure similar to that assumed in the presence of cognate tRNAs. This, in turn, reduces the energetic cost associated with "domain closure" of the 30S subunit and as a result, makes the process of tRNA selection more favorable in the presence of near-cognate aa-tRNAs (24, 25). In comparison, streptomycin, which decreases GTPase activation for cognate aa-tRNA and increases it for near-cognate aa-tRNAs, does not induce "domain closure". Instead, the antibiotic induces a lateral shift of helix 44 (h44), which contains A1492 and A1493; this

rearrangement is distinct than that triggered by the addition of paromomycin. This lateral shift appears to be sufficient to stabilize near-cognate tRNAs, whereas the prevention of "domain closure" destabilizes cognate tRNAs, which results in an overall increase in miscoding (26, 27).

These largely structure-based models for tRNA selection, whereby local changes in the decoding center drive global rearrangements in the small subunit, are also supported by genetic studies. In particular, mutations in the 30S subunit that destabilize interactions that are important for the transition from the "open" to "closed" state result in a hyperaccurate phenotype. These mutations are typically found on the ribosomal protein S12, specifically at its interface with h27/h44 of the 16S rRNA near the decoding center (28, 29). In contrast to the hyperaccurate mutants, error-prone (often referred to as *ribosomal ambiguity* (*ram*)) mutants reduce the energetics for transitioning to the "closed" state of the 30S by disrupting interactions important for maintaining the "open" state (30). Mutations of this class are associated with changes to the interfaces between ribosomal proteins S4 and S5 that are held together through electrostatic interactions in the "open" state. Therefore, disruption of these interactions eases the transition to the "closed" state, even in the presence of near-cognate tRNAs (31, 32).

Under typical circumstances, the ribosome only encounters mRNA composed of the four canonical nucleobases. In contrast, the tRNA anticodon is often modified, and these modifications impact how the anticodon base pairs with the codon. Similarly, mRNA appears to be modified, albeit to a lesser extent than tRNAs. The most abundant of these mRNA modifications include N^6-methyladenosine (m^6A), 5-methylcytosine (m^5C), and pseudouridine (Ψ) (33). Although these modifications do not change the Watson-Crick-base-pairing capabilities of the nucleotides, they affect the decoding process. For example, m^6A reduces the overall rate of peptide-bond formation by almost an order of magnitude (34, 35). In contrast, the introduction of Ψ to mRNA has little

effect on the speed of decoding but reduces accuracy on stop codons *in vitro* (36, 37). Regardless of their effect on decoding, the biological implications of these modifications are currently not fully understood, namely due to their low stoichiometries on mRNAs.

In contrast to these potentially intentional modifications, chemical damage to the mRNA nucleobase is largely detrimental to the decoding process. Most damage adducts occur as a result of reactivity between the mRNA and endogenous or exogenous agents (38). Some of the most common nucleotide-damaging agents include ultraviolet light, alkylating agents, and reactive oxygen species (ROS). In particular, ROS are produced endogenously as byproducts of metabolic reactions and increase under stress conditions (39). Of the many potential ROS adducts, 8-oxoguanosine (8-oxoG) is noteworthy due to its high abundance relative to other oxidized nucleotides and its association with neurodegenerative disease (40, 41). Furthermore, 8-oxoG significantly reduces the rate of peptide-bond formation to a point that it stalls protein synthesis and is likely to activate the process of no-go decay (NGD). Indeed, our group has shown that the introduction of 8-oxoG to the mRNA, independent of its position within the codon, slows down PT by three to four orders of magnitude (42). While the overall kinetic consequences of 8-oxoG on tRNA selection were recognized, the mechanistic details through which 8-oxoG interferes with translation remained unknown. Specifically, we were interested in understanding how 8-oxoG disrupted interactions with the anticodon within the decoding center of the ribosome.

Previous data from studies of the oxidative damage of DNA show that 8-oxodG can alter the base pairing preferences of dG by changing the conformation of the nucleotide (43). When 8-oxodG adopts the typical *anti*-conformation, the oxygen at carbon 8 is in steric clash with the phosphate backbone (Figure 1). In order to relieve this steric clash, the base can rotate around its glycosidic bond to the *syn* conformation, where it reveals a new hydrogen-bonding interface which

it uses to form a Hoogsteen base pair with dA (43). Different DNA polymerases read 8-oxodG as either a dG or dT at varying efficiencies, resulting in either accurate polymerization or a transversion. The efficiency of incorporating dCMP versus dAMP across 8-oxodG depends on the fidelity of the DNA polymerase. The steric constraints for base pairs in the active sites of high fidelity polymerases increase the frequency at which 8oxodG base pairs with dA, as this base pair is nearly identical in terms of its geometry to a normal Watson-Crick base pair than 8oxodG•C (44, 45). While much is known about the base pairing preferences of 8-oxodG during replication, the preference for the *syn* vs *anti* conformation of the base on the ribosome is not understood at all.

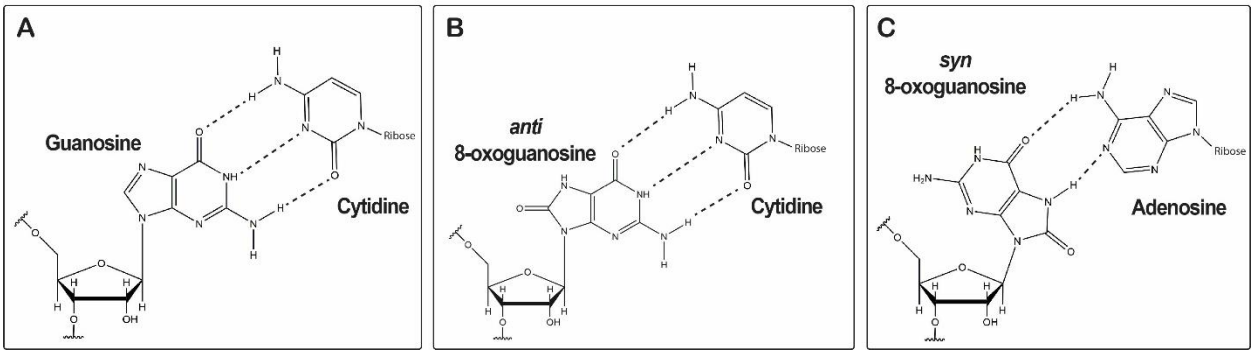

Figure 3.1: 8-oxoG alters the base-pairing properties of the nucleotide
A) Structure depicting the Watson-Crick base pair of unmodified guanosine and cytidine. B) Structure of 8-oxoG in the *anti* conformation forming a Watson-Crick base pair with cytidine, and C) in the *syn* conformation forming a Hoogsteen base pair with adenosine.

In this study, we take advantage of a well-defined *in vitro* translation system to examine the mechanism through which 8-oxoG in mRNA interferes with translation (46). We find that 8-oxoG significantly impacts the initial phase of tRNA selection, suggesting that 8-oxoG is interfering with the ability of the A-site codon to form a proper interaction with its corresponding anticodon. To address how 8-oxoG is disrupting this interaction in the context of the A site, we explored its base-pairing preferences by relaxing tRNA-selection conditions and reacting it with its cognate tRNA and all possible near-cognate tRNAs. Under these relaxed tRNA selection

conditions, we observed that 8-oxoG base pairs with either cytidine or adenosine independent of its location in either the first or second position of the codon. Our analysis also shows that 8-oxoG has a preference for base pairing with adenosine over cytidine under error-prone conditions, suggesting that it more frequently exists in the *syn* conformation than the *anti* one on the ribosome. Additionally, 8-oxoG disrupts the ability of the nucleotide to form base pairs with the remaining near-cognates (8oxoG•U and 8oxoG•G). Our results contribute to the mechanistic understanding of how 8-oxoG in mRNA disrupts translation.

MATERIALS AND METHODS

Materials

All reactions were performed in 1x polymix buffer (47), composed of 95 mM KCl, 5 mM NH_4Cl, 5 mM $Mg(OAc)_2$, 0.5 mM $CaCl_2$, 8 mM putrescine, 1 mM spermidine, 10 mM K_2HPO_4 (pH 7.5), 1 mM DTT.

70S ribosomes were purified from MRE600 *E. coli* via a double pelleting technique (32).

Translation factors were overexpressed and purified from *E. coli* (46).

Modified mRNAs containing 8-oxoG were purchased from either IDT, Dharmacon, or The Midland Certified Reagent Company. Unmodified control mRNAs were transcribed from a dsDNA template using T7 RNA polymerase and purified via denaturing PAGE (48). The sequence for the first position 8-oxoG mRNA was as follows: CAGAGGAGGUAAAAAA AUG (8-oxo-rG)UU UUG UAC AAA. The sequence for the second position 8-oxoG-Arg mRNA was as follows: CAGAGGAGGUAAAAAA AUG C(8-oxo-rG)C UUGUACAAA. The sequence for the second position 8-oxo-Gly mRNA was as follows: CAGAGGAGGUAAAAAA AUG G(8-oxo-rG)C UUG UAC AAA.

Charging of Aminoacyl-tRNA

[^{35}S]-fMet-tRNA^{fMet} was prepared as described (49). Pure tRNAs (tRNA^{Val}, tRNA^{Arg}, or tRNA^{Met} from ChemBlock) were aminoacylated by incubating them at 10 μM with the appropriate amino acid (0.4 mM), tRNA synthetase (~5 μM) and ATP (2 mM) in charging buffer composed of 100 mM K-HEPES (pH 7.6), 20 mM MgCl2, 10 mM KCl, 1 mM DTT. After incubation at 37°C for 30 minutes, the aa-tRNAs were purified by phenol/chloroform extraction and ethanol precipitated. The aa-tRNAs were resuspended in in 20 mM KOAc (pH 5.2) and 1 mM DTT. Other tRNAs were aminoacylated by incubating total tRNA mix (Roche) at 150 μM

in the presence of the corresponding amino acid and tRNA synthetase as above. The incubation and purification were conducted as that done for the pure tRNAs.

Formation of Ribosomal Initiation Complexes

Protocols were performed as described (50). Briefly, to generate initiation complexes (IC), the following components were incubated at 37°C for 30 min: 70S ribosomes (2μM), IF1, IF2, IF3, [^{35}S]-fMet-tRNA^{fMet} (3μM each), mRNA (6μM) in 1 × polymix buffer in the presence of 2 mM GTP. The complexes were then purified away from free tRNAs and initiation factors over a 500 μL sucrose cushion composed of 1.1 M sucrose, 20 mM Tris-HCl pH 7.5, 500 mM NH_4Cl, 0.5 mM EDTA, and 10 mM $MgCl_2$. The mixture was spun at 287,000 × g at 4°C for 2 hrs, and the resulting pellet was resuspended in 1 × polymix buffer and stored at -80°C. In order to determine the concentration of IC, the fractional radioactivity that pelleted was measured.

GTP Hydrolysis Assay

To assemble the ternary complexes, the following components were combined and incubated at 37°C for 15 minutes: 5 mCi/mL of [γ-^{32}P]-GTP, 20 μM EF-Tu, and 5 μM of unlabeled GTP. An equal volume of 30 μM aa-tRNA was then added to the reaction and allowed to incubate again at 37°C for 15 minutes. In order to purify away unbound GTP and aa-tRNA from the assembled ternary complexes, samples were passed twice over P-30 spin columns (Biorad). The ternary complex was then diluted to 1 μM in polymix buffer (0.5 μM in the final reaction) and mixed with an equal volume of 2 μM IC (1 μM in the final reaction) at 20°C in a quench-flow instrument (RQF-3, KinTek Corporation). The reactions were quenched through the addition of 40% formic acid. The inorganic phosphate product was separated from unreacted GTP using Polyethylenimine

(PEI) cellulose thin-layer chromatography (TLC) (Sigma) with 0.5 M potassium phosphate buffer pH 3.5 as a mobile phase. Fractional radioactivity corresponding to inorganic phosphate at each time-point was quantified using phosphorimaging and used to determine the observed rates of GTP hydrolysis.

Kinetics of Peptidyl Transfer

EF-Tu (30 μM final) was initially incubated with GTP (2 mM final) in polymix buffer for 15 mins at 37°C to exchange the bound GDP for GTP. To form the ternary complex, the mixture was incubated with aminoacyl-tRNAs (~6 μM) for 15 mins at 37°C. For reactions performed in the presence of antibiotics, streptomycin (100 μM final) or paromomycin (10 μg/mL final) were added to this mixture. The ternary complex mixture was then combined with an equivalent volume of IC at 37°C either by hand or using RQF-3 quench-flow instrument. The reaction was stopped at different time points using KOH to a final concentration of 500 mM. Dipeptide products were separated from free fMet using cellulose TLC plates that were electrophoresed in pyridine-acetate at pH 2.8 (51). The TLC plates were exposed to a phosphor screen overnight, and the screens were imaged using a Personal Molecular Imager (PMI) system. These images were quantified, and the fraction of dipeptide fMet at each time point was used to determine the rate of peptide bond formation using GraphPad Prism.

RESULTS

8-oxoG interferes with the initial phase of tRNA selection

Previous work from our group showed that the presence of 8-oxoG within the A-site codon, regardless of its position, has a drastic effect on the speed of translation and slight effect on accuracy. The modification reduced the PT rate by almost three orders of magnitude for cognate aa-tRNA, and slightly increased it for the near-cognate tRNAs interacting through 8-oxoG•A base pairs with the codon (42). We hypothesized that the adduct inhibits base pairing, and as a result, is likely to inhibit early stages of tRNA selection, particularly the codon-recognition step. For technical reasons, we could not directly measure the kinetics of this step. Instead, in order to address the potential effect of the modification on the initial phase of tRNA selection, we opted to measure the rate of GTP hydrolysis as it reports on the overall selectivity of initial selection (11). To accomplish this, we utilized a pre-steady-state-kinetics strategy in combination with our reconstituted *in vitro* bacterial translation system. This system allows us to monitor individual and specific amino-acid incorporation. Briefly, ternary complexes were generated by incubating EF-Tu with a specific aa-tRNA in the presence of radio-labeled [γ-^{32}P]-GTP. Purified ternary complexes were then incubated with initiation complexes programmed with intact mRNAs or 8-oxoG-containing ones, and rates of GTP hydrolysis were determined by stopping the reaction at various points.

In total, we analyzed 8 different complexes harboring 8-oxoG at different positions of the A-site codon and their corresponding unmodified mRNAs. In particular, we measured the rates of GTP hydrolysis for the following complexes: ^{8oxo}GUU, C^{8oxo}GC, G^{8oxo}GC and GA^{8oxo}G, and the corresponding intact ones; these complexes code for Val, Arg, Gly and Glu, respectively. As predicted, we measured rates of GTP hydrolysis that were significantly lower for the oxidized

mRNAs relative to the corresponding unmodified ones (> three orders of magnitude for three of the four complexes) More specifically, we measure rates of 42 s^{-1}, 24 s^{-1}, 47 s^{-1}, and 86 s^{-1}, respectively, whereas the same rates for the unmodified ones were <0.0001 s^{-1}, 0.064 s^{-1}, 0.033 s^{-1}, and 0.015 s^{-1}, respectively (Figure 2). Interestingly, this change in rates of GTP hydrolysis mirrors what we documented for PT, suggesting that most of the effects of the adduct on tRNA selection are due to alteration to the initial phase of the selection process.

8-oxoG impairs decoding in a manner similar to a mismatch with subtle but important distinctions

Thus far, our data has shown that the presence of 8-oxoG affects early stages of tRNA selection by potentially interfering with the codon-anticodon interaction. More specifically, we expect the modification to inhibit base pairing, resembling a mismatch. This would result in PT reactions with oxidized complexes behaving in a manner analogous to reactions involving near-cognate aa-tRNAs. To probe this prediction, we increased ribosomal promiscuity through the addition of aminoglycoside antibiotics to our *in vitro* PT reactions. This results in relaxed tRNA-selection parameters, which increases the incorporation of near-cognate aa-tRNAs; and based on our model, aa-tRNA reactivities should also increase with the oxidized complexes in the presence of these antibiotics.

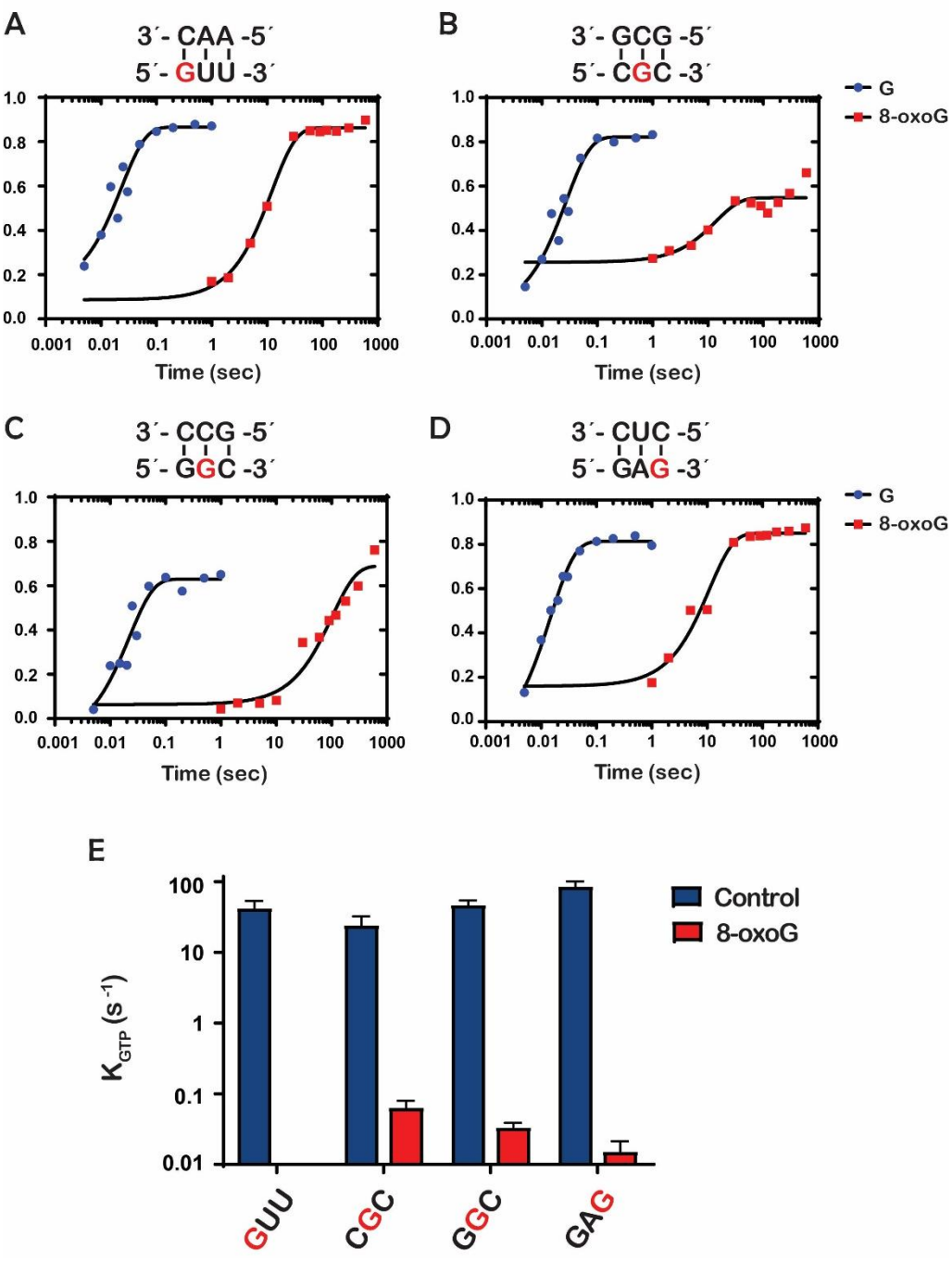

Figure 3.2: 8-oxoG inhibits GTP hydrolysis by EF-Tu
A-D) Representative time courses of GTP hydrolysis reactions between the indicated initiation and ternary complex (codon is shown at the bottom, while the anticodon is shown at the top). For each codon, time courses were performed in the presence of G (blue) or 8-oxoG (red) and the position of 8-oxoG within the codon is indicated in red. E) Bar graph showing the observed rate of GTP hydrolysis (k_{GTP}) for initiation complexes programmed with the indicated codon in the A site. 8-oxoG was introduced at the position depicted in red. Blue bars represent observed rates with unmodified complexes; red bars represent rates with 8-oxoG complexes. Plotted is the average of three independent experiments and the error bars represent the standard error of the mean.

We reacted the intact (CGC) complex and its oxidized counterpart ($C^{8oxo}GC$) with its cognate Arg-$tRNA^{Arg}$ ternary complex and every possible second-position-near-cognate ternary complex in the absence and presence of streptomycin or paromomycin. As expected, after 5 seconds of incubation, significant dipeptide formation was observed only in the presence of the cognate ternary complex for the intact CGC complex (Figure 3). Additionally, as we had reported earlier, the presence of 8-oxoG severely inhibited the formation of the cognate fMet-Arg dipeptide while increasing the incorporation of Leu-$tRNA^{Leu}$, for which the second position A of the anticodon base pairs with the 8-oxoG. The addition of antibiotics had no effect on the cognate reaction in the presence of intact mRNA. However, and as anticipated, the antibiotic significantly increased the formation of only the near-cognate fMet-His dipeptide. This is rationalized by the fact that $tRNA^{His}$ harbors U at the second position of its anticodon, which allows it to form a less deleterious wobble-base pair with the G of the mRNA's codon (52). Consistent with our model that 8-oxoG changes the decoding process in a manner resembling that of a near-cognate, the addition of antibiotics to the $C^{8oxo}GC$ complex increased the formation of fMet-Arg dipeptide and that of fMet-Leu. Interestingly, the antibiotics appear to have little to no effect on the reactivity of the $C^{8oxo}GC$ complex with His-$tRNA^{His}$. Together, these observations suggest that the effects of 8-oxoG on translation can be suppressed by antibiotics, but in a manner slightly distinct from a mismatch.

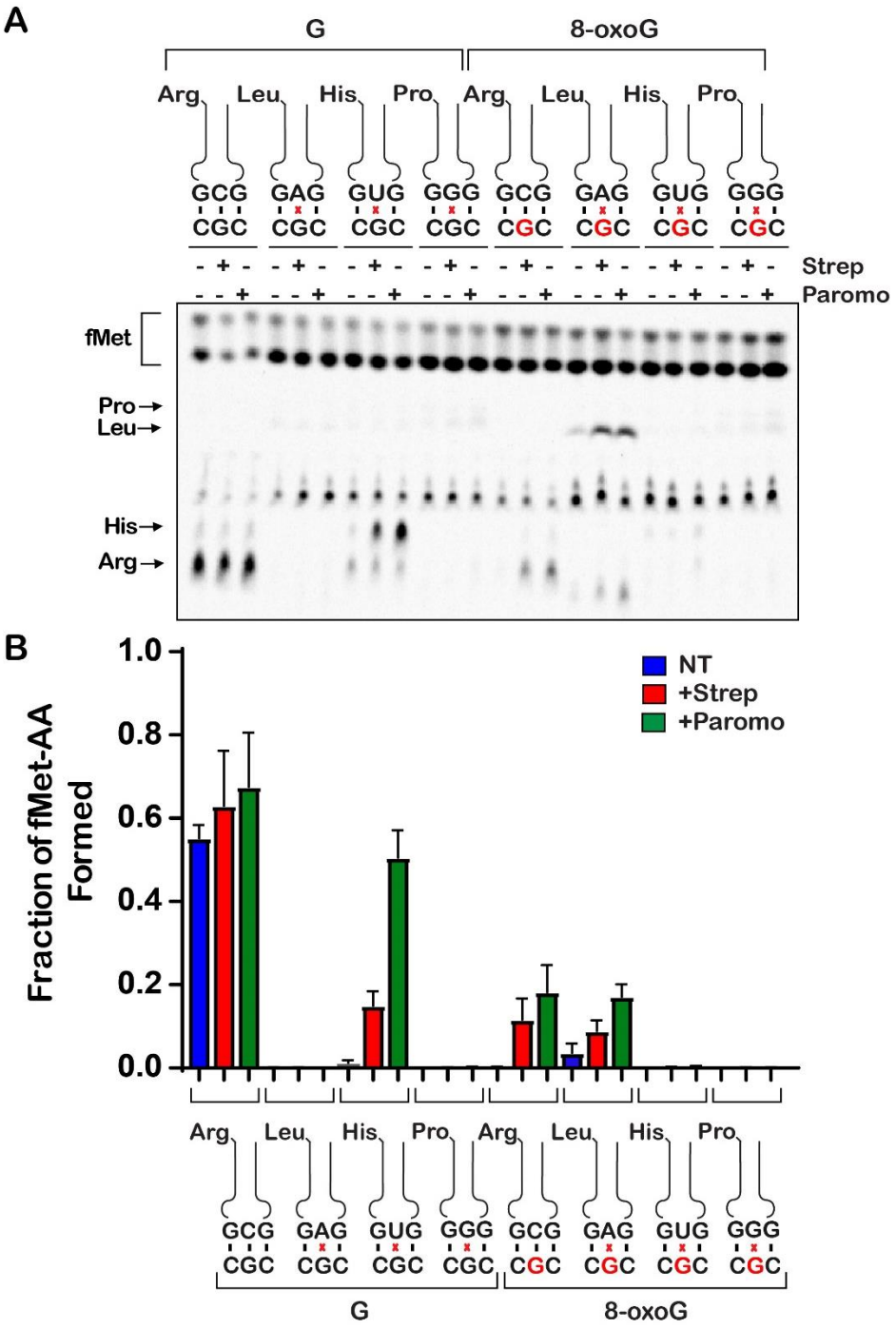

Figure 3.3: 8-oxoG in the second position of the codon changes the base pairing properties of guanosine on the ribosome

A) Phosphorimager scan of electrophoretic TLCs used to follow dipeptide-formation reactions (5-second incubation time) in the presence of the indicated initiation and ternary complexes in the absence and presence of the indicated antibiotics. B) Quantification of the dipeptide yield as performed in (A). Plotted is the average of three independent experiments and the error bars represent the standard deviations around the means.

To add more quantitative support for these differential reactivity profiles, we conducted full-time courses of the PT reactions in the absence and presence of streptomycin or paromomycin. Performing full-time courses allowed for us to measure the observed rate of peptide-bond formation (k_{pep}) which reports on the combined rates of aa-tRNA accommodation (k_5) and rejection (k_7), as well as the end point of each reaction (Fp), which reports on the effectiveness of proofreading (k_5 relative to k_{pep}) (9). In agreement with our end-point analysis, the antibiotics had little effect on the endpoints and the rate of the reactions between the native initiation complex and the cognate aa-tRNA (Figure 4A). This is in slight disagreement with previous reports showing that streptomycin reduces the rate of peptide bond formation for cognate reactions by approximately twofold (26, 53), whereas in our assays, streptomycin only slightly decreased these rates. We note that these earlier experiments utilized different buffer systems, for which the observed rate of peptide-bond formation in the presence of streptomycin is limited by GTP hydrolysis.

Interestingly, the addition of the antibiotics to the same reaction with the 8-oxoG-containing complex caused the observed rate of PT to increase twofold – we measured average rates of 0.0097 s^{-1}, 0.022 s^{-1}, and 0.049 s^{-1}in the absence of antibiotic and in the presence of streptomycin or paromomycin, respectively (Figure 4B). Additionally, the endpoint of the reactions increased by approximately an order of magnitude in the presence of the antibiotics, with measured Fp values of 0.027, 0.37, and 0.52 for no antibiotic, streptomycin, and paromomycin, respectively. Next, we performed reactions in the presence of the near-cognate aa-tRNAs. We started with the G•A mismatch reaction involving the Leu-$tRNA^{Leu}$ ternary complex. As our reactivity-survey assay indicated, the addition of antibiotics did not increase the rate or endpoint of PT with the intact complex but caused both to significantly increase for the oxidized complexes

(Figures 4C and 4D). For the G•G and 8-oxoG•G mismatches involving Pro-tRNA^{Pro} ternary complex, the addition of streptomycin had a barely detectable effect on the PT rate (Figures 4G and 4H). In contrast, the antibiotics increased the observed PT rate for the His-tRNA^{His}, which forms a wobble G•U mismatch with the mRNA, by more than an order of magnitude. Additionally, the Fp value for the same reaction increased by more than twofold as a result of antibiotic addition (Figure 4E). In contrast to the unmodified complex, His-tRNA^{His} failed to react with the 8-oxoG complex (Figure 4F). These observations suggest that the modification does not allow the mRNA to form a wobble base pair with U. Altogether, our findings suggest that oxidation of G changes the base-pairing preference for the modified nucleotides on the ribosome, likely due to its chemical nature as well as the geometry of the decoding center.

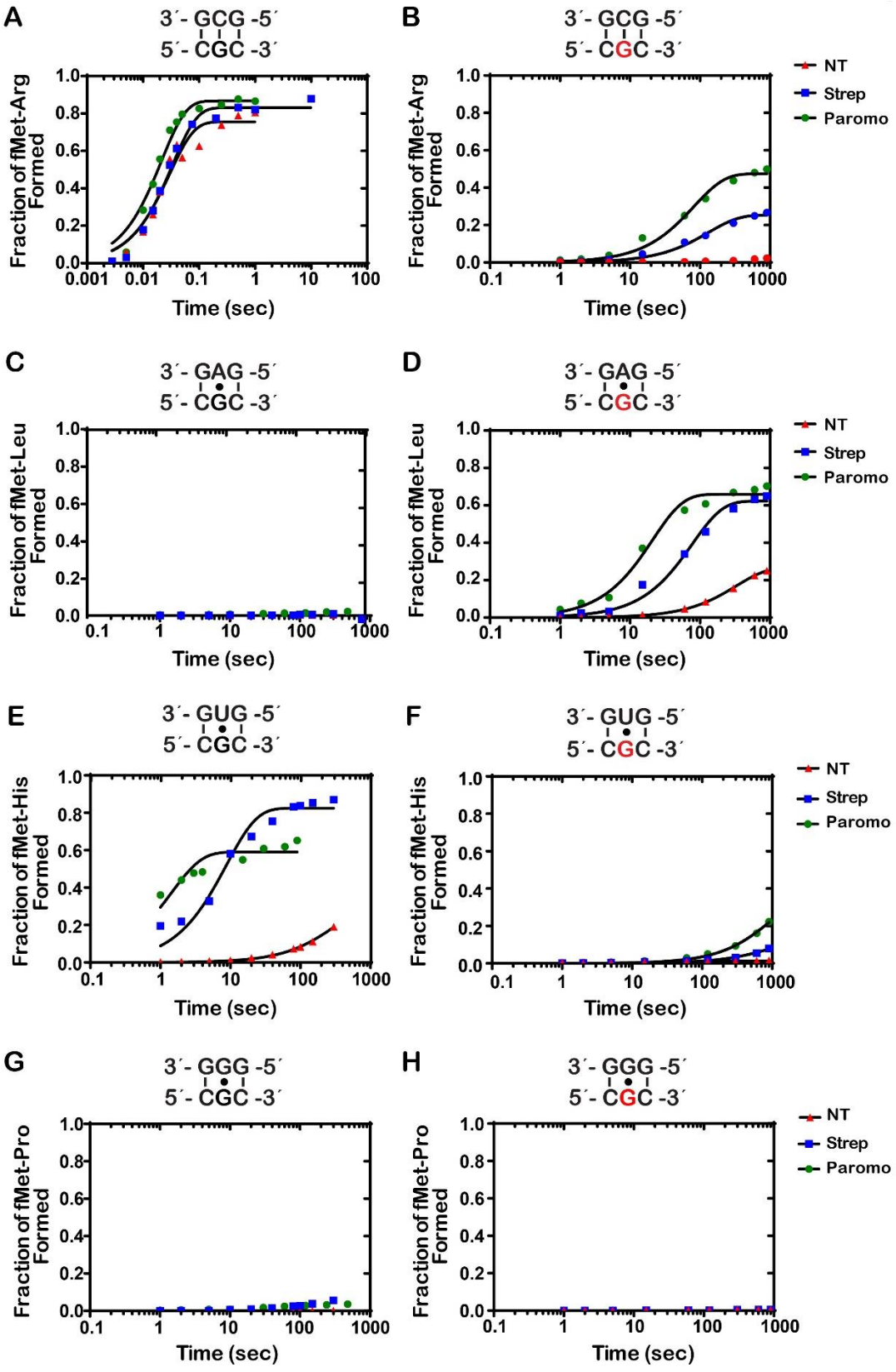
A
3′- GCG -5′
5′- CGC -3′
Fraction of fMet-Arg Formed
Time (sec)
B
3′- GCG -5′
5′- CGC -3′
Fraction of fMet-Arg Formed
Time (sec)
NT
Strep
Paromo
C
3′- GAG -5′
5′- CGC -3′
Fraction of fMet-Leu Formed
Time (sec)
D
3′- GAG -5′
5′- CGC -3′
Fraction of fMet-Leu Formed
Time (sec)
NT
Strep
Paromo
E
3′- GUG -5′
5′- CGC -3′
Fraction of fMet-His Formed
Time (sec)
F
3′- GUG -5′
5′- CGC -3′
Fraction of fMet-His Formed
Time (sec)
NT
Strep
Paromo
G
3′- GGG -5′
5′- CGC -3′
Fraction of fMet-Pro Formed
Time (sec)
H
3′- GGG -5′
5′- CGC -3′
Fraction of fMet-Pro Formed
Time (sec)
NT
Strep
Paromo

Figure 3.4: The addition of antibiotics increases the k_{pep} and Fp for cognate and a subset of near-cognate tRNAs in the presence of 8-oxoG at the second position of the codon
A-H) Representative time courses of peptide-bond-formation reactions between the indicated initiation and ternary complexes in the absence and presence of the indicated antibiotics. The time courses shown on the right panel were carried out with the unmodified complex, whereas ones shown on the left panel were carried out with the modified complex (8-oxoG drawn in red). Time courses were conducted at least in duplicates. We note that the observed rates varied from experiment to experiment due to differences in different preparation of aa-tRNA in the tRNA mix; the fold difference as a result of antibiotic addition, however, was reproducible.

To provide further support for our model that antibiotics can suppress the effect of 8-oxoG on decoding, we tested another set of complexes that displayed a different codon in the A site. In particular, we programmed ribosomes with the oxidized $G^{8oxo}GC$ codon and tested their reactivity with the cognate Gly-$tRNA^{Gly}$ and near-cognate Val-$tRNA^{Val}$ ternary complexes. Similar to what we observed for the $G^{8oxo}GC$ complex, both streptomycin increased the rate of peptide-bond formation significantly (Supplementary Figure S1). These observations suggest that aminoglycosides suppress the effect of the modification independent of the codon identity.

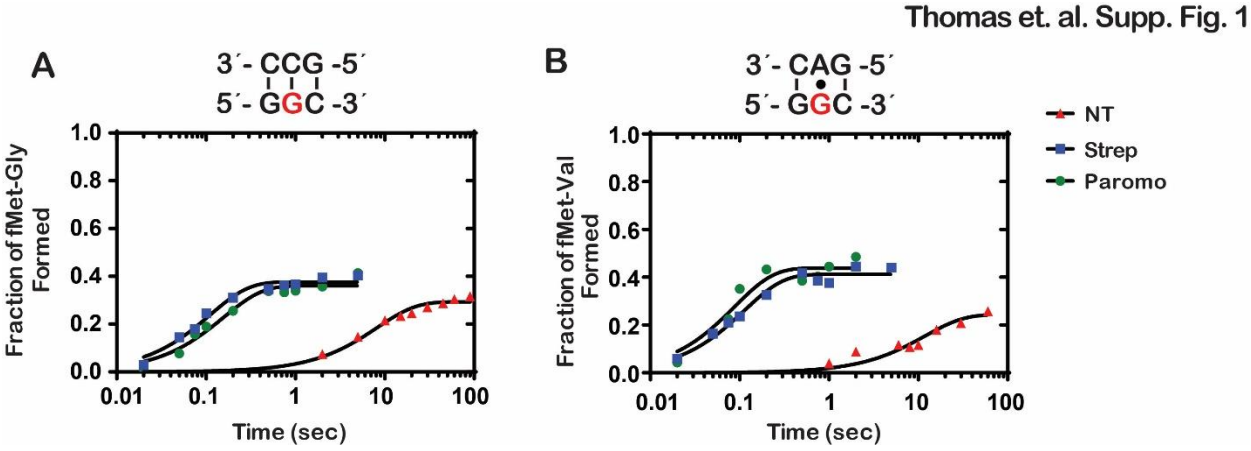

Supplementary Figure 3.S1: Streptomycin and paromomycin suppress the effects of 8-oxoG on k_{pep} for a complex displaying the $G^{8oxo}GC$ codon in the A site
A-B) Time courses of peptide-bond formation between the indicated initiation and ternary complexes either in the absence of antibiotics or in the presence of paromomycin or streptomycin.

The base-pairing preferences of 8-oxoG at the first position of the codon are slightly different from those observed at the second position

Our data thus far shows that when 8-oxoG is in the second position of a codon, it changes the base-pairing preferences of G on the ribosome. In order to investigate if the base-pairing preferences of 8-oxoG that we observed were specific to the second position, we performed the same peptidyl-transfer experiments with a codon containing 8-oxoG at the first position. We reacted the complex containing intact codon (GUU) and the complex containing the 8-oxoG codon ($^{8\text{-oxo}}$GUU) with the cognate Val-tRNA^{Val}, as well as all possible first-position-near-cognate aa-tRNAs in the presence of paromomycin or streptomycin. Once again, after 5 seconds of incubation with no antibiotic, significant amount of dipeptide was formed exclusively in the presence of the cognate ternary complex for the GUU codon, and the presence of 8-oxoG substantially decreased the formation of the cognate dipeptide (Figure 5). However, at this position and after 5 seconds of incubation, 8-oxoG did not result in any observable increase in the reactivity of the initiation complex with Phe-tRNA^{Phe}, which has an A at the third position of the anticodon (Figure 5). This is contrary to what we observed in the second position, where dipeptide is formed in the presence of the 8-oxoG•A base pair without the addition of antibiotics (Figure 3). We note that our source of the tRNA mix often contained low levels of charged tRNAs, even after extensive attempts at deacylation. Therefore, we observed some residual reactivity with the cognate Val-tRNA^{Val} in reactions containing the near-cognate tRNAs such as Phe-tRNA^{Phe}, but that did not affect our quantification since the two peptides migrate differently on our TLCs, allowing us to distinguish them.

Upon addition of antibiotics, we observed significant increases in dipeptide formation for the intact codon with two of the three near-cognate aa-tRNAs, namely Phe-tRNA^{Phe} and Ile-

$tRNA^{Ile}$, for which the third position of the anticodon is an A and a U, respectively. This differs from what we observed for the second-position mismatches, for which the addition of antibiotics increased the dipeptide formation only for the near-cognate tRNA with the G•U base pair. When we add the antibiotics to the reactions containing the 8-oxoG codon, we observe an increase in the incorporation of Val-$tRNA^{Val}$ and Phe-$tRNA^{Phe}$, for which the first position of the anticodon is a C and A, respectively. This is similar to what we observe for 8-oxoG in the second position of the codon. In both the first and second position of the codon, our data shows that 8-oxoG base pairs with adenosine as well as cytidine when tRNA selection is relaxed, suggesting that it is able to adopt both the *syn* or *anti* conformation on the ribosome.

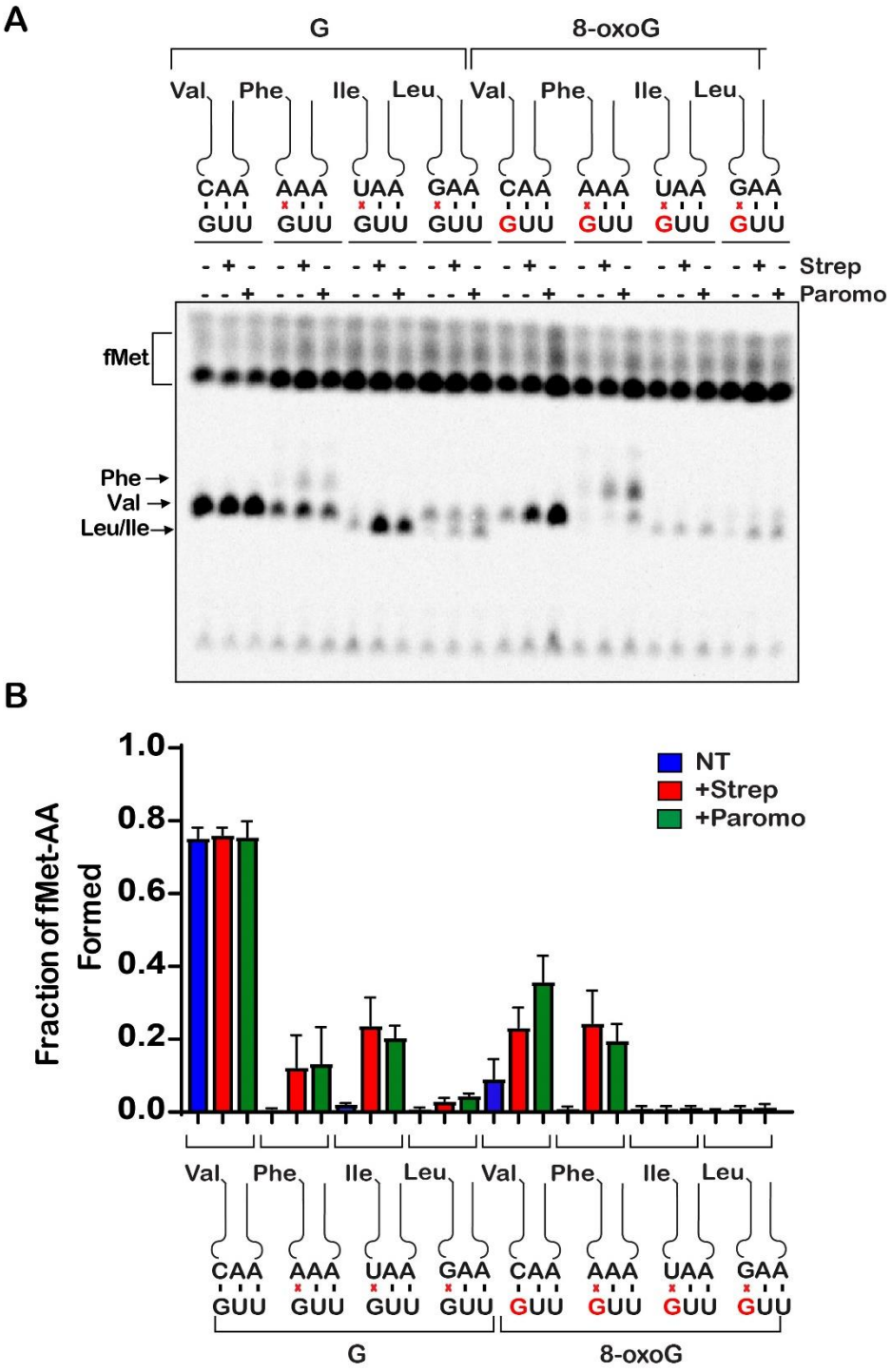

Figure 3.5: Antibiotics suppress the effects of 8-oxoG in the first position of the codon
A) Phosphorimager scan of electrophoretic TLCs used to follow dipeptide-formation reactions (5-second incubation time) in the presence of the indicated initiation and ternary complexes in the absence and presence of the indicated antibiotics. B) Quantification of the dipeptide yield as performed in (A). Plotted is the average of three independent experiments and the error bars represent the standard deviations around the means.

Again, to provide additional quantitative support for our reactivity profiles, we performed full-time courses of the PT reactions in the absence and presence of the aminoglycoside antibiotics. As expected, the addition of the antibiotics had no significant effect on the reaction of the intact GUU codon with the cognate Val-tRNA^{Val} (Figure 6A). We measured rates of 31 s^{-1}, 21 s^{-1}, and 25 s^{-1} and Fp values of 0.69, 0.72, and 0.73 for the no treatment, streptomycin, and paromomycin conditions, respectively. For the reactions between near-cognate Phe-tRNA^{Phe} and Ile-tRNA^{Ile} with the intact complex (G•A and G•U mismatches, respectively), the addition of antibiotics was found to result in an increase in the endpoint, but not the rate (Figures 6C and 6E). This is in direct contrast to what we observed for mismatches at the second position, for which the addition of the antibiotics substantially increased the rate and endpoint of PT for the G•U base pair only and no other mismatches (Figures 4E and 4C), consistent with the observations that decoding at the second position appears to be more stringent relative to that at the first one (34).

For the 8-oxoG-containing codon, we measured a rate and endpoint with Val-tRNA^{Val} (8-oxoG•C base pair) of 0.044 s^{-1} and 0.308, respectively. Both of these values are much higher than those measured for Phe-tRNA^{Phe} (8-oxoG•A mismatch); k_{pep} of 0.018 s^{-1} and Fp of 0.11 (Figures 6B, 6D). This differs from what we observed with 8-oxoG in the second position, where the rate and endpoint were higher for the reaction involving an 8oxoG•A interaction relative to the 8-oxoG•C (Figures 4B and 4D). These observations could be explained by at least two scenarios: 1) the frequency of rotation of 8-oxoG around its glycosidic bond might be different depending on its position within the codon; 2) the rate of dissociation of Phe-tRNA^{Phe} from the 8-oxoGUU complex is slow, when 8-oxoG is in the *syn* conformation, allowing the tRNA to sample the *anti* conformation to form a Watson-Crick base pair and proceed with tRNA selection. Interestingly, the 8-oxoG•A Phe-tRNA^{Phe} reaction was found to benefit much more from the addition of

antibiotics relative to the 8-oxoG•C Val-tRNA^{Val} reaction. For the Val-tRNA^{Val} reaction (8-oxoG•C base pair), the observed rate and endpoint increased by a mere twofold to fourfold in the presence of streptomycin and paromomycin (Figure 4B). In contrast, in the presence of Phe-tRNA^{Phe} (8-oxoG•A base pair), the observed rate increased by more than an order of magnitude and the endpoint increased by approximately sixfold (Figure 4D). These observations are consistent with the second scenario, whereby 8-oxoG prefers the *syn* conformation in the decoding center, but the addition of antibiotics stabilizes the tRNA long enough to allow it to sample the *anti* conformation. If the tRNA harbors a C at that position, the selection process can proceed.

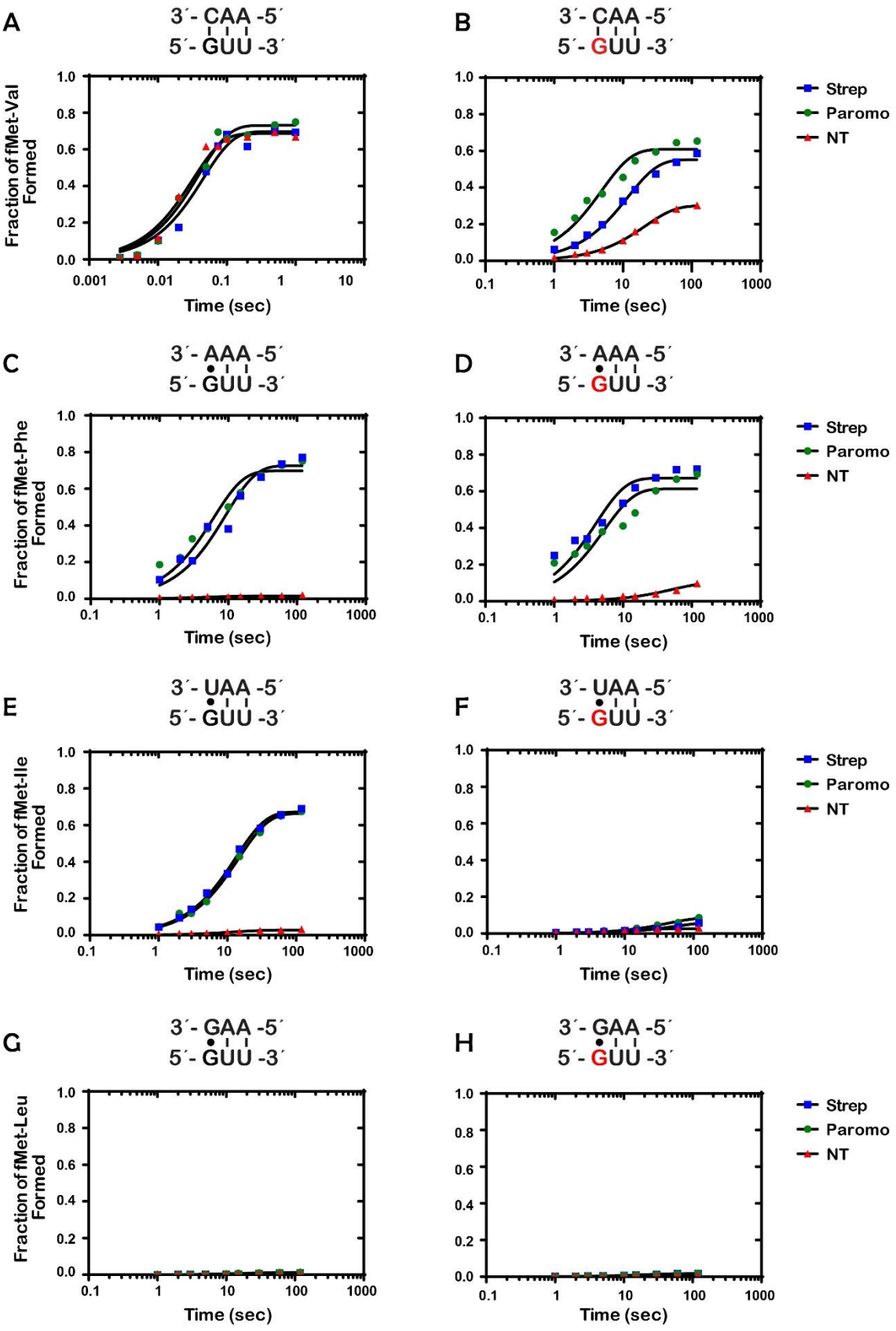
A
3´- CAA -5´
5´- GUU -3´
Fraction of fMet-Val Formed
Time (sec)
B
3´- CAA -5´
5´- GUU -3´
Strep
Paromo
NT
Time (sec)
C
3´- AAA -5´
5´- GUU -3´
Fraction of fMet-Phe Formed
Time (sec)
D
3´- AAA -5´
5´- GUU -3´
Strep
Paromo
NT
Time (sec)
E
3´- UAA -5´
5´- GUU -3´
Fraction of fMet-Ile Formed
Time (sec)
F
3´- UAA -5´
5´- GUU -3´
Strep
Paromo
NT
Time (sec)
G
3´- GAA -5´
5´- GUU -3´
Fraction of fMet-Leu Formed
Time (sec)
H
3´- GAA -5´
5´- GUU -3´
Strep
Paromo
NT
Time (sec)

Figure 3.6: Antibiotics drastically increase k_{pep} and Fp for reactions between the ^{8oxo}GUU complex with Phe-tRNA^{Phe} (8-oxoG•A base pair), and only slightly for reactions with Val-tRNA^{Val} (8-oxoG•C)

A-H) Representative time courses of peptide-bond-formation reactions between the indicated initiation and ternary complexes (codon is shown at the bottom, while the anticodon is shown at the top) in the absence and presence of the indicated antibiotics. The time courses shown on the right panel were carried out with the unmodified complex, whereas ones shown on the left panel were carried out with the modified complex (8-oxoG drawn in red). Time courses were conducted at least in duplicates; the fold difference as a result of antibiotic addition was reproducible.

Error-prone and hyperaccurate ribosomes suppress and exaggerate the effects of 8-oxoG on decoding, respectively

To provide further support for our model that altering tRNA selection parameters changes the effect of 8-oxoG on decoding independent of drug addition, we utilized error-prone as well as hyperaccurate ribosome mutants and assessed their effect on PT in the presence of 8-oxoG. We chose the well-studied *rpsD12* and *rpsL141* mutants as representatives for the error-prone and hyperaccurate types, respectively (54). As expected, the mutations had no effect on the observed PT rate or endpoints for the intact complex in the presence of the cognate aa-tRNA (Figure 7A). In contrast, and in agreement with our model, in the presence of 8-oxoG the error-prone mutation increased the observed rate of formation of fMet-Arg dipeptide by sevenfold, whereas the hyperaccurate decreased it by approximately fourfold (Figure 7B). Similarly, and consistent with their effect on decoding, the error-prone mutation slightly increased the observed PT rate for the near-cognate (G•A base pair), whereas the hyperaccurate one slightly decreased the rate (Figure 7C). In the presence of 8-oxoG, the hyperaccurate mutation suppressed the modification-induced misincorporation of Leu-tRNA^{Leu} (8-oxoG•A base pair), for which we observe an almost ninefold decrease in the observed PT rate, while the error-prone mutation increased the misincorporation by fivefold (Figure 7D). These effects of ribosome mutations on peptide-bond formation in the presence of 8-oxoG appear not to depend on the identity of the codon. We measure similar effects

on complex programmed with the $G^{8oxo}GC$ codon (Supplementary Figure S2). Interestingly, for both the no antibiotic and antibiotic treatments, the endpoints for PT reactions involving the 8oxoG•A interactions were at least twofold relative to those measured for ones involving the 8oxoG•C base pairs (Figure 7B and 7D). Collectively our data utilizing drug- as well as mutation-induced alteration of the tRNA-selection process support our model that 8-oxoG can base pair in either the *syn* or *anti* conformation in the context of the A site, with a preference for the *syn* conformation. Additionally, our data shows that 8-oxoG disrupts the ability of guanosine to mispair with uridine, suggesting that the lesion modifies the conformation in which guanosine can miscode.

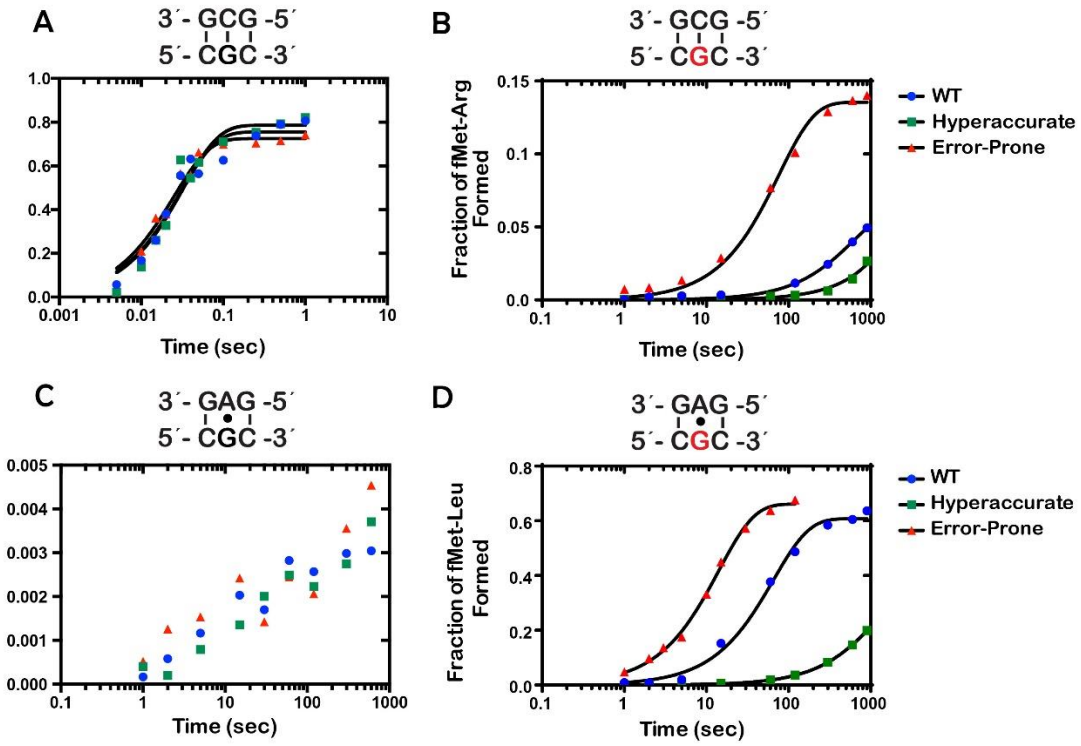

Figure 3.7: Hyperaccurate and error-prone ribosomes suppress and amplify the effects of 8-oxoG, respectively

A-D) Representative time courses of peptide-bond formation between the indicated initiation and ternary complexes with the depicted ribosome mutant. The time courses shown on the right panel were carried out with the unmodified complex, whereas ones shown on the left panel were carried out with the modified complex (8-oxoG drawn in red). Time courses were conducted at least in duplicates for constructs containing 8-oxoG; the fold difference was reproducible.

DISCUSSION

Recent reports from a number of groups have shown that modification of the mRNA occurs at levels that could potentially affect its function (33). Emerging from these studies are the observations that ribosomal function as well as the decoding process could be significantly altered as a consequence of these modifications. For some adducts, such as m^6A which are deliberately modified by cellular enzymes, the modifications appear to play roles in regulating gene expression (55). In contrast, for most unintended adducts, like those that result from chemical damage, the modifications are a burden to the translation machinery and pose challenges to the speed and accuracy of the ribosome. We previously chose to study the effects of the oxidized base 8-oxoG due to its high prevalence, especially under certain conditions, as well as its unique chemical properties (40–43). Introducing the adduct to the mRNA, regardless of its position within the A-site codon, slowed down PT significantly. Previous studies regarding the impact of 8-oxoG on DNA replication show that the modification can increase C to A transversions by preferentially mispairing with A (56). Interestingly, 8-oxoG was found to only slightly increase misincorporation of near-cognate aa-tRNAs during translation. These findings suggested that 8-oxoG interfered with tRNA selection. Here, we expanded on these studies by characterizing the mechanism by which 8-oxoG affects the decoding process. A priori, we hypothesized that base-pairing interaction with the modified nucleotide resembles a mismatch. As a result, 8-oxoG fails to trigger the required conformational changes in the decoding center to proceed through the tRNA selection process. Consistent with this proposal, we find the modification to severely inhibit GTP hydrolysis by EF-Tu, suggesting that it affects the initial phase of the selection process (Figure 2). Furthermore, the introduction of miscoding antibiotics or ribosomes with error-prone mutations was found to partially rescue the effect of the modification, as would be expected if 8-oxoG•C and 8-oxoG•A

base pairs were to resemble mismatches. Indeed, when we add the antibiotics to the reactions of intact codons and near-cognate aa-tRNAs, we see similar increases in k_{pep} and/or Fp.

While the 8-oxoG•C and 8-oxoG•A base pairs resemble mismatches in both the first and second position of the codon, we observe that 8-oxoG has distinct base pairing preferences based on its position within the codon. In the absence of antibiotics, 8-oxoG in the second position prefers to base pair with A, while 8-oxoG in the first position prefers to base pair with C (Figures 4 and 6). Structural studies of the A site show that the interactions between the second position codon and its corresponding anticodon are monitored by the universally conserved A-minor interactions of A1492, as well as G530 of the 16S rRNA and S50 of the ribosomal protein S12. Meanwhile, the interactions between the first position codon and its corresponding anticodon are only monitored by the A-minor interactions of A1493. Monitoring at both positions work to ensure that only Watson-Crick base pairs are recognized as acceptable interactions (20, 21, 57). We speculate that the bulky conformation of the *anti*-8-oxoG•C base pair is not recognized as an acceptable interaction in the highly-monitored second position, thus explaining why we observe a preference for the *syn*-8oxoG•A. Alternatively, the *anti* conformation of the modified base might be very short lived that during codon recognition tRNAs harboring a C at the second position dissociate before they can sample it. In the less stringently monitored first position, we observed a preference for the *anti*-8-oxoG•C base pair in the absence of antibiotics, which could be explained by decreased dissociation rates for near-cognate tRNAs at this position (58).

Upon addition of antibiotics, the average k_{pep} and Fp for the 8oxoG•A in the first position exceeded that of 8-oxoG•C, more closely resembling the trends we observe in the second position of the codon (Figures 4 and 6). Additionally, we observe higher k_{pep} and/or Fp values for 8oxoG•A than 8-oxoG•C in the presence of error-prone ribosomes. Previous studies have shown that 8-oxoG

prefers to exist in the *syn* conformation because of steric repulsion between the 8-oxo and the phosphate backbone (43). This is consistent with our model that 8-oxoG primarily exists in the *syn* conformation on the ribosome, and under normal conditions, is recognized as a mismatch when it base pairs with A and is rejected during codon recognition. When error-prone conditions, which suppress the effect of mismatches, are introduced in this case, the 8oxoG(syn)•A base pair can move through codon recognition and into proofreading, and its Fp values are almost restored to those observed in the presence of a G•U base pair (Figure 7). We speculate that 8-oxoG does not exist in the *anti* conformation as frequently, but upon addition of antibiotics, the codon-anticodon interaction is stabilized long enough to allow for the 8-oxoG to change from the *syn* to the *anti* conformation and proceed with codon recognition.

The hypothesis that 8-oxoG primarily exists in the *syn* conformation on the ribosome is also supported by its ability to disrupt base pairing with U. We observe significant reductions in k_{pep} and/or Fp values in the presence of an 8-oxoG•U base pair in error-prone conditions compared to G•U, regardless of its position within the codon (Figures 4E, 4F, 6E, and 6F). This was a surprising observation because the G•U wobble conformation should not be disrupted by the introduction of the oxygen at carbon 8; therefore, we expected to see an increase in 8-oxoG•U mispairing in the presence of antibiotics. In order to form a wobble base pair with U, 8-oxoG needs to be in the *anti* conformation (52). We speculate that the inability of the antibiotics to increase miscoding in the presence of 8-oxoG•U is due to 8-oxoG primarily existing in the *syn* conformation on the ribosome. Additionally, we cannot exclude the possibility that the 8-oxoG•U wobble base pair is structurally unfavorable in the A site; however, further studies would need to be performed to test this hypothesis.

Interestingly, circular dichroism (CD) analysis of RNA duplexes suggest that 8-oxoG modification has little to no effect on the geometry of the A helix adopted by the RNA (59). Similarly, X-ray and NMR analysis of DNA duplexes harboring 8-oxodG•dA or 8-oxodG•dC revealed little to no distortion of the helical structure of the molecule (60–62). However, thermal stability analysis of short modified RNAs shows that the lesion decreases the melting temperature of the 8-oxoG•C duplex by as much as 10°C relative to G•C suggesting that there are energetic penalties associated with this base pair (63). The 8-oxoG•A base pair, in contrast, is significantly stabilized relative to the G•A base pair. Even with this increased stability, the Tm of duplexes containing the 8-oxoG•A base pairs is on average 5°C lower than that of the canonical G•C base pair. These observations suggest that even though the geometry of the 8-oxoG•A base pair is not likely to change the overall structure of the codon-anticodon helix, the energetics of the interaction between the mRNA and tRNA is not as favorable as would be expected for a cognate one.

In comparison to the ribosome, DNA polymerases display varying efficiencies for incorporating dCMP or dAMP opposite to 8-oxodG dependent on the type of the polymerase. For example, replicative polymerases incorporate dCMP across 8-oxodG with frequencies ranging from 1:14 to 90:1 relative to dAMP incorporation (44). In addition, these polymerases are more efficient at extending beyond the lesion when 8-oxodG is base paired with dA relative to dC, suggesting that the polymerases tolerate the mispair presumably due to its similarity to Watson-Crick base pairs. Indeed, structural analysis of DNA polymerases bound with modified primer-template complexes rationalized some of these observed effects on the accuracy of DNA replication as well as the variation in the efficiencies of misincorporation rates (64–66). These studies revealed that both base pairs are accommodated in the active site of the polymerases, but their conformations as well as their interactions with the side chains of the proteins are dependent

on the identity of the protein. For instance, in the case of T7 DNA polymerase, the 8-oxodG•A base pair adopts a geometry nearly identical to that of a Watson-Crick base pair, rationalizing the ability of the mispair to escape the proofreading function of the enzyme (67). In contrast to replicative polymerases, translesion enzymes, like those used to replicate over thymine dimers, tend to be relatively more accurate (68). At a structural level, this can be explained by the slightly larger active site employed by these enzymes to allow access for large adduct, which in turn allows for the formation of the 8-oxodG•C base pair. Although we lack equivalent structural data of the ribosome bound to 8-oxoG-containing mRNA, our data suggests that either base pair can form under normal conditions with a preference for 8-oxoG to base pair with A. However, the geometry of the base pair is slightly distorted such that it fails to trigger the required conformational changes, even in the presence of miscoding antibiotics. Furthermore, we hypothesize that the *anti* conformation of 8-oxoG, which is required for base pairing with C, rapidly rotates to the preferred *syn* conformation before EF-Tu is activated. In the presence of the antibiotic, the cognate tRNA is stabilized long enough for the adduct to adopt the canonical *anti* conformation, activating EF-Tu, and in doing so, suppressing the effect of the modification on tRNA selection.

The ability of ribosomes to bypass oxidative lesions, such as 8oxoG, may serve as an advantage under oxidative stress conditions. Previous data from our group showed that the presence of 8-oxoG can cause ribosomal stalling and activation of No-Go Decay pathways (42). This stalling generates incomplete peptides that are recognized as such and degraded through proteolysis. In the presence of error-prone ribosomes, we observe increased decoding of the 8-oxoG adduct as either a G or U. Previous work has shown that the ability of error-prone ribosomes to generate mistranslated proteins rather than stall may serve as a signal for the activation of stress response pathways *in vivo* (69). Indeed, *E. coli* that expressed error-prone ribosomes were better

able to survive hydrogen peroxide treatment than those expressing wild-type ribosomes. Interestingly, natural *E. coli* vary over 10-fold in their mistranslation rates, suggesting that miscoding is either tolerated or selected for in certain environments (70). The tendency towards error-prone translation in the presence of oxidative damage, such as 8-oxoG, may serve as an important adaptive mechanism through which cells tolerate high-stress environments.

ACKNOWLEDGMENTS

We thank members of the H.S.Z. laboratory for useful discussions on earlier versions of this manuscript.

FUNDING

This work was supported by the National Institutes of Health [R01GM112641 to H.S.Z.].

REFERENCES

1. Zaher,H.S. and Green,R. (2009) Fidelity at the Molecular Level: Lessons from Protein Synthesis. *Cell*, **136**, 746–762.

2. Rodnina,M. V., Gromadski,K.B., Kothe,U. and Wieden,H.J. (2005) Recognition and selection of tRNA in translation. *FEBS Lett.*, **579**, 938–942.

3. Thompson,R.C. (1988) EFTu provides an internal kinetic standard for translational accuracy. *Trends Biochem. Sci.*, **13**, 91–93.

4. Rodnina,M. V, Fricke,R., Kuhn,L. and Wintermeyer,W. (1995) Codon-dependent conformational change of elongation factor Tu preceding GTP hydrolysis on the ribosome. *EMBO J.*, **14**, 2613–9.

5. Liu,W., Chen,C., Kavaliauskas,D., Knudsen,C.R., Goldman,Y.E. and Cooperman,B.S. (2015) EF-Tu dynamics during pre-translocation complex formation: EF-Tu·GDP exits the ribosome via two different pathways. *Nucleic Acids Res.*, **43**, 9519–9528.

6. Villa,E., Sengupta,J., Trabuco,L.G., LeBarron,J., Baxter,W.T., Shaikh,T.R., Grassucci,R.A., Nissen,P., Ehrenberg,M., Schulten,K., *et al.* (2009) Ribosome-induced changes in elongation factor Tu conformation control GTP hydrolysis. *Proc. Natl. Acad. Sci.*, **106**, 1063–1068.

7. Hopfield,J.J. (1974) Kinetic proofreading: a new mechanism for reducing errors in biosynthetic processes requiring high specificity. *Proc. Natl. Acad. Sci. U. S. A.*, **71**, 4135–9.

8. Ninio,J. (1975) Kinetic amplification of enzyme discrimination. *Biochimie*, **57**, 587–595.

9. Pape,T., Wintermeyer,W. and Rodnina,M. (1999) Induced fit in initial selection and proofreading of aminoacyl-tRNA on the ribosome. *EMBO J.*, **18**, 3800–3807.

10. Johansson,M., Bouakaz,E., Lovmar,M. and Ehrenberg,M. (2008) The Kinetics of Ribosomal Peptidyl Transfer Revisited. *Mol. Cell*, **30**, 589–598.

11. Gromadski,K.B. and Rodnina,M. V. (2004) Kinetic Determinants of High-Fidelity tRNA Discrimination on the Ribosome. *Mol. Cell*, **13**, 191–200.

12. Rosenberger,R.F. and Foskett,G. (1981) An estimate of the frequency of in vivo transcriptional errors at a nonsense codon in Escherichia coli. *Mol. Gen. Genet.*, **183**, 561–3.

13. Edelmann,P. and Gallant,J. (1977) Mistranslation in E. coli. *Cell*, **10**, 131–137.

14. Bouadloun,F., Donner,D. and Kurland,C.G. (1983) Codon-specific missense in vivo. *Embo J*, **2**, 1351–1356.

15. E.B.,K. and P.J.,F. (2007) The frequency of translational misreading errors in E. coli is largely determined by tRNA competition. *Rna*, **13**, 87–96.

16. Clemons,W.M., May,J.L.C., Wimberly,B.T., McCutcheon,J.P., Capel,M.S. and Ramakrishnan,V. (1999) Structure of a bacterial 30S ribosomal subunit at 5.5 Å resolution. *Nature*, **400**, 833–840.

17. Loveland,A.B., Demo,G., Grigorieff,N. and Korostelev,A.A. (2017) Ensemble cryo-EM elucidates the mechanism of translation fidelity. *Nature*, **546**, 113–117.

18. Fislage,M., Zhang,J., Brown,Z.P., Mandava,C.S., Sanyal,S., Ehrenberg,M. and Frank,J. (2018) Cryo-EM shows stages of initial codon selection on the ribosome by aa-tRNA in ternary complex with GTP and the GTPase-deficient EF-TuH84A. *Nucleic Acids Res.*, **46**, 5861–5874.

19. Valle,M., Sengupta,J., Swami,N.K., Grassucci,R.A., Burkhardt,N., Nierhaus,K.H., Agrawal,R.K. and Frank,J. (2002) Cryo-EM reveals an active role for aminoacyl-tRNA in the accommodation process. *EMBO J.*, **21**, 3557–3567.

20. Wimberly,B.T., Carter,A.P., Clemons,W.M., Brodersen,D.E., Morgan-Warren,R.J., Ramakrishnan,V., Vonrhein,C. and Hartsch,T. (2000) Structure of the 30S ribosomal subunit. *Nature*, **407**, 327–339.

21. Ogle,J.M., Murphy IV,F. V., Tarry,M.J. and Ramakrishnan,V. (2002) Selection of tRNA by the ribosome requires a transition from an open to a closed form. *Cell*, **111**, 721–732.

22. Schmeing,T.M., Voorhees,R.M., Kelley,A.C., Gao,Y.-G., Murphy,F.V.I., Weir,J.R. and Ramakrishnan,V. (2009) The Crystal Structure of the Ribosome Bound to EF-Tu and Aminoacyl-tRNA. *Science (80-.).*, **326**, 688–695.

23. Thompson,R.C. and Stone,P.J. (1977) Proofreading of the codon-anticodon interaction on ribosomes (Escherichia coli/protein synthesis/GTP hydrolysis/polypeptide elongation factor Tu). *Biochemistry*, **74**, 198–202.

24. Pape,T., Wintermeyer,W. and Rodnina,M. V. (2000) Conformational switch in the decoding region of 16S rRNA during aminoacyl-tRNA selection on the ribosome. *Nat. Struct. Biol.*, **7**, 104–107.

25. Ramakrishnan,V., Carter,A.P., Clemons,W.M., Brodersen,D.E., Morgan-Warren,R.J. and Wimberly,B.T. (2000) Functional insights from the structure of the 30S ribosomal subunit and its interactions with antibiotics. *Nature*, **407**, 340–348.

26. Gromadski,K.B. and Rodnina,M. V. (2004) Streptomycin interferes with conformational coupling between codon recognition and GTPase activation on the ribosome. *Nat. Struct. Mol. Biol.*, **11**, 316–322.

27. Demirci,H., Iv,F.M., Murphy,E., Gregory,S.T. and Albert,E. (2013) A structural basis for streptomycin-induced misreading of the genetic code. *Nat. Commun.*, 10.1038/ncomms2346.A.

28. Anderson,W.F., Gorini,L. and Breckenridge,L. (2006) Role of ribosomes in streptomycin-activated suppression. *Proc. Natl. Acad. Sci.*, **54**, 1076–1083.

29. Ozaki,M., Mizushima,S. and Nomura,M. (1969) Identification and functional characterization of the protein controlled by the streptomycin-resistant locus in E. coli. *Nature*, **222**, 333–9.

30. Rosset,R. and Gorini,L. (1969) A ribosomal ambiguity mutation. *J. Mol. Biol.*, **39**, 95–112.

31. Andersson,D.I. and Kurland,C.G. (1983) Ram ribosomes are defective proofreaders. *MGG Mol. Gen. Genet.*, **191**, 378–381.

32. Zaher,H.S. and Green,R. (2010) Hyperaccurate and Error-Prone Ribosomes Exploit Distinct Mechanisms during tRNA Selection. *Mol. Cell*, **39**, 110–120.

33. Roundtree,I.A., Evans,M.E., Pan,T. and He,C. (2017) Dynamic RNA Modifications in Gene Expression Regulation. *Cell*, **169**, 1187–1200.

34. Hudson,B.H. and Zaher,H.S. (2015) O6-Methylguanosine leads to position-dependent effects on ribosome speed and fidelity. *Rna*, **21**, 1648–1659.

35. Choi,J., Ieong,K.W., Demirci,H., Chen,J., Petrov,A., Prabhakar,A., O'Leary,S.E., Dominissini,D., Rechavi,G., Soltis,S.M., *et al.* (2016) N6-methyladenosine in mRNA disrupts tRNA selection and translation-elongation dynamics. *Nat. Struct. Mol. Biol.*, **23**, 110–115.

36. Karijolich,J. and Yu,Y.T. (2011) Converting nonsense codons into sense codons by targeted pseudouridylation. *Nature*, **474**, 395–399.

37. Fernández,I.S., Ng,C.L., Kelley,A.C., Wu,G., Yu,Y.T. and Ramakrishnan,V. (2013) Unusual base pairing during the decoding of a stop codon by the ribosome. *Nature*, **500**, 107–110.

38. Wurtmann,E.J. and Wolin,S.L. (2009) RNA under attack: Cellular handling of RNA damage RNA under attack: Cellular handling of RNA damage E. J. Wurtmann et.al. *Crit. Rev. Biochem. Mol. Biol.*, **44**, 34–49.

39. Finkel,T. and Holbrook,N.J. (2000) Oxidants, oxidative stress and the biology of ageing. *Nature*, **408**, 239–47.

40. Shan,X. and Lin,C. liang G. (2006) Quantification of oxidized RNAs in Alzheimer's disease. *Neurobiol. Aging*, **27**, 657–662.

41. Hofer,T., Badouard,C., Bajak,E., Ravanat,J.L., Mattsson,Å. and Cotgreave,I.A. (2005) Hydrogen peroxide causes greater oxidation in cellular RNA than in DNA. *Biol. Chem.*, **386**, 333–337.

42. Simms,C.L., Hudson,B.H., Mosior,J.W., Rangwala,A.S. and Zaher,H.S. (2014) An Active Role for the Ribosome in Determining the Fate of Oxidized mRNA. *Cell Rep.*, **9**, 1256–1264.

43. Cheng,X., Kelso,C., Hornak,V., de los Santos,C., Grollman,A.P. and Simmerling,C. (2005) Dynamic behavior of DNA base pairs containing 8-oxoguanine. *J. Am. Chem. Soc.*, **127**, 13906–18.

44. Mcculloch,S.D., Kokoska,R.J., Garg,P., Burgers,P.M. and Kunkel,T.A. (2009) The efficiency and fidelity of 8-oxo-guanine bypass by DNA polymerases δ and η. *Nucleic Acids Res.*, **37**, 2830–2840.

45. Hsu,G.W., Ober,M., Carell,T. and Beese,L.S. (2004) Error-prone replication of oxidatively damaged DNA by a high-fidelity DNA polymerase. *Nature*, **431**, 217–21.

46. Zaher,H.S. and Green,R. (2009) Quality control by the ribosome following peptide bond

formation. *Nature*, **457**, 161–166.

47. Jelenc,P.C. (1979) Nucleoside triphosphate regeneration decreases the frequency of. *Proc. Natl. Acad. Sci. U. S. A.*, **76**, 3174–3178.

48. Zaher,H.S. and Unrau,P.J. (2004) T7 RNA Polymerase Mediates Fast Promoter-Independent Extension of Unstable Nucleic Acid Complexes †. *Biochemistry*, **43**, 7873–7880.

49. Walker,S.E. and Fredrick,K. (2008) Preparation and evaluation of acylated tRNAs. *Methods*, **377**, 364–377.

50. Pierson,W.E., Hoffer,E.D., Keedy,H.E., Simms,C.L., Dunham,C.M. and Zaher,H.S. (2016) Uniformity of Peptide Release Is Maintained by Methylation of Release Factors. *Cell Rep.*, **17**, 11–18.

51. Youngman,E.M., Brunelle,J.L., Kochaniak,A.B. and Green,R. (2004) The active site of the ribosome is composed of two layers of conserved nucleotides with distinct roles in peptide bond formation and peptide release. *Cell*, **117**, 589–99.

52. Varani,G. and McClain,W.H. (2000) The G·U wobble base pair: A fundamental building block of RNA structure crucial to RNA function in diverse biological systems. *EMBO Rep.*, **1**, 18–23.

53. Cochella,L., Brunelle,J.L. and Green,R. (2007) Mutational analysis reveals two independent molecular requirements during transfer RNA selection on the ribosome. *Nat. Struct. Mol. Biol.*, **14**, 30–36.

54. Andersson,D.I., Bohman,K., Isaksson,L.A. and Kurland,C.G. (1982) Translation rates and misreading characteristics of rpsD mutants in Escherichia coli. *MGG Mol. Gen. Genet.*, **187**, 467–472.

55. Yue,Y., Liu,J. and He,C. (2015) RNA N6-methyladenosine methylation in post-transcriptional gene expression regulation. *Genes Dev.*, **29**, 1343–1355.

56. Cheng,K.C., Cahill,D.S., Kasai,H., Nishimura,S. and Loeb,L.A. (1992) 8-Hydroxyguanine, an abundant form of oxidative DNA damage, causes G → T and A → C substitutions. *J. Biol. Chem.*, **267**, 166–172.

57. Carter,A.P., Brodersen,D.E., Morgan-warren,R.J., Hartsch,T., Wimberly,B.T. and Ramakrishnan,V. (2001) Crystal Structure of an Initiation Factor Bound to the 30S Ribosomal Subunit. *Science (80-.).*, **291**, 498–501.

58. Gromadski,K.B., Daviter,T. and Rodnina,M. V. (2006) A uniform response to mismatches in codon-anticodon complexes ensures ribosomal fidelity. *Mol. Cell*, **21**, 369–377.

59. Choi,Y.J., Gibala,K.S., Ayele,T., Deventer,K. V. and Resendiz,M.J.E. (2017) Biophysical properties, thermal stability and functional impact of 8-oxo-7,8-dihydroguanine on oligonucleotides of RNA-a study of duplex, hairpins and the aptamer for preQ1 as models. *Nucleic Acids Res.*, **45**, 2099–2111.

60. Ikehara,M., Kawase,Y. and Ohtsuka,E. (1992) Nmr studies of a dna containing 8-methoxydeoxyguanosine. *Nucleosides and Nucleotides*, **11**, 261–272.

61. Lipscomb,L.A., Peek,M.E., Morningstar,M.L., Verghis,S.M., Miller,E.M., Rich,A., Essigmann,J.M. and Williams,L.D. (1995) X-ray structure of a DNA decamer containing 7,8-dihydro-8-oxoguanine. *Proc. Natl. Acad. Sci. U. S. A.*, **92**, 719–23.

62. Plum,G.E., Grollman,A.P., Johnson,F. and Breslauer,K.J. (1995) Influence of the Oxidatively Damaged Adduct 8-Oxodeoxyguanosine on the Conformation, Energetics, and Thermodynamic Stability of a DNA Duplex. *Biochemistry*, **34**, 16148–16160.

63. Singh,S.K., Szulik,M.W., Ganguly,M., Khutsishvili,I., Stone,M.P., Marky,L.A. and Gold,B. (2011) Characterization of DNA with an 8-oxoguanine modification. *Nucleic Acids Res.*, **39**, 6789–6801.

64. Freudenthal,B.D., Beard,W.A. and Wilson,S.H. (2013) DNA polymerase minor groove interactions modulate mutagenic bypass of a templating 8-oxoguanine lesion. *Nucleic Acids Res.*, **41**, 1848–1858.

65. Vasquez-Del Carpio,R., Silverstein,T.D., Lone,S., Swan,M.K., Choudhury,J.R., Johnson,R.E., Prakash,S., Prakash,L. and Aggarwal,A.K. (2009) Structure of human DNA polymerase κ inserting dATP opposite an 8-OxoG DNA lesion. *PLoS One*, **4**.

66. Batra,V.K., Shock,D.D., Beard,W.A., McKenna,C.E. and Wilson,S.H. (2011) Binary complex crystal structure of DNA polymerase reveals multiple conformations of the templating 8-oxoguanine lesion. *Proc. Natl. Acad. Sci.*, **109**, 113–118.

67. Brieba,L.G., Eichman,B.F., Kokoska,R.J., Doublié,S., Kunkel,T.A. and Ellenberger,T. (2004) Structural basis for the dual coding potential of 8-oxoguanosine by a high-fidelity DNA polymerase. *EMBO J.*, **23**, 3452–3461.

68. Sale,J.E. (2013) Translesion DNA synthesis and mutagenesis in eukaryotes. *Cold Spring Harb. Perspect. Biol.*, **5**, a012708.

69. Fan,Y., Wu,J., Ung,M.H., De Lay,N., Cheng,C. and Ling,J. (2015) Protein mistranslation protects bacteria against oxidative stress. *Nucleic Acids Res.*, **43**, 1740–1748.

70. Mikkola,R. and Kurland,C.G. (2017) Selection of laboratory wild-type phenotype from natural isolates of Escherichia coli in chemostats. *Mol. Biol. Evol.*, **9**, 394–402.

Chapter 4

Decoding on the ribosome depends on the structure of the mRNA phosphodiester backbone

This chapter is currently published in the Proclamations of the National Academy of Sciences as Hannah E. Keedy*, Erica N. Thomas*, and Hani S. Zaher (2018) Decoding on the ribosome depends on the structure of the mRNA phosphodiester backbone. *Authors contributed equally to this manuscript.

ABSTRACT

During translation, the ribosome plays an active role in ensuring that mRNA is decoded accurately and rapidly. Recently, biochemical studies have also implicated certain accessory factors in maintaining decoding accuracy. However, it is currently unclear whether the mRNA itself plays an active role in the process beyond its ability to base pair with the tRNA. Structural studies revealed that the mRNA kinks at the interface of the P and A sites. A magnesium ion appears to stabilize this structure through electrostatic interactions with the phosphodiester backbone of the mRNA. Here we examined the role of the kink structure on decoding using a well-defined *in vitro* translation system. Disruption of the kink structure through site-specific phosphorothioate modification resulted in an acute hyperaccurate phenotype. We measure rates of peptidyl transfer for near-cognate tRNAs that are severely diminished and in some instances are almost one 100-fold slower than unmodified mRNAs. In contrast to peptidyl transfer, the modifications had little effects on GTP hydrolysis by elongation factor thermal unstable (EF-Tu), suggesting that only the proofreading phase of the tRNA selection process depends critically on the kink structure. Although the modifications appear to have no effect on typical cognate interactions, peptidyl transfer for a tRNA that uses atypical base pairing is compromised. These observations suggest that the kink structure is important for decoding in the absence of Watson-Crick or G-U Wobble base pairing at the third position. Our findings provide evidence for a previously unappreciated role for the mRNA backbone in ensuring uniform decoding of the genetic code.

Keywords: Ribosome, Decoding, mRNA Structure, tRNA Selection, Phosphorothioate Substitution

SIGNIFICANCE STATEMENT

Reading of the genetic code is an intricate process in which the ribosome plays an active role in ensuring that translation proceeds rapidly and accurately. Studies have revealed that the mRNA adopts an unusual structure between the P and A sites of the small ribosomal subunit, where it is significantly kinked. In this work we probed the role of the kink structure in decoding. Substitutions that disrupt this structure were found to increase the accuracy of decoding. Conversely, peptide bond formation on difficult-to-decode codons was severely reduced when this kink structure was perturbed. Our data suggests that the rigid nature of the mRNA backbone is important for ensuring efficient codon-anticodon interactions under suboptimal conditions.

INTRODUCTION

The accurate decoding of the genetic code depends critically on the ability of the ribosome to select the aminoacyl tRNA (aa-tRNA) that matches the mRNA in its A site. During this process of tRNA selection, the ribosome employs multiple strategies to maintain the low error frequency of 10^{-4}-10^{-3} per one amino-acid-incorporation event (1-4). The aa-tRNA is delivered to the ribosome in a ternary complex with elongation factor thermal unstable (EF-Tu) and GTP. The hydrolysis of GTP by EF-Tu essentially divides the tRNA selection processes into two stages: initial selection and proofreading (5). Dividing the selection process gives the ribosome two opportunities to reject the incorrect aa-tRNA. This mechanism of kinetic proofreading (6, 7) utilizes both thermodynamic differences as well as induced fit to accelerate the dissociation rates of incorrect aa-tRNAs and forward rates for correct aa-tRNAs (8-10). In particular, during the initial selection phase, near cognate ternary complexes rapidly fall off the ribosome, whereas GTP is rapidly hydrolyzed for cognate ternary complexes. Similarly, during the proofreading phase following the dissociation of EF-Tu, near-cognate aa-tRNAs are readily rejected, whereas cognate aa-tRNAs are readily accommodated into the active site to participate in peptidyl transfer (PT) (8).

More than half a century of biochemical studies on the ribosome have defined many of the molecular elements responsible for the observed accuracy during protein synthesis (reviewed in) (11). The ribosome itself plays a critical role in dictating the overall fidelity of this process (12, 13). Indeed, some of the first error-prone and hyperaccurate mutations to be identified mapped to ribosomal proteins. For instance, many mutations in the ribosomal proteins genes *rpsD* and *rpsE* have long been documented to confer a ribosome ambiguity phenotype (*ram*) (14-19). On the other hand, mutations in the *rpsL* gene result in a restrictive phenotype. Most of these mutations also confer resistance to, and in some cases dependence on, the error-inducing antibiotic streptomycin

(20, 21). In contrast to ribosomal proteins, mutations to the ribosomal RNA (rRNA) rarely appear naturally, due to incomplete penetrance of these mutations, as rRNA genes are typically found in numerous copies in the genome. Nonetheless, screens using high copy plasmids carrying the rrn operon of *E. coli* have been used to isolate rRNA variants that alter the decoding properties of the ribosome (22, 23). More recent studies using orthogonal ribosomes have also been successful in isolating mutants that otherwise would be dominant negative. Interestingly, most of these mutations appear to map to functionally important parts of the ribosome such as the decoding center or intersubunit bridges (24).

In addition to the ribosome, translation factors play a critical role in maintaining the fidelity of protein synthesis. For example, mutations in elongation and release factors (RFs) have been found to increase the error frequency during translation (25, 26). In addition, tRNAs arguably play one of the most important roles in the decoding process during both the aminoacylation reaction as well as the tRNA selection process. This is best exemplified by suppressor tRNAs that decode stop codons and result in missense suppression. While the miscoding properties of most of these RNAs can be easily rationalized by alteration to the anticodon, which allows them to base pair with the incorrect codon, some, I which mutations far from the anticodon appear to be responsible for their phenotype, are more complex. For instance, the Hirsch $tRNA^{Trp}$ suppressor tRNA (CCA anticodon) harbors a G24A mutation in the D arm enabling it to decode the tryptophan UGG and UGA stop codons (27). Biochemical studies of this tRNA showed that this variant tRNA accelerates forward rates of tRNA selection even in the presence of mismatched codon-anticodon interaction, underlining the critical role of the tRNA during the selection process (28).

Emerging from recent structural studies of ribosomal complexes are some key hints about the molecular mechanics of the decoding process and how perturbation to the translation

machinery disrupts it (29, 30). In particular, during the tRNA selection process, the decoding center of the ribosome undergoes local conformational changes that in turn drive larger changes within the small ribosomal subunit (31, 32). This so-called "domain closure" of the small subunit is also accompanied by changes to the A-site tRNA that are manifested by a large conformational change in its structure. This structural change is likely responsible for relaying a signal to the GTPase activation center of the large ribosomal subunit, leading to the subsequent accommodation of the tRNA into the peptidyl-transferase center (33, 34). These structures also provided some important mechanistic clues about how classical mutations in the ribosome perturb decoding. They appear to alter the thermodynamics of the interchangeability between the "open" and "closed" state of the ribosome (32). The *rpsD* and *rpsE* mutations of error-prone ribosomes disrupt interactions that are necessary to maintain the open conformation, whereas the *rpsL* mutations of hyperaccurate ribosomes disrupt interactions necessary for the closed conformation. In addition to the ribosome, the accompanying conformational changes in the tRNA as it moves into the A site play an integral role during protein synthesis (33, 35). Structural studies of the Hirsch suppressor tRNA revealed tRNA distortion was critical for decoding (36). This increased flexibility of the tRNA allows increased GTPase activation of EF-Tu even in the presence of a near-cognate tRNA (28).

What is clear from the abundance of biochemical and structural studies on the ribosome is that decoding is an intricate process that takes cues from almost every single factor of the translation machinery. What has been less understood is the extent to which the structure of the mRNA itself is important for this process. Nonetheless, biochemical studies on the role of the ribose backbone during decoding showed the substitutions of the 2'-OH groups of the A-site mRNA residue by deoxy or fluoro groups to have only modest effect on tRNA selection (37). This

is in contrast to structural studies, which showed the hydroxyl groups to be important for A-minor interactions with the decoding center nucleotides (31, 32).

Equivalent studies of the role of the phosphodiester backbone of the mRNA on ribosome function are lacking. Interestingly, crystal structures of the ribosome revealed the mRNA adopts a kink-like structure between the P and A sites (38, 39). A magnesium ion stabilizes this structure through electrostatic interactions with the non-bridging oxygens of the phosphodiester backbone of the mRNA (39). While the kink has been speculated to be critical for frame maintenance by preventing slippage (39), this has not been directly tested. Whether the structure contributes to tRNA selection is yet unknown. Here, we perturbed the mRNA structure by introducing stereospecific phosphorothioate substitutions in the mRNA at the interface of the P and A site and assessed their effect on decoding using a well-defined *in vitro* system. We found that substitution of either of the nonbridging oxygens results in a hyperaccurate phenotype; however, substitution of the *pro*-Sp oxygen, one of the oxygens involved in coordinating the divalent metal, with sulfur has a more drastic effect. In the presence of the *Rp*-phosphorothioate, PT rates for near-cognate aa-tRNAs were reduced by about 10-fold relative to the native mRNA. In contrast, the same rates were more than 100-fold slower for the *Sp*-phosphorothioate. Peptide release on near-stop codons was similarly affected, suggesting that the kink is critical for the process by which A-site ligands interact with the ribosome. In an effort to determine whether the substitutions affect both phases of tRNA selection, we measured the rates of GTP hydrolysis by near-cognate ternary complexes in the presence of the modifications. Either substitution resulted in a modest two- to threefold reduction in the observed rate, suggesting that magnesium coordination by the mRNA is important only for the proofreading phase of the selection process. Interestingly, while both substitutions appear to have no effect on most cognate aa-tRNA selection, the *Sp*-phosphorothioate substitution

significantly reduced the PT rate for a difficult-to-decode cognate codon. In particular, PT for the AUA codon, which is decoded by the anticodon-modified Ile-tRNA$^{Ile}_{(k2_{CAU})}$, is approximately fivefold slower in the presence of *Sp*-modified mRNA relative to the unmodified or the *Rp*-modified mRNAs. Finally, to expand on the potential role of the mRNA backbone on tRNA selection, we investigated the effect of the deoxy substitutions on peptide-bond formation for cognate and near-cognate ternary complexes. Similar to previous observations (37), substitution of any of the three 2'-OH of the A-site codon by a deoxy does not alter peptide-bond formation in the presence of cognate aa-tRNA. However, peptide-bond formation was drastically inhibited for these modified mRNAs in the presence of a near-cognate aa-tRNA. Collectively our findings provide some of the first hints at the integral role of the mRNA structure in decoding and how its perturbation could have profound consequences on the speed of protein synthesis.

RESULTS

Experimental approach

To investigate the role of the mRNA-kink structure in tRNA selection, we decided to destabilize magnesium-binding at the interface of the P and A site of the small subunit. The divalent metal ion is held in place by a network of electrostatic interactions that include three non-bridging oxygen atoms of the mRNA phosphodiester backbone (Fig. 1*A*). As a starting point, we chose to introduce sulfur substitutions right between the initiation codon and the second codon of a model mRNA. Namely, we sought to substitute the *pro*-Sp oxygen of the phosphodiester linkage between the third nucleotide of the P-site codon and the first nucleotide of the A-site codon (Fig. 1*A*). However, since the smallest model mRNA (~25 nt) is too long to efficiently separate the resulting two diastereomers from chemical synthesis, we chose to generate the mRNAs from two pieces. This allowed us to synthesize the phosphorothioate-containing RNA as a 9-mer, which is readily separated into the *Rp* and *Sp* diastereomers using reverse-phase HPLC methods (Fig. 1*B*). Subsequent near quantitative ligation using T4 RNA ligase 2 to an upstream RNA oligonucleotide containing the necessary Shine-Dalgarno sequence gave us the full-length model mRNA (Fig. 1*C*).

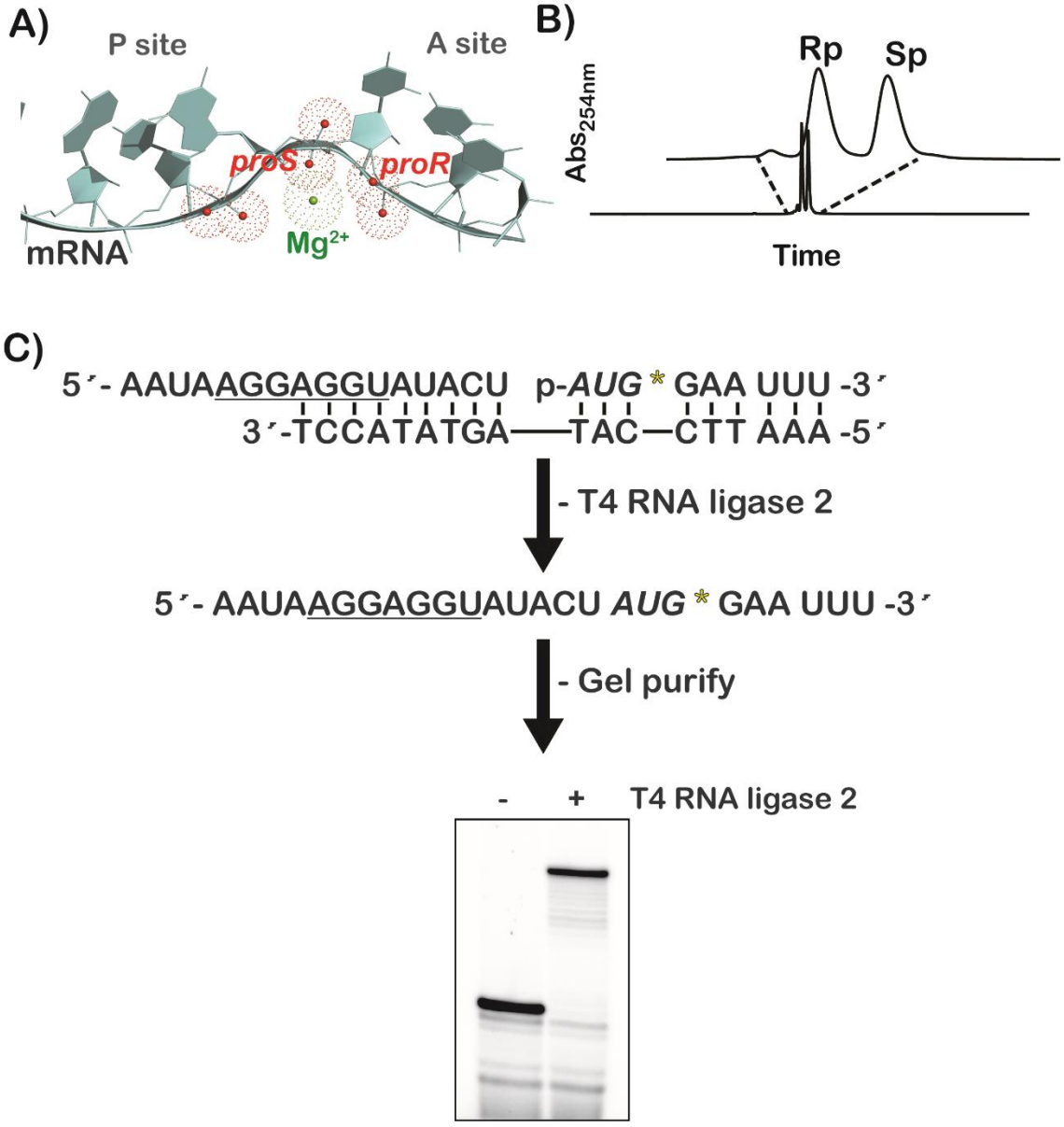

Fig. 4.1 Structure of the mRNA on the ribosome and preparation of phosphorothioate-modified mRNAs. A) Overview of the mRNA structure (PDB 2J00) highlighting the kink structure dividing the P and A sites of the ribosome. The non-briding oxygen atoms (red) coordinating a magnesium ion (green) are shown. B) A representative HPLC chromatogram showing the separation of the two phosphorothioate diastereoisomers of the downstream RNA sequence. C) Schematic of the procedure used to synthesize the full-length modified mRNA. Sequence of the two pieces is shown annealed to a DNA splint. The bottom panel shows a representative denaturing PAGE used to follow the ligation reaction using a radio-labeled downstream sequence.

The modified mRNA was then used in our *in vitro* reconstituted system (40) to make initiation complexes. Ribosomes were incubated with initiation factors (IFs) 1, 2 and 3, f-[^{35}S]-Met-tRNA^{fMet}, and GTP in the presence of native or modified mRNAs. The initiation complexes were then purified away from the IFs and unbound mRNA through ultracentrifugation over a sucrose cushion. The first set of initiation complexes displayed the Glu GAA codon. Peptide-bond formation was commenced by incubating initiation complexes with ternary complexes comprised of aa-tRNA, EF-Tu, and GTP. Following quenching and hydrolysis of the ester linkage between the peptide and the tRNA with KOH, dipeptides were resolved from unreacted fMet using electrophoretic TLC and were visualized by phosphorimaging.

Phosphorothioate substitutions at the interface of the P and A site result in stringent tRNA selection.

For our initial studies we conducted a surveying approach (41) in an effort to gain an unbiased view of the modifications' effects on the decoding process. Three initiation complexes programmed with the native mRNA or with *Rp*- or *Sp*-phosphorothioate modified mRNAs were reacted with the 20 canonical aa-tRNA isoacceptors for 30 seconds (Fig. 2). As expected, all three complexes, which displayed the GAA codon in the A site, reacted efficiently with the cognate Glu-tRNA^{Glu} ternary complex. In contrast, replacement of either of the non-bridging oxygen atoms by sulfur had a profound effect on the reactivity of near-cognate ternary complexes. In particular, whereas dipeptide formation was observed for a number of near-cognate aa-tRNAs (including but not limited to Asp-tRNA^{Asp} and Lys-tRNA^{Lys}) in the presence of the native complex (O), significantly less dipeptide was observed in the presence of the *Rp* complex, and it was nearly undetectable for the *Sp* complex (Fig. 2). These observations suggested that the structure of the

mRNA backbone, particularly at the interface of the A and P sites of the ribosome, plays an important role during tRNA selection.

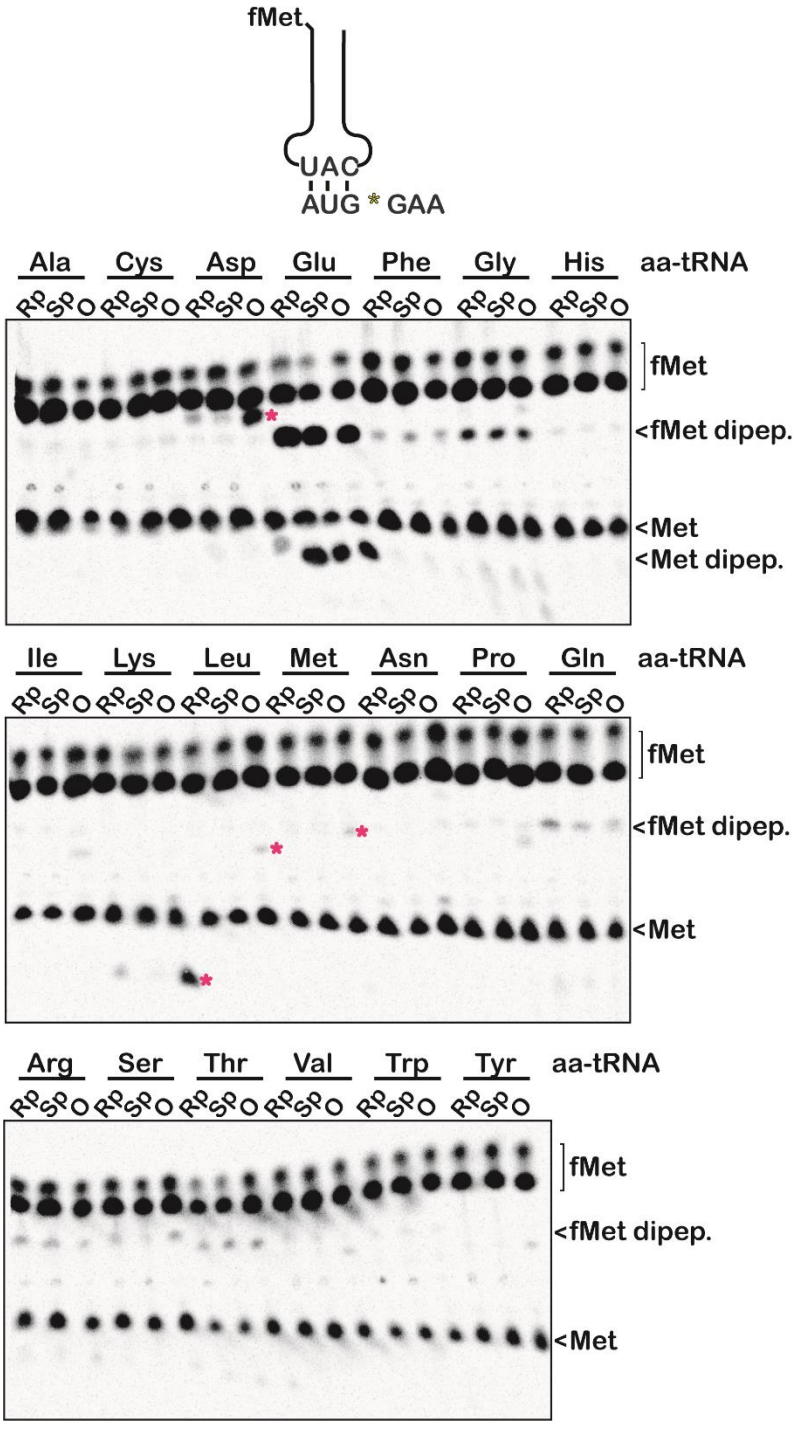

Fig. 4.2 Phosphorothioate mRNAs suppress the incorporation of near-cognate amino acids. Phosophorimager scans of electrophoretic TLCs showing the reactivity profile of the initiation complexes –programmed with the indicated native and phosphorothioate-modified mRNAs– with the 20 aa-tRNA isoacceptors. A schematic of the initiation complex is shown at the top with fMet-tRNA^{fMet} occupying the P site and the Glu GAA codon occupying the A site. Differential reactivities with near-cognate aa-tRNA are marked by asterisks. Note that for this particular reactivity survey the formylation of fMet was incomplete and as a result residual Met is observed. This does not affect the analysis because of differences in migration on the TLC between fMet and Met as well as the corresponding dipeptides.

Although the endpoint of the dipeptide survey reactivities provided some important clues about the effect of the substitutions on the accuracy of peptide-bond formation, these assays fail to provide more quantitative information about the extent to which fidelity is improved. As a result, we resorted to a pre-steady-state kinetics approach to measure the rate of peptidyl transfer (PT) for the cognate Glu-tRNA^{Glu} ternary complex as well as for the near-cognate Lys-tRNA^{Lys} and Asp-tRNA^{Asp} ternary complexes. Consistent with our end-point analysis in Fig. 2, the modifications appear to have little effect on the PT rates for the cognate aa-tRNA (Fig. 3*A*). More specifically, we measure a rate of ~20 s^{-1} for the O mRNA and ~ 15 s^{-1} for the *Rp*- and *Sp*-phosphorothioate mRNAs. In contrast to the cognate reaction, both substitutions had strong effects on the near-cognate PT rates, with the *Sp*-phosphorthioate having the most drastic effect. In the presence of Lys-tRNA^{Lys}, PT rates for the O, *Rp*- and *Sp*-phosphorothioate mRNA-containing complexes were 0.10 s^{-1}, 0.0093 s^{-1}, and 0.0055 s^{-1}, respectively. In addition, the *Sp*-phosphorothioate complex displayed a drastic endpoint defect, for which the fraction of fMet that converted to fMet-Lys dipeptide was 27% (Fig. 3*B*). Conversely, the same reactions with the unmodified and Rp-phosphorothioate went to near completion (~86%). These effects of the phosphorothioate substitutions on near-cognate Lys-tRNA^{Lys} selection were, by and large, similar to those measured for Asp-tRNA^{Asp} selection. We measured PT rates of 0.056 s^{-1}, 0.0089 s^{-1}, and 0.017 s^{-1} for the unmodified, *Rp*- and *Sp*-phosphorothioate complexes, respectively (Fig. 3*C*). In addition, similar

to the Lys-tRNA^{Lys} reaction, the modifications appear to significantly improve proofreading by the ribosome as evidenced by the reduced end points. The *Sp*-phosphorothioate complex displayed an even better rejection of the Asp-tRNA^{Asp}, for which we measure an end point of 0.035. In comparison, the end points for the O and *Rp*-phosphorothioate complexes were 0.33 and 0.11, respectively (Fig. 3*C*). Collectively these observations suggest that disruption of interactions between the phosphodiester backbone of the mRNA and divalent metals induces a hyperaccurate phenotype.

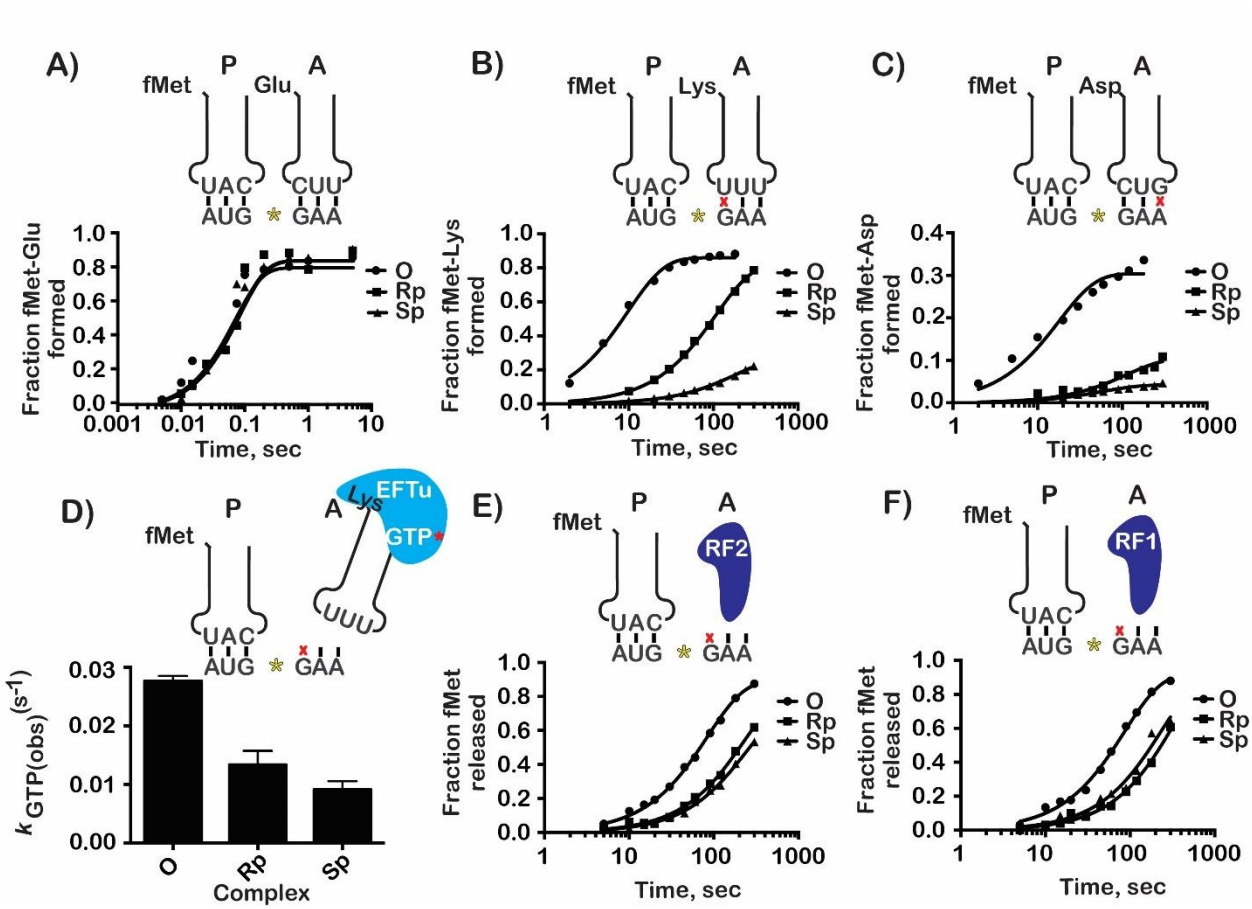

Fig. 4.3 The *Sp*-phosphorothioate substitution of the kink oxygen results in a severe hyperaccurate phenotype. A) Representative time courses for PT reactions between the indicated complexes and the cognate Glu-tRNA^{Glu} ternary complex. B) Representative time course for PT reactions between the indicated complexes and the near-cognate Lys-tRNA^{Lys} ternary complex. C) Representative time courses for PT reactions between the indicated complexes and the near-cognate Asp-tRNA^{Asp} ternary complex. D) Bar graph showing the observed rate of GTP hydrolysis for modified, *Rp*- and *Sp*- complexes with the near-cognate Lys-tRNALys ternary complex. Unlike

PT reactions, which were all conducted at 37°C, these reactions were conducted at 20°C. Shown are the means of three independent time courses with the error bar representing the standard deviation from the mean. E) Representative time courses for RF2-mediated hydrolysis on the indicated complexes. F) Representative time courses for RF1-mediated hydrolysis reaction on the indicated complexes.

The accuracy of the initial phase of tRNA selection is not significantly impacted by the phosphorothioate substitutions.

As our peptide-formation assays report on the overall process of tRNA selection, the observed effects of substitutions could, in principle, be the result of defects in the initial phase or proofreading phase of the process. GTP hydrolysis by EF-Tu reports on the GTPase activation of the factor, which in turn reports on the accuracy of the overall initial phase. We measured the rate for GTP hydrolysis for the native and *Rp*- and *Sp*-phosphorothioate complexes in the presence of the near-cognate Lys-tRNA^{Lys} ternary complex. In contrast to our observations for peptide-bond formation, the substitution had only a modest effect on the observed rate of GTP hydrolysis (Fig. 3*D*). For the *Rp*-modified complex, the observed rate is merely twofold slower relative to the native complex. Similarly, the observed rate for the *Sp*-modified complex was threefold slower (Fig. 3*D*). Hence, it appears that the kink structure of the mRNA plays little to no role during the initial phase of the selection process. Instead, given that we measured rates for peptide-bond formation that are almost two order of magnitude slower under the same conditions, the kink structure is likely to play an important role during the proofreading phase. Disruption of this structure appears to reduce the accommodation rates and increases the rejection rates of near-cognate aa-tRNAs.

Phosphorothioate substitutions increase the fidelity of RFs

Next, we sought to explore the effects of phosphorothioate substitutions on the accuracy of peptide release by RFs. In particular, we were interested in examining whether the kink structure affects protein-mRNA interaction during peptide release misrecognition of sense codons. The GAA codon displayed in the A site of our complexes is a near-stop for both RF1 and RF2, as both recognize the UAA codon. As a result, we could address the effect of the substitutions on the accuracy of both factors. Although the modifications appear to affect both RF1- and RF2-mediated hydrolysis (Fig. 3*E* and *F*), the extent of these effects was much smaller than those observed for PT, and on average they were two- to threefold slower relative to the native mRNA. We measured rates of hydrolysis for RF2 of 0.012 s^{-1}, 0.0045 s^{-1}, and 0.0041 s^{-1} for the unmodified and *Rp*- and *Sp*-phosphorothioate complexes, respectively (Fig. 3*E*). Similarly, in the presence of RF1, we measured hydrolysis rates of 0.012 s^{-1}, 0.0030 s^{-1}, and 0.0044 s^{-1} for the unmodified and *Rp*- and *Sp*-phosphorothioate complexes, respectively (Fig. 3*F*). Interestingly, and in contrast to tRNA selection, peptide release on the *Sp* complex was faster (ableit only slightly) than its *Rp* counterpart. These observations are consistent with data from our group and others that show the process of RF selection to be different than its tRNA selection counterpart (42, 43). For instance, whereas certain base modifications appear to be detrimental for peptide-bond formation, they have little effect on peptide release (44, 45). Nevertheless, the observation that phosphorothioate substitutions affect peptide release (with little distinction between the two diastereomers) highlights the importance of the mRNA backbone structure during the recognition of A-site ligands regardless of their identity.

The effects of the phosphorothioate substitutions are not dependent on the A-site codon identity

Our analysis, so far, has focused on one particular mRNA sequence, so our next logical step was to expand our analysis to assess whether the effects of the substitutions we observed are specific or general in nature. Our analysis on the GAA mRNA revealed that both the *Rp*- and *Sp*-phosphorothioate substitutions appear to severely reduce the observed PT rates for near-cognate aa-tRNAs (Fig.3). To simplify our approach, in the next set of experiments we chose to synthesize the modified mRNA in one piece and generate mixed complexes with a racemic mixture of the mRNA. The new complexes displayed the CAA Gln codon in the A site. Again, we started our analysis by carrying out a survey for all aa-tRNA-isoacceptors reactivities (Fig. S1*A*). The reactivity profile for the new complexes was nearly identical to the one observed for the previous complexes (compare Fig. 3*A* to S1*A*). The native and phosphorothioate-modified complexes reacted efficiently with the cognate Gln-tRNA^{Gln} ternary complex. In contrast, the native complex reacted much better with the near-cognate Asp-tRNA^{Asp} and His-tRNA^{His} ternary complexes relative to the modified one (Fig. S1*A*). Furthermore, both RFs 1 and 2 appear to recognize the native complex better than the modified one, for which we observe significant fMet release from fMet-tRNA^{fMet} only for the native complex. Therefore, our survey analysis suggests that effect of the phosphorothioate substitution on A-site-ligand binding is general in nature.

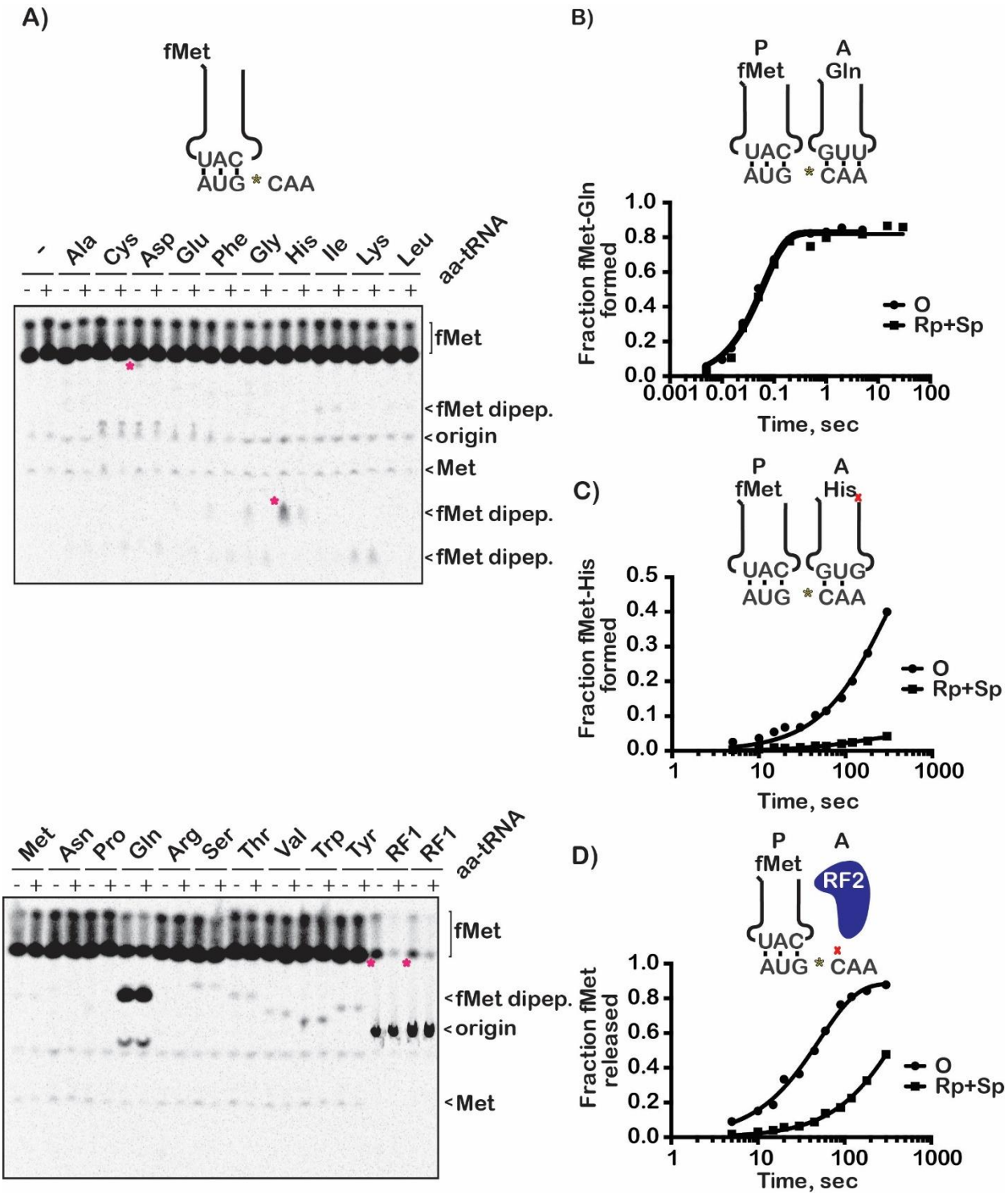

Fig. 4.S1 Reactions with a different mRNA yield similar results. A) Reactivity profile of the depicted complex, which displays the Gln CAA codon in the A site, with the indicated aa-tRNAs and RF. Products were separated on electrophoretic TLCs and visualized using phosphorimaging. Differential reactivities are marked by asterisks. B) Representative time courses of PT reactions between the indicated complexes (programmed with a native mRNA or racemic mixture of

phosphorothioate mRNAs) and the cognate Gln-tRNA^{Gln}. C) Representative time courses of PT reactions between the indicated complexes and the near-cognate His-tRNA^{His}. D) Representative time courses for RF2-mediated hydrolysis reaction on the indicated complexes.

To gain a more quantitative understanding of the effects on decoding, we measured the PT rates for the cognate and a near-cognate tRNA as well as the release rate for RF2. Similar to our observations for the previous complexes, the modification had almost no effect on the PT rate for the cognate Gln-tRNA^{Gln} complex. We measured rates of 17 s^{-1} and 15 s^{-1} for the unmodified and modified mRNAs, respectively (Fig. S1*B*). Also in agreement with our surveying analysis, the modification had a drastic effect on the His-tRNA^{His} near-cognate reaction. Although the PT rate appears to be unaffected (in fact slightly increased from 0.0037 s^{-1} to 0.0069 s^{-1}), the end point of the reaction was dramatically reduced from ~0.6 to ~0.05 (Fig. S1*C*). These findings suggest that the modification is likely to increase the rate of aa-tRNA rejection during the proofreading phase of tRNA selection. Finally, and as expected the modification reduced the rate of RF2-mediated peptide release by almost one order of magnitude (Fig. S1*D*). The observation that modification of two independent mRNA sequences has near-identical effects on peptide-bond formation and peptide release greatly suggests that the effect of the phosphorothioate substitution is independent of the mRNA sequence. This in turn adds more support for the hypothesis that the mRNA-kink structure plays a key role in ribosome function.

Phosphorothioate modification reduces peptide-bond formation for a subset of cognate aa-tRNAs

To this point, our analysis revealed that perturbation of the mRNA structure results in aggressive proofreading by the ribosome with little to no effect on cognate tRNA selection. This in turn begs the question as to why the mRNA evolved to adopt this conformation on the ribosome.

It is highly likely that the structure plays a role in frame maintenance, as has been suggested by structural biologists (39). However, for our next experiments we were motivated by data on ribosome variants that showed certain hyperaccurate rRNA variants to also significantly compromise PT for a subset of cognate aa-tRNAs, in particular those that exploit unusual base pairs at the wobble position (46). For example, to avoid mispairing with the AUG Met codon, the AUA Ile codon in *E. coli* does not base pair with an anticodon using the typical A:U base pair at the third position. Instead, the corresponding C in the anticodon is modified to lysidine (^{k2}C). Studies by Ortiz-Meoz and Green showed that mutations in helix 69 of the large subunit, while having no effect on most cognate tRNAs, significantly slow down the PT rate for tRNA$^{Ile}_{(k2_C)}$ (46). As a result, we wondered whether the mRNA-kink structure is similarly critical for decoding the AUA codon by Ile-tRNA$^{Ile}_{(k2_C)}$.

To explore this hypothesis, ribosomes were programmed with three mRNAs: native, *Rp*- and Sp-phosphorothioate modified mRNAs, all displaying the AUA codon in the A site. In agreement with our earlier observation, the observed PT rate for the *Rp*-phosphorothioate-programmed complexes with the cognate Ile-tRNA^{Ile} was indistinguishable from that for the native complexes (~ 10s^{-1}, Fig. 4*A*). In contrast, the same rate for the *Sp*-modified complex was almost an order of magnitude slower (Fig. 4*A*). These findings again suggest that the *pro*-S oxygen plays a more important role in maintaining the mRNA structure. We note that, similar to what we observed for the two previous complexes, the AUA complexes exhibited defects in their reactivity similar to those in near-cognate aa-tRNAs. In the presence of Met-tRNA^{Met}, we measure rates of peptide-bond formation of 0.41 s^{-1}, 0.022 s^{-1}, and 0.0082 s^{-1} for the native and *Rp*- and *Sp*-modified complexes, respectively (Fig. 4*B*). These observations suggest that the *pro*-S oxygen, and likely its ability to coordinate magnesium, is critical for decoding under less-than-ideal conditions.

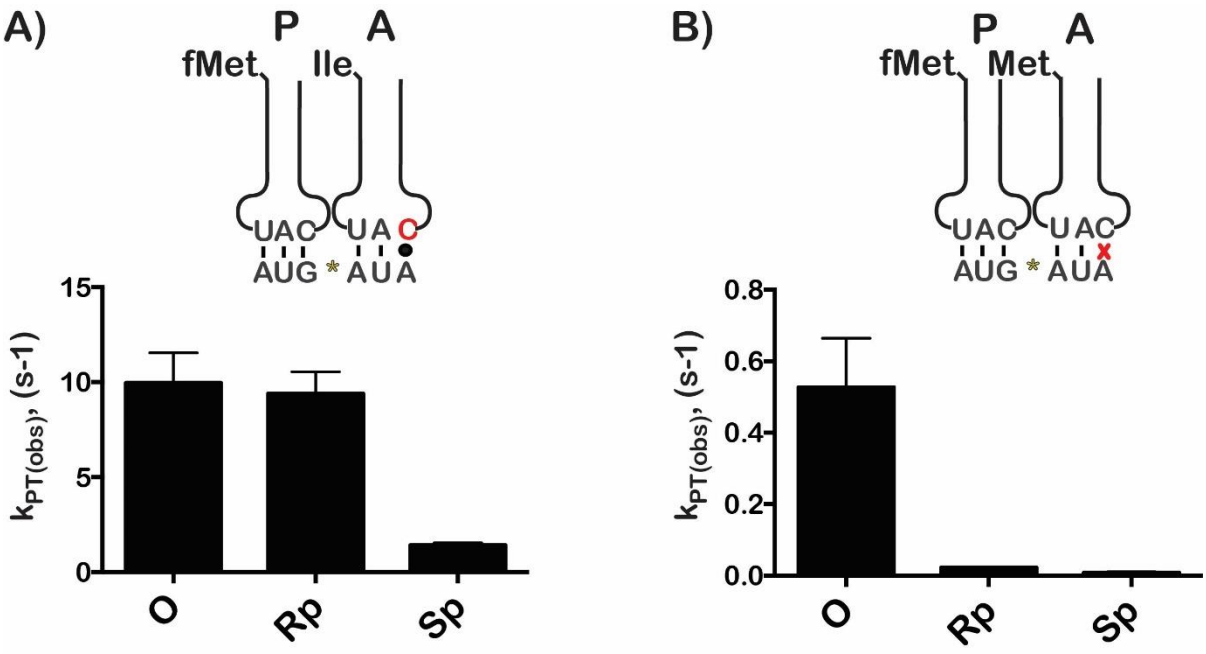

Fig. 4.4 Substitution of the *pro*-S oxygen reduces the rate of peptide-bond formation in the presence of atypical tRNA-mRNA interactions. A) Bar graph showing the PT rate for unmodified, *Rp*- and *Sp*- complexes, all displaying the Ile AUA codon in the A site (depicted above), with the cognate Ile-tRNA^{Ile}. The corresponding Ile-tRNA harbors the lysidine (k^2C) modification at the wobble position. B) Observed PT rates for the near-cognate Met-tRNA^{Met} in the presence of the indicated complexes. Graphs show the means of three independent time courses; error bars represent the SD from the mean.

Peptide release is not impacted by phosphorothioate modification of the mRNA

Our analysis thus far has suggested the kink structure to be likely important for decoding a subset of sense codons. As a result, the next logical step was to assess its effects on canonical peptide release. As before, we prepared unmodified- and phosphorothioate-mRNA-containing initiation complexes that displayed the UAA stop codon in the A site. Similar to our observations for PT, the rates of peptide release were found to be unaffected by the presence of the phosphorothioate modification at the interface of the P and the A site of the mRNA. For RF1 we measured rates of 0.35 s^{-1} and 0.49 s^{-1} for the native and modified mRNA, respectively (Fig. 5*A*). Likewise, for RF2, we measured rates of 0.76 s^{-1} and 0.93 s^{-1} for the same set of mRNAs (Fig. 5*B*).

These observations are in agreement with our model that the kink structure is not important for decoding (sense and missense codons) under optimal conditions.

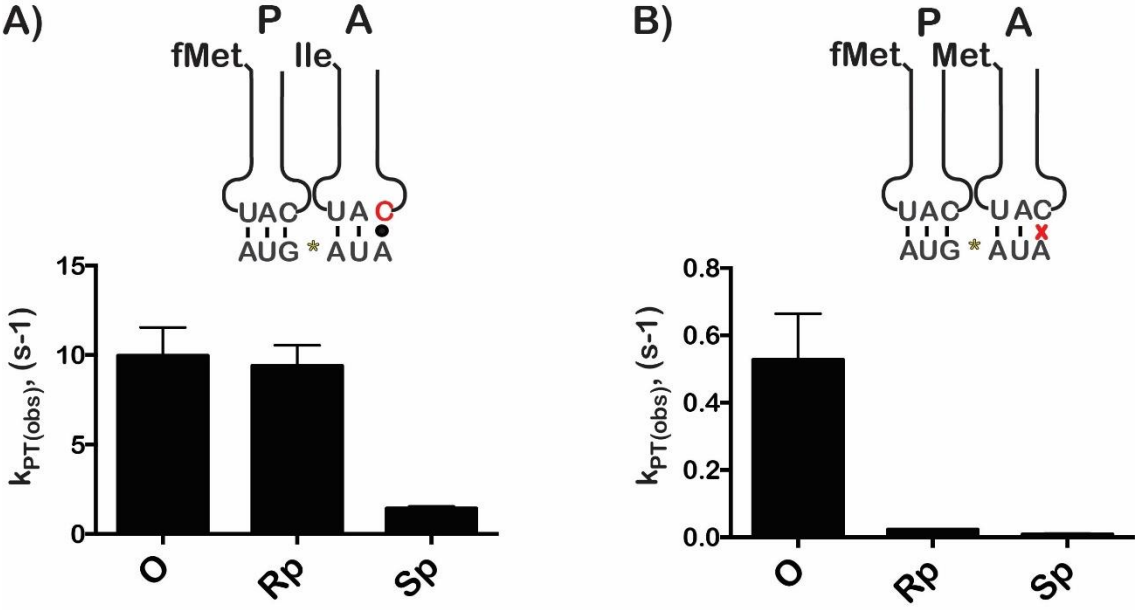

Fig. 4.5 Peptide release is not impacted by phosphorothioate modification at interface of the P-site and A-site codons. A) and B) Representative time courses for peptide release between the indicated initiation complexes (programmed with either a native mRNA or racemic mixture of phosphorothioate mRNAs) and RF1 and RF2, respectively.

Phosphorothioate substitutions between the first and second nucleotide of the A-site codon also result in a hyperaccurate phenotype

In addition to the *pro*-S oxygen between the P and A site, the kink-stabilizing magnesium ion also appears to be coordinated by the *pro*-R oxygen between the first and second position of the A-site codon (39). Consequently, substitution of this oxygen is very likely to perturb the mRNA structure and, in turn, produce a phenotype similar to the one we saw with substitutions at the P/A interface. We used the same strategy as before to generate native as well as modified complexes and assessed the effect of the sulfur substitution on PT rate for cognate and near-cognate aa-tRNAs.

Consistent with earlier observations, both *Rp*- and *Sp*-phosphorothioate substitutions at the second position of the A site have minimal effect on peptide-bond formation for the cognate aa-

tRNA (Fig. 6*A*). Furthermore, the same substitutions significantly reduced the PT rates for the two tested near-cognate ternary complexes, Lys-tRNA^{Lys} and Asp-tRNA^{Asp} (Fig. 6*B* and 6*C*). However, whereas the *pro*-S oxygen at the P/A interface appears to have a larger effect on decoding near-cognate aa-tRNAs, at this position in the A site the *Rp*-phosphorothioate substitution had a much more pronounced effect on the selection of these very same aa-tRNAs. In particular, PT rates for lys-tRNA^{lys} were 0.080 s^{-1}, 0.0039 s^{-1}, and 0.011 s^{-1} for the native and *Rp*- and Sp-phosphorothioate complexes, respectively. Similarly, PT rates for Asp-tRNA^{Asp} were 0.035 s^{-1}, 0.0049 s^{-1}, and 0.0050 s^{-1} for the native, *Rp*- and *Sp*-phosphorothioate complexes, respectively. Furthermore, the end points for the same reactions were 0.51, 0.11, and 0.21, respectively, suggesting that the modification also increases the rejection rate for the near-cognate aa-tRNAs during the proofreading phase of the selection. Interestingly, at this position, the substitution does not appear to affect peptide-release by RF1 (Fig. 6*D*) and only slightly for that by RF2 (Fig. 6*E*). These observations again highlight the distinction between tRNA and RF selections, with the latter being more robust to perturbations. Nevertheless, taken together, our data suggests that coordination of the magnesium ion by the phosphodiester backbone of the mRNA, and likely the resulting mRNA structure, plays a significant role during decoding.

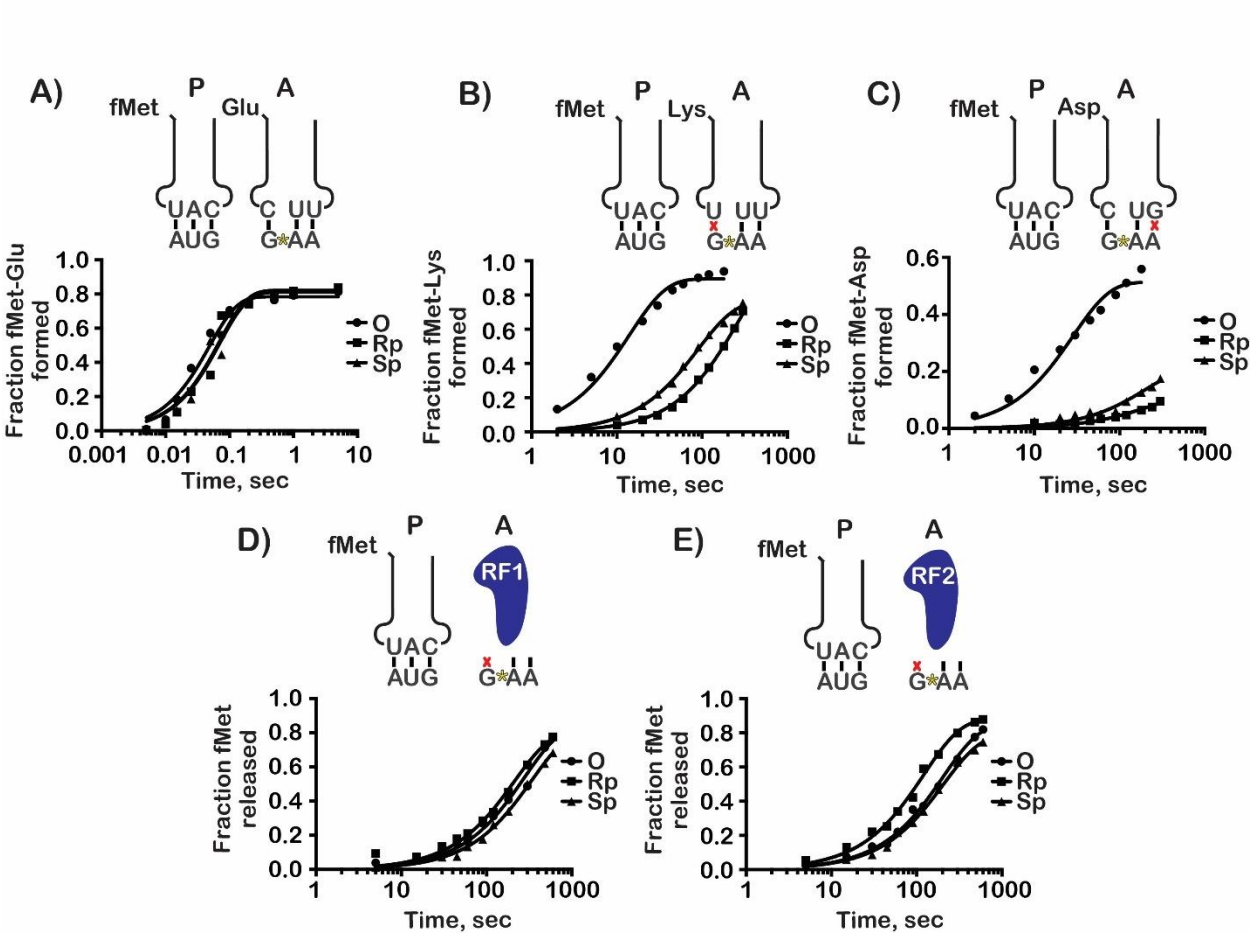

Fig. 4.6 Phosphorothioate modification at the second position of the A-site codon results in a hyperaccurate phenotype. A) Representative time courses of peptide-bond formation between the depicted unmodified or modified complexes with the cognate Glu-tRNA^{Glu}. The phosphorothioate modification is between the G and A of the A-site GAA codon (as shown above). B) and C) Time courses of PT reactions with the near-cognate Lys-tRNA^{Lys} and Asp-tRNA^{Asp} ternary complexes, respectively. D) and E) Time courses for RF1- and RF2-mediated hydrolysis reactions, respectively.

Phosphorothioate substitutions between the second and third nucleotide of the A-site codon has little effect on the accuracy of tRNA selection

Unlike that of the P/A interface and the first position of A-site codon, the phosphate of the second position of the A-site codon does not appear to coordinate a divalent metal (Fig. 1*A*). Therefore, phosphorothioate substitution at this position should serve as a nice control for effects resulting from mere sulfur introduction into the backbone of the mRNA versus magnesium-

structural stabilization effects. We used the same GAA-codon-containing mRNA but introduced the sulfur substitution between the last two nucleotides (GA-S_p-A) to generate modified initiation complexes. As expected, the substitution had no effect on the observed rate of peptide-bond formation by the cognate Glu-tRNA^{Glu} ternary complex (Fig. 7*A*). In the presence of the near-cognate Lys-tRNA^{Lys} ternary complex, we observed a modest threefold decrease for the modified complex (Fig. 7*B*). In comparison, we saw a twentyfold decrease in the observed rate for the same mRNA when it was modified at the first position (Fig. 6*B*), which was also accompanied by a fourfold reduction in the end point of the reaction. These observations suggest that while the introduction of sulfur on its own has some effects on the accuracy of peptide-bond formation, magnesium coordination by the nonbridging oxygen atoms of the mRNA backbone and hence its structure plays a far more important role in decoding accuracy.

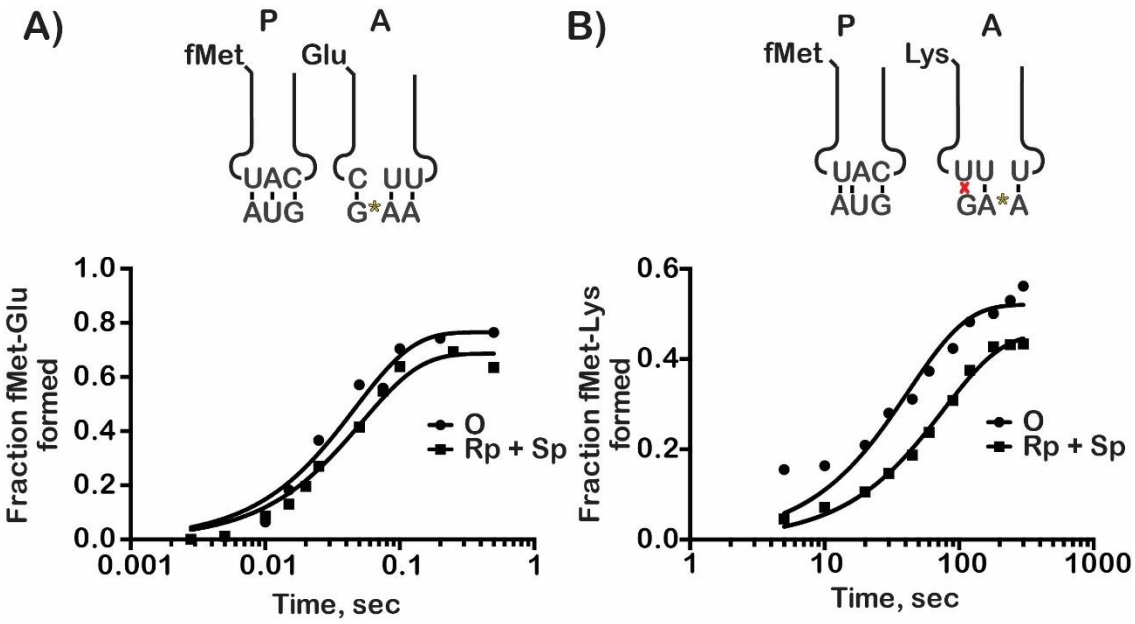

Fig. 4.7 Phosphorothioate substitution between the second and third nucleotide of the A-site codon does not significantly impact peptidyl transfer. A) and B) Representative time courses for PT between the indicated initiation complexes and the cognate Glu-tRNA^{Glu} and near-cognate Lys-tRNA^{Lys}, respectively. The phosphorothioate modification is between the second and third nucleotide of the A-site codon (as shown above).

The presence of a deoxyribose sugar between the A and P-site codons results in a hyperaccurate phenotype

Thus far, our studies have focused on the role of the phosphodiester backbone on the accuracy of tRNA selection and suggests an important role for its structure during tRNA selection. As a logical next step, we sought to examine the role of the ribose backbone in the accuracy of decoding. Initial structural studies of the small subunit highlighted the potential role for the chemical structure of ribose in decoding. These studies suggested that the A-site 2'-OH groups to be important for distinguishing between cognate and near-cognate tRNAs (31, 32). In particular, rRNA residues G530, A1492, and A1493 were shown to monitor the minor groove of the cognate codon-anticodon helix by forming hydrogen bonds with the 2'-OH groups. However, recent structural studies from a different group suggested that the hydrogen bonding was identical for both cognate and near-cognate codons (38) and that accuracy originates from energetic penalties associated with base pair mismatches being forced to adopt a Watson-Crick base-pair geometry. Previous biochemical studies by Simpson and colleagues explicitly addressed the role of the 2'-OH groups of the A site in decoding (37). Interestingly, single substitution of any of the 2'-OH groups by a deoxy only marginally affected peptide-bond formation. Multiple deoxy substitutions, on the other hand, severely inhibited tRNA selection parameters. In contrast, 2'-Fluro substitutions of all three hydroxyl groups of the A site has little to no effect on tRNA selection. These findings suggested that hydrogen bonds with the ribose backbone are not important for decoding; instead shape complementarity of the bases and their partners appears to be paramount. We note that, these studies looked at the role of the 2'-OH groups on the accuracy of the decoding process through competition assays. These assays suggested that individual substitutions to have no effect on

fidelity. However, their effect on peptide-bond formation in the presence of near-cognate aa-tRNAs was not directly measured.

Motivated by these earlier findings, we next explored the role of the 2'OH groups of the ribose backbone in discriminating against near-cognate tRNAs. As in the phosphorothioate assays, we prepared initiation complexes that displayed the Glu GAA in the A site. In addition to the native complex, we generated four more that harbored one deoxy substitution at the third position of the P-site codon or at the first, second, or third position of the A-site codon. As had been seen earlier, these substitutions had a negligible effect on the rate of peptide-bond formation in the presence of the cognate aa-tRNA (Fig. 8*A*). In contrast, the substitutions had drastic effects on peptidyl transfer in the presence of the near-cognate Lys-tRNA^{Lys}, with the substitutions of the A-site codon having the most profound effect (Fig. 8*B*). More specifically, introducing the deoxy modification to the third position of the P-site codon resulted in a tenfold decrease observed rate of peptidyl transfer, with no appreciable effect on the end point (Fig. 8*B*). In contrast, although the observed rates for A-site-substituted complexes does not vary much from the unmodified one, the end points for these reactions were severely diminished (1-2% of the initiation complexes reacted with the ternary complex) (Fig. 8*B*). Hence, substitution of the hydroxyl groups of the A-site codon appears to result in aggressive proofreading by the ribosome.

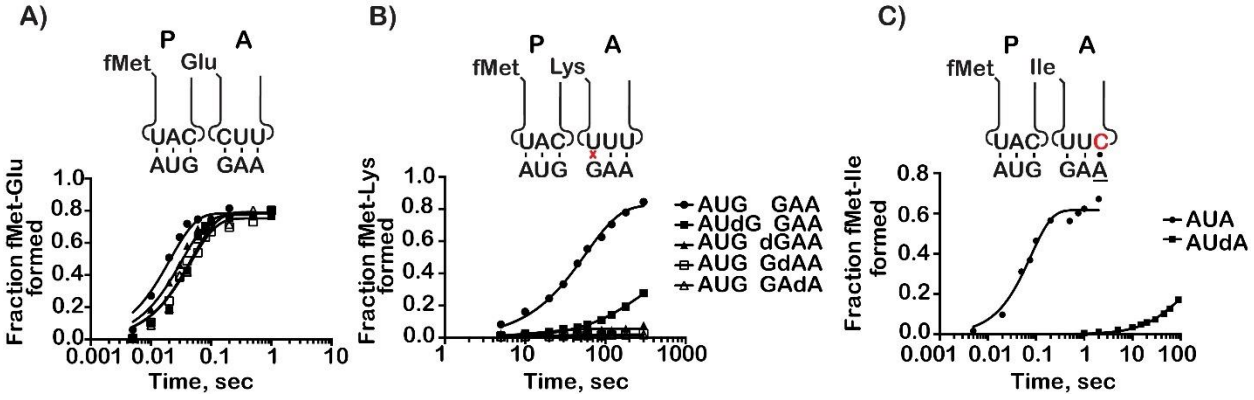

Fig. 4.8 Deoxyribose substitutions in the A-site codon result in a severe hyperaccurate phenotype. A) Representative time courses for PT reactions between the initiation complexes programmed with the indicated native and deoxyribose-modified mRNAs and the cognate Glu-tRNA^{Glu} ternary complex. B) Representative time course for PT between complexes displaying the native AUA codon or the deoxy-modified one at the third position of the codon (AUdA) and the cognate Ile-tRNA^{Ile} ternary complex. The corresponding Ile-tRNA harbors the lysidine (k^2C) modification at the wobble position.

DISCUSSION

Decades of biochemical and structural studies on translation have shown almost every component of the translational machinery, including the ribosomal RNA and proteins, tRNAs, and translation factors, to be important for faithful and rapid decoding (11, 29). In contrast, the role of the mRNA substrate itself during the process has been largely overlooked. Beyond its primary role in interrogating the incoming tRNA to ensure matched codon-anticodon interactions are maintained, the mRNA is arguably perceived as a mere onlooker during elongation. It is worth noting that the tRNA substrate was also viewed similarly until structural and biochemical data provided compelling evidence to the contrary (28, 36). For instance, the tRNA is very dynamic during the selection process, adopting distinct conformations as it moves into the A site and eventually participating in peptidyl transfer (47, 48). Perturbance to this conformational flexibility has significant consequences on the fidelity of protein synthesis, allowing tRNAs to read the incorrect codon (49). In addition to its role in decoding, the tRNA plays an important role in the chemistry of peptide-bond formation and peptide release (50-54). The hydroxyl group of the terminal ribose (A76) of the tRNA and its ability to form a hydrogen-bonding network is important for PT (54) and appears to be absolutely required for peptide release (55, 56). Similar to the findings of studies on the functional importance of the tRNA structure, it is highly likely that the mRNA structure plays an extensive role in many aspects of protein synthesis.

Early structural studies of the decoding process revealed a central role for the ribose backbone of the mRNA in maintaining codon-anticodon interactions (31). These include A-minor interactions between the mRNA and decoding center rRNA nucleotides. In addition to interacting with O2 and N4 of the respective purine and pyrimidine bases of the codon/anticodon, the rRNA residues also hydrogen bond with the 2’-OH groups of the mRNA (31). Disruption of these

interactions by substituting the ribose groups by 2'-deoxy ribose or 2'-fluoro, as expected, results in increased dissociation of the A-site tRNAs (57). However, these substitutions also result in increased translocation rates (57) suggesting that disruption of the interactions between the mRNA and tRNAs are required to remodel the mRNA during translocation. In contrast to their role in translocation, the 2'-OH groups of the A-site codon appear to be dispensable for tRNA selection (37); instead, shape complementarity appears to be the driving force for decoding. While these limited studies have highlighted the importance of the ribose backbone of mRNA during translation, the importance of the phosphodiester backbone has not been explored. In functional RNAs, the phosphodiester backbone plays an important role in coordinating divalent metals (58), which are important for maintaining the overall structure of the molecule; in certain cases, the metal is directly responsible for the function of the RNA (59, 60). In the case of the ribosome, atomic-resolution structures have revealed a number of locations where metals appear to play an important role (39). However, the contribution of most of these sites to the function of the ribosome has not been directly tested. Naturally, the main limitation to carrying out such studies is the difficulty of conducting atomic mutagenesis on the rRNA and, in particular, substitutions of nonbridging oxygen atoms to interfere with metal binding. In contrast to the ribosome, these types of phosphorothioate substitutions approaches have been instrumental in working out mechanisms of ribozymes (61).

In addition to rRNA, structural studies have shown the mRNA backbone to be directly involved in coordinating at least one divalent metal at the interface of the P/A sites of the small subunit (38, 39). More important, the metal appears to play a critical role in maintaining an unusual structure of the mRNA characterized by a kink. This in turn allows rRNA nucleobases of the small subunit to sandwich themselves (through base stacking) between the P and the A site and in the

process divide the two sites (38, 39). These initial studies speculated that this structure is important for preventing slippage and hence frameshifting during translocation (39). In contrast to its supposed role in frame maintenance, the role of the kink in decoding has not been considered previously. By disrupting the interaction between the mRNA and the divalent metal (and very possibly the kink structure) through phosphorothioate substitutions we were able to show the structure to be likely important for uniform decoding. In particular, whereas the substitutions appear to have little to no effect on PT for cognate tRNAs that utilize typical Watson-Crick as well as G-U wobble base pairs, they dramatically reduced PT for an aa-tRNA that uses atypical base pairing at the third position. Substitution of the *pro*-S oxygen at the kink (one of the atoms involved in coordinating the crucial divalent metal) reduced the PT rate for Ile-tRNA^{Ile}($k2_C$) by more than fivefold (Fig. 4*A*). Consistent with its role in boosting tRNA selection under compromised conditions, altering the kink structure also resulted in a severe hyperaccurate phenotype (Figs. 3, 4 and S1). As a case in point, the rate of the peptide bond reaction and the endpoint for the near-cognate Lys-tRNA^{Lys} on the Sp-GAA codon is ~twenty fold slower and approximately fourfold lower than that for the unmodified mRNA (Figs. 3*B* and 3*C*). We note that these observed effects of the phosphorothioate substitutions on the tRNA selection, through which the effective accuracy is improved by almost two orders of magnitude, are much more dramatic than those observed in the hyperaccurate-variant ribosomes. Restrictive mutations in the ribosomal protein S12, for instance, have been documented to improve accuracy by less than 10-fold (62). Similarly, mutations in H69 have been shown to improve accuracy by only threefold (46). These observations argue that, beyond its requirement to base pair with the tRNA, the mRNA structure is at least as equally critical for tRNA selection as are the rRNA and ribosomal proteins.

Arguably one of the key questions that came out of this study is how the kink structure might be affecting the interaction between the mRNA and the incoming tRNA. While our data alone do not answer this question, one could take advantage of the available structural and biochemical information to come up with scenarios to explain our findings. Disruption of the kink structure appears to affect later steps of tRNA selection more severely than early steps (Fig. 3). In particular, in the presence of the *S*p-phosphorothioate modification, PT reactions with near-cognates exhibited drastic end-point defects (Fig. 3*B* and *C*), but a modest decrease in observed rate of GTP hydrolysis (Fig. 3*D*). Hence, interfering with magnesium binding at the P/A interface appears to increase the rate of near-cognate tRNA rejection. It is plausible that the kink structure serves to rigidify the mRNA in the A site; as a result, the mRNA is more dynamic in its absence. Consequently, the dissociation rate of the tRNA is likely to increase during the proofreading phase. For typical cognate aa-tRNAs, the proceeding step of accommodation is so rapid that the increase in the dissociation rate is not realized to an extent that would affect the overall selection process. For near-cognate aa-tRNAs, accommodation is much slower; as a result, the effects of the kink disruption on codon recognition are felt, reducing the overall rate of peptide-bond formation. These ideas are corroborated by the observations that disruption of potential hydrogen bonds with the 2'-OH of the A-site codon has modest effect on cognate tRNA selection, but drastically diminishes peptide-bond formation in the presence of near-cognate aa-tRNAs (Fig. 8).

In an alternative scenario, the kink structure could play a role relaying signals between the P and the A sites of the ribosome. This idea is motivated by earlier studies by our group showing that mismatches in the P site severely compromise the fidelity of the next bout of tRNA selection (63, 64). These earlier findings as well as the observations we report here are consistent with a model in which the extended mRNA-tRNA interaction is important for decoding.

Notwithstanding, whatever the mechanism by which the kink affects decoding may be, our findings provide some new unappreciated insights into the role of the substrate mRNA in ensuring protein synthesis proceeds uniformly. The observation that a mere atomic substitution of one of the nonbridging oxygen atoms could drastically modify tRNA selection parameters argues that decoding is an intricate process that evolved to take advantage of all available interactions for optimal gene expression. In addition to this role in tRNA selection, the mRNA structure is highly likely to be important for frame maintenance. Indeed, mutations and perturbations even farther from the A site in the E site have been shown to increase frameshifting (64). It will be exciting to directly probe the role of the kink in translocation and to explore whether phosphorothioate substitutions affect frameshifting.

EXPERIMENTAL PROCEDURES

Materials and reagents.

Unmodified mRNAs were synthesized using *in vitro* runoff transcription by T7 RNA polymerase (66). Double-stranded DNA templates were amplified from single-stranded oligonucleotides that were purchased from IDT. The final DNA templates had the following sequences:

AUG-GAA (Met-Glu):

*TAATACGACTCACTATA*GGGTTAACTTTAGAAGGAGGTATACT**ATG**GAATAACTCGCA

TGCCCACTTGTCGATCACCGCCCTTGATTTGCCCTTCTGT

AUG-CAA (Met-Gln):

*TAATACGACTCACTATA*GGGTTAACTTTAGAAGGAGGTATACT**ATG**CAATAACTCGCA

TGCCCACTTGTCGATCACCGCCCTTGATTTGCCCTTCTGT

AUG-AUA (Met-Ile):

*TAATACGACTCACTATA*GGGTTAACTTTAG<u>AAGGAGGT</u>ATACT**ATG**ATATAACTCGCA

TGCCCACTTGTCGATCACCGCCCTTGATTTGCCCTTCTGT

The T7 promoter is italicized, the Shine-Dalgarno sequence is underlined, and the initiation codon is in bold.

AUG-$_s$CAA (Met-Gln)-modified mRNA with the sequence AAGGAGGTAAAAAAAATG$_s$CAAAAGTAA ("s" indicates the site of the phosphorothioate modification) was purchased from Dharmacon. AUG-$_s$GAA, AUG-$_s$AUA and AUG-G$_s$AA phosphorothioate-modified mRNAs were generated from two chemically synthetized ribo-oligonucleotides that were purchased from IDT. The upstream sequence of AAUA<u>AGGAGGU</u>AUACU was common to all of them. The downstream oligonucleotides had the following sequences: AUG$_s$GAAUUU, AUG$_s$AUAUUU and AUGG$_s$AAUUU, respectively. Before generating the full-length mRNAs, the modified oligonucleotides were separated into the *R*p and *S*p diastereoisomers using reverse phase chromatography as described earlier (66). In particular, 10 nmoles of RNA was injected into an Agilent 1100 HPLC system equipped with a C18 column (Zorbax ODS, 5 μm, 4.6 × 250 mm). The following conditions were used for the purification: the column was equilibrated with 100 mM ammonium acetate buffer pH 7 containing 3% acetonitrile; 5 minutes following injection, acetonitrile concentration was linearly increased to 13% over a 15-minute period and kept there for an additional 5 minutes. During the purification, the column was maintained at 45°C. The purified RNA was dried using a SpeedVac concentrator at ambient temperature overnight. The purified oligonucleotides were resuspended in water and then phosphorylated using polynucleotide kinase (NEB) in the presence of ATP. Prior to initiating

the ligation reaction, the upstream and the phosphorylated purified modified oligonucleotides were annealed to a DNA splint with final concentrations of 13 μM upstream RNA sequence, 10 μM modified phosphorylated oligonucleotide and 11 μM DNA splint. The DNA splints had the following sequence: AAATTCCATAGTATACCT for the AUG-$_s$GAA and AUG-G$_s$AA mRNAs and AAATAT CATAGTATACCT for the AUG-$_s$AUA mRNA. Ligation was carried out using T4 RNA ligase 2 (NEB) and incubation at 37°C for 2 hr. The ligated products were purified away from the substrate RNA and DNA splint using denaturing PAGE.

Tight-coupled 70S ribosomes were purified using a double pelleting strategy as described (68). Briefly clarified lysate was centrifuged at 107100 × g for 16 hr over a sucrose cushion at 4°C; ribosome pellet was resuspended, and the centrifugation step was repeated. Ribosomes were stored in polymix buffer (69) (95 mM KCl, 5 mM NH_4Cl, 5 mM Mg(OAc)2, 0.5 mM CaCl2, 8 mM putrescine, 1 mM spermidine, 5 mM potassium phosphate at pH 7.5, 1 mM DTT), aliquoted, flash frozen and stored at -80°C. His-tagged IF1, IF3 (45) and IF2 (70) were purified over Ni-NTA resin as described earlier (45). Purification of the His-tagged 20 aa-tRNA synthetases, RF1 and RF2 was carried out as described in (70). EF-Tu and EF-G were also purified over Ni-NTA resin; following purification the His tag was removed using TEV protease (71). *E. coli* $tRNA^{fMet}$, RNA^{Met}, RNA^{Glu}, RNA^{Lys} , RNA^{Arg}, RNA^{Val}, RNA^{Phe} and RNA^{Tyr} was purchased from ChemBlock.

tRNA aminoacylation

[^{35}S]-fMet-$tRNA^{fMet}$ was prepared as described (72) using Met-tRNA synthetase and Methionyl-tRNA formyltransferase in the presence of [^{35}S]-Met (Perkin Elmer) and 10-

formyltetrahydrofolate formyl donor at 37°C. Purified tRNAs were aminoacylated as described (41) by incubating them in the presence of the appropriate tRNA synthetase, the corresponding amino acid and ATP. All other tRNAs were charged by incubating *E. coli* total tRNA (Roche) with the applicable tRNA synthetase and the equivalent amino acid in the presence of ATP.

Ribosome complex formation

Initiation complex were generated as described previously (45) by mixing 2 μM 70S ribosomes with 3 μM IF1, IF2, IF3, [^{35}S]-fMet-tRNA^{fMet}, 6 μM mRNA, and 2 mM GTP in polymix buffer. Following incubation at 37°C for 2 minutes, the mixture was placed on ice before adding $MgCl_2$ to a final concentration of 10 mM. The complex was purified away from IFs, and unbound tRNA and mRNA through centrifugation over a sucrose cushion (1.1 M sucrose, 20 mM Tris pH 7.5, 500 mM NH_4Cl, 10 mM $MgCl_2$, 0.5 mM EDTA) at 223424 × g in an MLA-130 rotor (Beckman) for 2 hours at 4°C. The purified pelleted complexes were resuspended in polymix buffer (using the original volume). Small aliquots were taken before and after centrifugation for scintillation counting to estimate complex recovery and concentration.

Dipeptide-formation and release assays

Ternary complexes were generated by first incubating 30 μM EFTu with 2 μM GTP to exchange bound GDP at 37°C for 15 minutes before adding the appropriate aa-tRNA to a final concentration of 4 μM. The mixture was further incubated for an additional 15 minutes. Peptide-bond formation was initiated by mixing equal volume of initiation complex and ternary complex at 37°C. For fast reactions, the mixing was done on an RQF-3 quench flow apparatus (KinTek) at 37°C. The reactions were quenched by the addition of KOH to a final concentration of 1 M.

Dipeptides were resolved from unreacted fMet using cellulose TLC plates electrophoresed in a PyrAC buffer (3.48 M acetic acid, 62 mMpyridine) and Stoddard's solvent at 1200 V (40). The TLCs were dried and exposed to phosphoscreens before imaging on a Biorad personal imager phosphorimager. The fractional reactivity corresponding to the dipeptide was quantified as a function of time using Bio-Rad Quantity One software. The resulting data was fit to a single-exponential function using GraphPad prism software. All reactions were conducted at least in duplicates.

Peptide release was carried out by mixing 2 μM initiation complex with 10 μM RF1 and RF2 in polymix buffer at 37°C. Reactions were stopped through the addition of formic acid to a final concentration of 5% or EDTA to a final concentration of 20 mM. Released fMet was resolved from fMet-tRNA^{fMet} using electrophoretic TLCs as described above.

ACKNOWLEDGMENTS

The authors wish to thank Bob Kranz and Allen Buskirk for commenting on earlier versions of the manuscript and members of the Zaher lab for useful discussion. This work was supported by the NIH (R01GM112641 to H.S.Z.).

AUTHOR CONTRIBUTIONS

HEK, ENT and HSZ designed the experiments. HEK and ENT carried out the experiments. HEK, ENT and HSZ analyzed the data and wrote the manuscript.

REFERENCES:

1. Rosenberger RF & Foskett G (1981) An estimate of the frequency of in vivo transcriptional errors at a nonsense codon in Eschericia-coli. *Mol Gen Genet* 183(3):561-563.

2. Edelmann P & Gallant J (1977) Mistranslation in E. coli. *Cell* 10(1):131-137.

3. Bouadloun F, Donner D, & Kurland CG (1983) Codon-specific missense errors in vivo. *EMBO J.* 2(8):1351-1356.

4. Kramer EB & Farabaugh PJ (2007) The frequency of translational misreading errors in E. coli is largely determined by tRNA competition. *RNA* 13(1):87-96.

5. Thompson RC (1988) EFTu provides an internal kinetic standard for translational accuracy. *Trends Bioch Sci* 13(3):91-93.

6. Hopfield JJ (1974) Kinetic proofreading: a new mechanism for reducing errors in biosynthetic processes requiring high specificity. *Proc Natl Acad Sci USA* 71(10):4135-4139.

7. Ninio J (1975) Kinetic amplification of enzyme discrimination. *Biochimie* 57(5):587-595.

8. Pape T, Wintermeyer W, & Rodnina M (1999) Induced fit in initial selection and proofreading of aminoacyl-tRNA on the ribosome. *EMBO J* 18(13):3800-3807.

9. Johansson M, Bouakaz E, Lovmar M, & Ehrenberg M (2008) The kinetics of ribosomal peptidyl transfer revisited. *Mol Cell* 30(5):589-598.

10. Gromadski KB & Rodnina MV (2004) Kinetic determinants of high-fidelity tRNA discrimination on the ribosome. *Mol Cell* 13(2):191-200.

11. Zaher HS & Green R (2009) Fidelity at the molecular level: lessons from protein synthesis. *Cell* 136(4):746-762.

12. Crick FH (1963) On the genetic code. *Science* 139:461-464.

13. McLaughl.Cs, Dondon J, Grunberg.M, Michelso.Am, & Saunders G (1966) Stability of the messenger RNA-sRNA-ribosome complex. *Cold Spring Harb Symp Quant Biol* 31:601-610.

14. Gorini L, Jacoby GA, & Breckenr.L (1966) Ribosomal ambiguity. *Cold Spring Harb Symp Quant Biol* 31:657-664.

15. Rosset R & Gorini L (1969) A ribosomal ambiguity mutation. *J Mol Biol* 39(1):95-112.

16. Zimmermann RA, Garvin RT, & Gorini L (1971) Alteration of a 30S ribosomal protein accompanying the ram mutation in Escherichia coli. *Proc Natl Acad Sci USA* 68(9):2263-2267.

17. Birge EA & Kurland CG (1970) Reversion of a streptomycin-dependent strain of Escherichia coli. *Mol Gen Genet* 109(4):356-369.

18. Brownstein Bl & Lewandowein LJ (1967) A mutation suppressing streptomycin dependence. I. An effect on ribosome function. *J Mol Biol* 25(1):99-109.

19. Stoffler G, Deusser E, Wittmann HG, & Apirion D (1971) Ribosomal proteins. XIX. Altered S5 ribosomal protein in an Escherichia coli revertant from strptomycin dependence to independence. *Mol Gen Genet* 111(4):334-341.

20. Gorini L & Kataja E (1964) Phenotypic repair by streptomycin of defective genotypes in E. coli *Proc Natl Acad Sci USA* 51(3):487-493.

21. Ozaki M, Mizushim.S, & Nomura M (1969) Identification and Functional Characterization of the Protein controlled by the Streptomycin-resistant Locus in E. coli. *Nature* 222(5191):333-339.

22. O'Connor M & Dahlberg AE (1995) The involvement of two distinct regions of 23 S ribosomal RNA in tRNA selection. *J Mol Biol* 254(5):838-847.

23. O'Connor M, Thomas CL, Zimmermann RA, & Dahlberg AE (1997) Decoding fidelity at the ribosomal A and P sites: influence of mutations in three different regions of the decoding domain in 16S rRNA. *Nucleic Acids Res* 25(6):1185-1193.

24. McClory SP, Leisring JM, Qin D, & Fredrick K (2010) Missense suppressor mutations in 16S rRNA reveal the importance of helices h8 and h14 in aminoacyl-tRNA selection. *RNA* 16(10):1925-1934.

25. Carr-Schmid A, Durko N, Cavallius J, Merrick WC, & Kinzy TG (1999) Mutations in a GTP-binding motif of eukaryotic elongation factor 1A reduce both translational fidelity and the requirement for nucleotide exchange. *J. Biol Chem* 274(42):30297-30302.

26. Ito K, Uno M, & Nakamura Y (1998) Single amino acid substitution in prokaryote polypeptide release factor 2 permits it to terminate translation at all three stop codons. *Proc Natl Acad Sci USA* 95(14):8165-8169.

27. Hirsh D (1971) Tryptophan transfer RNA as the UGA suppressor. *J Mol Biol* 58(2):439-458.

28. Cochella L & Green R (2005) An active role for tRNA in decoding beyond codon:anticodon pairing. *Science* 308(5725):1178-1180.

29. Voorhees RM & Ramakrishnan V (2013) Structural basis of the translational elongation cycle. *Annu Rev Biochem* 82:203-236.

30. Schmeing TM & Ramakrishnan V (2009) What recent ribosome structures have revealed about the mechanism of translation. *Nature* 461(7268):1234-1242.

31. Ogle JM, *et al.* (2001) Recognition of cognate transfer RNA by the 30S ribosomal subunit. *Science* 292(5518):897-902.

32. Ogle JM, Murphy FV, Tarry MJ, & Ramakrishnan V (2002) Selection of tRNA by the ribosome requires a transition from an open to a closed form. *Cell* 111(5):721-732.

33. Loveland AB, Demo G, Grigorieff N, & Korostelev AA (2017) Ensemble cryo-EM elucidates the mechanism of translation fidelity. *Nature* 546(7656):113-117.

34. Schmeing TM, *et al.* (2009) The crystal structure of the ribosome bound to EF-Tu and aminoacyl-tRNA. *Science* 326(5953):688-694.

35. Voorhees RM, Schmeing TM, Kelley AC, & Ramakrishnan V (2010) The mechanism for activation of GTP hydrolysis on the ribosome. *Science* 330(6005):835-838.

36. Schmeing TM, Voorhees RM, Kelley AC, & Ramakrishnan V (2011) How mutations in tRNA distant from the anticodon affect the fidelity of decoding. *Nat Struct Mol Biol* 18(4):432-436.

37. Khade PK, Shi X, Joseph S (2013) Steric complementarity in the decoding center is important for tRNA selection by the ribosome. *J Mol Biol* 425:3778-3789.

38. Demeshkina N, Jenner L, Westhof E, Yusupov M, & Yusupova G (2012) A new understanding of the decoding principle on the ribosome. *Nature* 484(7393):256-259.

39. Selmer M, *et al.* (2006) Structure of the 70S ribosome complexed with mRNA and tRNA. *Science* 313(5795):1935-1942.

40. Youngman EM, Brunelle JL, Kochaniak AB, & Green R (2004) The active site of the ribosome is composed of two layers of conserved nucleotides with distinct roles in peptide bond formation and peptide release. *Cell* 117(5):589-599.

41. Pierson WE, *et al.* (2016) Uniformity of Peptide Release Is Maintained by Methylation of Release Factors. *Cell reports* 17(1):11-18.

42. Freistroffer DV, Kwiatkowski M, Buckingham RH, & Ehrenberg M (2000) The accuracy of codon recognition by polypeptide release factors. *Proc Natl Acad Sci USA* 97(5):2046-2051.

43. Petropoulos AD, McDonald ME, Green R, & Zaher HS (2014) Distinct roles for release factor 1 and release factor 2 in translational quality control. *J Biol Chem* 289(25):17589-17596.

44. Hudson BH & Zaher HS (2015) O6-Methylguanosine leads to position-dependent effects on ribosome speed and fidelity. *RNA* 21(9):1648-1659.

45. Simms CL, Hudson BH, Mosior JW, Rangwala AS, & Zaher HS (2014) An active role for the ribosome in determining the fate of oxidized mRNA. *Cell reports* 9(4):1256-1264.

46. Ortiz-Meoz RF & Green R (2011) Helix 69 is key for uniformity during substrate selection on the ribosome. *J Biol Chem* 286(29):25604-25610.

47. Agirrezabala X, *et al.* (2008) Visualization of the hybrid state of tRNA binding promoted by spontaneous ratcheting of the ribosome. *Mol Cell* 32(2):190-197.

48. Agirrezabala X, *et al.* (2011) Structural insights into cognate versus near-cognate discrimination during decoding. *EMBO J* 30(8):1497-1507.

49. Ortiz-Meoz RF & Green R (2010) Functional elucidation of a key contact between tRNA and the large ribosomal subunit rRNA during decoding. *RNA* 16(10):2002-2013.

50. Schmeing TM, Huang KS, Kitchen DE, Strobel SA, & Steitz TA (2005) Structural insights into the roles of water and the 2' hydroxyl of the P site tRNA in the peptidyl transferase reaction. *Mol Cell* 20(3):437-448.

51. Trobro S & Aqvist J (2005) Mechanism of peptide bond synthesis on the ribosome. *Proc Natl Acad Sci USA* 102(35):12395-12400.

52. Dorner S, Panuschka C, Schmid W, & Barta A (2003) Mononucleotide derivatives as ribosomal P-site substrates reveal an important contribution of the 2'-OH to activity. *Nucleic Acids Res* 31(22):6536-6542.

53. Dorner S, Polacek N, Schulmeister U, Panuschka C, & Barta A (2002) Molecular aspects of the ribosomal peptidyl transferase. *Biochem Soc Trans* 30(Pt 6):1131-1136.

54. Zaher HS, Shaw JJ, Strobel SA, & Green R (2011) The 2'-OH group of the peptidyl-tRNA stabilizes an active conformation of the ribosomal PTC. *The EMBO J* 30(12):2445-2453.

55. Shaw JJ, Trobro S, He SL, Aqvist J, & Green R (2012) A Role for the 2' OH of peptidyl-tRNA substrate in peptide release on the ribosome revealed through RF-mediated rescue. *Chem Biol* 19(8):983-993.

56. Brunelle JL, Shaw JJ, Youngman EM, & Green R (2008) Peptide release on the ribosome depends critically on the 2' OH of the peptidyl-tRNA substrate. *RNA* 14(8):1526-1531.

57. Khade PK & Joseph S (2011) Messenger RNA interactions in the decoding center control the rate of translocation. *Nat Struct Mol Biol* 18(11):1300-1302.

58. Draper DE, Grilley D, & Soto AM (2005) Ions and RNA folding. *Annu Rev Biophys Biomol Struct* 34:221-243.

59. Bowman JC, Lenz TK, Hud NV, & Williams LD (2012) Cations in charge: magnesium ions in RNA folding and catalysis. *Curr Opin Struct Biol* 22(3):262-272.

60. Fedor MJ & Williamson JR (2005) The catalytic diversity of RNAs. *Nat Rev Mol Cell Biol* 6(5):399-412.

61. Frederiksen JK & Piccirilli JA (2009) Identification of catalytic metal ion ligands in ribozymes. *Methods* 49(2):148-166.

62. Zaher HS & Green R (2010) Hyperaccurate and error-prone ribosomes exploit distinct mechanisms during tRNA selection. *Mol Cell* 39(1):110-120.

63. Zaher HS & Green R (2009) Quality control by the ribosome following peptide bond formation. *Nature* 457(7226):161-166.

64. Zaher HS & Green R (2010) Kinetic basis for global loss of fidelity arising from mismatches in the P-site codon:anticodon helix. *RNA* 16(10):1980-1989.

65. Devaraj A, Shoji S, Holbrook ED, & Fredrick K (2009) A role for the 30S subunit E site in maintenance of the translational reading frame. *RNA* 15(2):255-265.

66. Zaher HS & Unrau PJ (2004) T7 RNA polymerase mediates fast promoter-independent extension of unstable nucleic acid complexes. *Biochemistry* 43(24):7873-7880.

67. Frederiksen JK & Piccirilli JA (2009) Separation of Rna Phosphorothioate Oligonucleotides by Hplc. *Method Enzymol* 468:289-309.

68. Cochella L, Brunelle JL, & Green R (2007) Mutational analysis reveals two independent molecular requirements during transfer RNA selection on the ribosome. *Nat Struct Mol Biol* 14(1):30-36.

69. Jelenc PC & Kurland CG (1979) Nucleoside triphosphate regeneration decreases the frequency of translation errors. *Proc Natl Acad Sci USA* 76(7):3174-3178.

70. Shimizu Y, *et al.* (2001) Cell-free translation reconstituted with purified components. *Nat Biotechnol* 19(8):751-755.

71. Blanchard SC, Gonzalez RL, Kim HD, Chu S, & Puglisi JD (2004) tRNA selection and kinetic proofreading in translation. *Nat Struct Mol Biol* 11(10):1008-1014.

72. Walker SE & Fredrick K (2008) Preparation and evaluation of acylated tRNAs. *Methods* 44(2):81-86.

Chapter 5

Conclusions and Future Directions

ABSTRACT

The focus of my thesis work has been on understanding how changes to mRNA structure impact the accuracy and fidelity of translation, which is a vital step in the transmission of genetic information. This was accomplished through several *in vitro* studies designed to understand the precise effect each mRNA modification had on the speed and accuracy of decoding, as well as changes in specific miscoding events. Through these studies, we uncover the base pairing preference of the most common oxidative damage adduct of mRNA, 8-oxoguanosine, in the context of the A-site of the ribosome. We confirm that the alkylative damage adduct, N(1)-methyladenosine, stalls the ribosome and provide evidence to support that it severely distorts the codon-anticodon helix. Additionally, we show that alkylative damage of RNA increases the activity of *trans*-translation in bacteria, suggesting that it stalls ribosomes. In another project, we show that the kink structure that the mRNA phosphodiester backbone assumes in the A site of the ribosome is only important to decoding under non-optimal conditions. Overall, this work has contributed to our understanding of the importance of mRNA structure during translation.

The impact of N(1)-methyladenosine on peptidyl transfer *in vitro*

N(1)-methyladenosine (m^1A) has recently emerged as a potential regulatory modification of mRNA; however, no demethylases have been shown to exist specifically for removing m^1A from mRNA. Additionally, no "reader" proteins that recognize m^1A have been identified (1). On the contrary, one study shows that the presence of m^1A in the coding region of mRNA significantly increases ribosome stalling (2) and another study demonstrates that m^1A increases local duplex melting (3), suggesting that it is detrimental to decoding. To understand the magnitude by which m^1A decreases the rate of peptidyl transfer as well as to understand if it impacts miscoding, *in vitro* peptide-bond formation assays were performed using our well-established reconstituted bacterial translation system (4).

We show that m^1A in the second position of the codon significantly decreases the rate and endpoint of peptide-bond formation, confirming its activity as a disruptive adduct of mRNA. Furthermore, we demonstrate that the addition of the aminoglycoside antibiotic, paromomycin, does not rescue the effect of m^1A on peptidyl transfer. This suggests that m^1A causes the codon to behave more as a non-cognate than a near-cognate codon, because if m^1A were only disrupting its own ability to form base pairs, the reaction should have at least been partially rescued by the addition of the antibiotic (5, 6). From these results, we predict that the positively charged resonance structure introduced to adenosine by the addition of the methyl group to N1 disrupts its neighboring nucleotides from forming base pairs.

In order to understand the details of how m^1A disrupts interactions between codons and aa-tRNAs or release factors, structural studies will need to be performed. These studies will help to confirm that m^1A is disrupting the codon-anticodon helix and elucidate the details of how neighboring hydrogen bonds might be disrupted by this lesion. Additionally, they will reveal

how m^1A is disrupting the interaction between the codon and release factor. Future kinetic and structural studies using stop codons containing m^1A may also reveal interesting changes to the recognition of stop codons by release factors.

Several studies in which m^1A-sequencing was performed revealed that it is enriched around the start codon and 3' of the first splice site in human cells (7, 8). If these studies are accurate, it would be interesting to investigate if m^1A has an intentional role to regulate translation initiation. We predict that the presence of the adduct would prevent proper translation initiation, and potentially cause the ribosome to continue scanning past the ^{m1}AUG and initiate at a downstream start codon. However, a third study that performed m^1A-sequencing showed that the adduct is significantly rarer than the previous studies reported, detecting only nine modified sites in cytosolic and mitochondrial mRNAs with no enrichment pattern (9). Much work remains to be performed to resolve these discrepancies; however, our data supports the theory that m^1A is primarily a damage adduct that is highly disruptive to decoding.

Ribosome rescue from alkylated transcripts in bacteria

While several studies have been performed to investigate the impact of alkylative adducts of mRNA on decoding *in vitro*, less is known about how this damage affects translation *in vivo* (10). Previous work from our group showed that the most common oxidative damage adduct, 8-oxoguanosine (8-oxoG), significantly reduces the rate of peptide-bond formation *in vitro* when it is present in mRNA. Additionally, this study revealed that when the no-go decay quality control pathway in eukaryotes is compromised, 8-oxoG accumulates to higher levels than in wild-type cells, suggesting that no-go decay may have evolved to cope with damaged mRNA (11). The cellular response to alkylative damage as well as mRNA damage in bacteria had not been previously explored. We hypothesized that alkylative damage of mRNA stalls translation *in vivo*,

and that the main bacterial ribosome rescue pathway, known as *trans*-translation, is responsible for rescuing these stalled ribosomes. To address these hypotheses, we introduced alkylative damage *in vivo* and visualized the resulting activity of the *trans*-translation pathway.

We first confirmed that two common alkylating agents, MMS and MNNG, caused accumulation of damage adducts in *E. coli* and identified the specific adducts introduced by each agent. Cells were treated with either alkylating agent and the resulting RNA adducts were quantified via LC-MS/MS. We measured significant increases in several disruptive adducts, including m^1A and m^3C after treatment with MMS or MNNG, and m^6G after treatment with MNNG. Our results support previous data demonstrating that mRNA is more susceptible to alkylative damage than DNA, as the hydrogen-bonding interface between double-stranded DNA impedes the accumulation of m^1A and m^3C (12, 13).

After demonstrating the accumulation of multiple disruptive RNA adducts after alkylating agent treatment, we then sought to observe ribosome stalling *in vivo*. To accomplish this, we utilized a previously modified-transfer-messenger RNA (tmRNA) that His_6-tags incomplete peptides from stalled ribosomes rather than tagging them for degradation by cellular proteases (14). We then treated these cells with MMS or MNNG and observed significant increases in His_6 levels via Western blot, suggesting that *trans*-translation is being activated upon nucleotide damage. To demonstrate that the observed increase in tmRNA activity was due to RNA damage rather than the production of truncated transcripts from damaged DNA, we performed a transcriptional runoff assay and treated cells with agents that exclusively introduce damage to DNA. We then observed His_6 levels in each of these samples and observed that while double-stranded DNA breaks do increase His_6 tagging, these levels significantly decrease after transcriptional runoff. Additionally, His_6 levels in the MMS and MNNG samples after

transcriptional runoff do slightly decrease, but not to the same extent as the samples treated with the DNA damaging agent. From these results, we conclude that while some His_6 tagging in the MMS and MNNG is due to the production of truncated transcripts from damaged DNA, most of the activity is due to damaged mRNA, demonstrating that *trans*-translation is responsible for rescuing ribosomes stalled by alkylative damage *in vivo*.

We also hypothesized that the *trans*-translation pathway is important for bacteria to efficiently recover from alkylative damage. To test this, we treated both WT *E. coli* and those lacking tmRNA (Δ*ssrA*) with the alkylating agents and monitored their growth post-treatment. While the growth curves of the untreated WT and Δ*ssrA* cells were indistinguishable, Δ*ssrA* cells after treatment with either MMS or MNNG recovered approximately 1.5 hours after WT cells. This demonstrates that a functional *trans*-translation system is required for efficient recovery post-alkylative damage. We predict that the Δ*ssrA* cells are still able to recover post-alkylative damage treatment because *E. coli* contain two additional ribosome rescue factors, ArfA and ArfB. ArfA is known to function as a backup for *trans*-translation, as its expression increases when tmRNA activity is limited. Future experiments can include performing qPCR in the WT and Δ*ssrA* to observe if ArfA activity increases. ArfB does not appear to function solely as a backup for tmRNA, so it would be interesting to investigate if it plays a role in rescuing ribosomes from damaged transcripts.

Here, we provide the first evidence that alkylative damage causes ribosomal stalling *in vivo*, and that *trans*-translation in bacteria is responsible for rescuing ribosomes stalled on alkylated transcripts. Another type of mRNA damage that can cause ribosome stalling is oxidative damage. To show that *trans*-translation is the pathway responsible for rescuing ribosomes stalled by other types of nucleotide damage besides alkylative damage, future

experiments will include repeating the tmRNA His_6-tagging analyses after treatment with oxidizing agents, such as hydrogen peroxide.

The mechanism through which tmRNA recognizes ribosomes stalled by alkylated transcripts is not understood. Previous studies have shown that tmRNA requires that no more than six nucleotides are present downstream of the P-site to rescue stalled ribosomes (15, 16). If the alkylative adduct exists in the middle of the transcript, we predict that the stalled ribosome triggers the cleavage of the mRNA at or within these six nucleotides. Previous reports have suggested that the tmRNA-complex recruits RNase R to degrade the non-stop mRNA (17, 18); however, RNase R is an exonuclease so it is not able to perform the initial endonucleolytic cleavage necessary for tmRNA to act on a ribosome stalled by a damage adduct. A previous report from our group shows that the collision of upstream ribosomes with the stalled ribosome induces no-go decay in eukaryotes (19). This involves the cleavage of the mRNA between the stalled and the colliding ribosome, and the endonuclease that performs this cleavage remains unidentified. It is possible that a similar process exists in bacteria, where the colliding ribosomes induces cleavage of mRNA so that the complex can become a target for *trans*-translation. To identify this potential endonuclease, a genetic screen could be performed to identify mutants that reduce His_6-tagging by tmRNA after treatment with alkylative damaging agents.

Recent *in vitro* studies have shown that when mRNA damaged with MMS was treated with AlkB, which is a hydroxylase in *E. coli* that has been shown to demethylate RNA and single-stranded DNA (20), translation was enhanced (21). Additionally, the same study showed that the treatment of tRNA with an alkylating agent inhibited aminoacylation, but that this inhibition was substantially relieved upon treatment with AlkB. To show that AlkB has the same effect *in vivo*, we can overexpress the protein in *E. coli* expressing tmRNA-His_6 and observe

differences in His_6-levels after treatment with alkylating agents. If there is a reduction in His_6-levels in the cells overexpressing AlkB, this would support the *in vitro* study that AlkB demethylates RNA and restores translation.

The treatment of *E. coli* with alkylating agents also revealed that activation of Ada increases proportionally to tmRNA activity. Ada is a key player in the adaptive response in *E. coli*, during which it serves as a suicide enzyme that transfers alkyl groups from O^6- alkyl guanine, O^4-alkyl thymine, and the oxygen of the phosphodiester backbone of DNA to one of its cysteine residues (22, 23). Once it is methylated, Ada serves as a transcriptional activator, inducing the expression of itself and other genes involved in the adaptive response (24, 25). One open question is whether Ada can transfer alkyl groups from damaged RNA, such as m^6G, resulting in the same activation of the adaptive response. One ongoing study in our group involves damaging mRNA with MMS and subsequently transfecting the mRNA into *E. coli* and observing if Ada is activated. If Ada activation is observed, this will provide evidence to support the hypothesis that Ada responds to both DNA as well as mRNA damage.

The base pairing preference of 8-oxoguanosine on the ribosome

8-oxoguanosine (8-oxoG) is the most common oxidative damage adduct of DNA and RNA (26, 27). Studies investigating 8-oxodG in DNA have shown that the lesion is mutagenic, as it has dual-coding potential due to its ability to change from an *anti* to a *syn* conformation and reveal an alternate hydrogen-bonding interface where is can form a Hoogsteen base pair with adenosine (28). This change in conformation relieves the steric hindrance that the O8 experiences with the phosphate backbone when 8-oxoG is in the *anti* conformation. A previous report by our group demonstrated that 8-oxoG in mRNA drastically reduced the rate of peptidyl transfer *in vitro* in the presence of an 8-oxoG•C base pair while slightly increasing the rate of

miscoding for 8-oxoG•A (11). However, the underlying mechanism for this disruption of tRNA selection was unaddressed. Here, *in vitro* peptidyl transfer studies in the presence of error-prone conditions demonstrate that 8-oxoG predominantly adopts a *syn* conformation in the A site.

We initially hypothesized that 8-oxoG is interfering with initial codon selection rather than the steps further downstream in tRNA selection. The irreversible hydrolysis of GTP separates initial codon selection and downstream reactions (29), so to test our initial hypothesis, we performed GTP hydrolysis assays in the presence and absence of 8-oxoG at all three positions of the codon. We observe a decrease in the rate of GTP hydrolysis that is similar to the decrease we previously observed for the rate of peptidyl-transfer in the presence of 8-oxoG. From this, we conclude that 8-oxoG is predominantly interfering with early-stage tRNA selection, likely during initial codon selection.

We then set out to investigate the preferred base pairing conformation of 8-oxoG in both the first and second position of the codon. To accomplish this, we took advantage of the ability of aminoglycoside antibiotics to relax tRNA selection conditions (5, 6, 30, 31). We performed *in vitro* peptidyl transfer reactions in the presence or absence of aminoglycoside antibiotics as well as in the presence of the cognate and all possible near-cognate aa-tRNAs. We observed that the average rate and endpoint of peptidyl transfer in the presence of 8-oxoG•A base pairs exceeded that of 8-oxoG•C base pairs in both the first and second positions of the codon. We also performed peptidyl transfer reactions in the presence of error prone ribosomes and observed higher rate and endpoint values for 8-oxoG•A than 8-oxoG•C. These results support the hypothesis that 8-oxoG primarily exists in the *syn* conformation on the ribosome, but that the 8-oxoG•A base pair is recognized as a mismatch and rejected during tRNA selection under normal conditions.

The next steps of investigating the base pairing preference of 8-oxoG on the ribosome include performing structural studies to investigate not only the changes that occur in the codon-anticodon helix in the presence of 8-oxoG, but also how the hydrogen bonds of the rRNA residues that are important for monitoring this interaction are altered by 8-oxoG in both the *syn* and *anti* conformation. Structural studies of DNA polymerases with templates containing 8-oxodG in the active site demonstrate that the fidelity of the polymerase determines how frequently the adduct codes for dC or for dA. Lower fidelity polymerases can incorporate bulkier base pairs, such as 8-oxodG•dC, in their active sites so they less frequently miscode for dA. On the contrary, high fidelity polymerases have a smaller active site, and the 8-oxodG•A base pair adopts a geometry that is very similar to that of a Watson Crick base pair, so these polymerases are more likely to miscode in the presence of the adduct (32–35). Similar structural studies of 8-oxoG in the A site of the ribosome will help to elucidate why this lesion generally causes stalling rather than bypass under normal conditions.

Additionally, we hypothesized that *E. coli* containing error-prone ribosomes would be better able to survive oxidative stress conditions due to their ability to bypass oxidative lesions rather than stall protein synthesis. This would provide a selective advantage for organisms living in highly oxidative environments, such as pathogens that deal with the reactive oxygen species associated with immune responses. To test this, we treated either WT *E. coli* or cells expressing error-prone ribosomes with hydrogen peroxide and observed recovery either by performing spot assays or monitoring growth curves. No significant difference in ability to recovery post-oxidative treatment was observed between the strains. Interestingly, one previous study did observe a 30% - 70% decrease in survival rates during oxidative damage of WT *E. coli* compared to those expressing error-prone ribosomes post-oxidative treatment (36), but the

mutations to generate error-prone ribosomes in this study were in the same ribosomal protein but at a different locus than the mutation we utilized. Overall, the results of this study were inconclusive but do not support the conclusion that all error-prone ribosomes provide a selective advantage for bacterial recovery following oxidative stress.

The importance of the phosphodiester backbone kink structure during decoding

While much is known about the importance of rRNA and tRNA structure with regards to the decoding process, less is known about how mRNA structure impacts translation. Structural studies have revealed that the mRNA adopts a kink-like structure in the context of the ribosome between the P and A sites (37, 38). A magnesium ion stabilizes this structure through electrostatic interactions with the non-bridging oxygens of the phosphodiester backbone of the mRNA (38). Whether or not this structure contributes to tRNA selection remained unknown. To address this question, we utilized our reconstituted *in vitro* translation system in combination with an mRNA construct that contains stereospecific phosphorothioate substitutions to disrupt this kink structure.

When we substituted either of the non-bridging oxygen atoms between the A- and P-site codons with sulfur to disrupt the coordination of the magnesium ion, we observed that tRNA selection became more stringent. The phosphorothioate-modified mRNAs were less reactive with near-cognate tRNAs than the unmodified mRNA control. Interestingly, reactivity with cognate aa-tRNAs remained unaffected. This suggested that the structure of the mRNA backbone at the interface of the A and P sites plays an important role in tRNA selection. When extended reactions were performed, both the *Sp*- and *Rp*- phosphorothioate substitutions reduced the rate of peptide-bond formation in the presence of near-cognate aa-tRNAs, but the *Sp* substitution resulted in a more severe endpoint defect, suggesting that the *pro*-S oxygen is more

important for coordinating the kink structure than the *pro*-R oxygen. We also analyzed the rate of peptide release for these constructs, and while there was a slight decrease in rate for the *Sp* and *Rp*-phosphorothioate-modified mRNA compared to the control, it was not as significant as the effects observed on tRNA selection.

To investigate the phase of tRNA selection impacted by the substitution, we performed GTP hydrolysis assays and demonstrated that the initial phase of tRNA selection is not significantly impacted by the substitutions. This suggests that the kink structure plays an important role during the later proofreading phase. Additionally, we investigated the impact of phosphorothioate substitutions between the first and second position as well as the second and third positions of the A-site codon on tRNA selection. Structural studies show that the kink-stabilizing magnesium ion also appears to be coordinated by the *pro*-R oxygen between the first and second position of the A-site codon, but not by oxygens in the backbone between the second and third position of the A-site codon [38, 39]. For the phosphorothioate substitutions between the first and second position but not the second and third position, we observed effects on tRNA selection that were similar to those observed for the substitutions at the P/A interface. This served as a control to show that the effects on tRNA selection were due to the disruption of magnesium coordination which likely also disrupts the kink structure.

The results that the disruption of the kink structure decreases the rate of miscoding in the presence of near-cognate aa-tRNAs while having no effect on the rate of the reaction in the presence of the cognate aa-tRNA begs the question as to why the mRNA evolved to adopt this kink structure if it makes decoding less accurate. We hypothesized that a subset of cognate aa-tRNAs that exploit unusual base pairs at the wobble position would be negatively impacted by the loss of this kink structure, as the substitution might not provide promiscuous enough

conditions to allow for tRNA selection to occur. To this end, we utilized the AUA Ile codon which does not base pair with the anticodon in the typical A•U base pair at the third position. Instead, the C in the anticodon is modified to lysidine (^{k2}C) in order to avoid base pairing with the AUG Met codon (39). When we perform the peptidyl transfer reactions with unmodified or *Rp*- phosphorothioate-programmed complexes in the presence of the cognate Ile-tRNA^{Ile}, the rates were indistinguishable. However, the rate for the *Sp*-modified complex was about an order of magnitude slower. This supports the hypotheses that the kink structure is critical for decoding under less-than-ideal conditions and that the *pro*-S oxygen is more important for coordinating the kink structure than the *pro*-R oxygen.

While our study shows that the kink structure is important for tRNA selection, previous studies speculated that this structure is important for preventing slippage during translocation (40). This slippage of the mRNA template causes frameshifting, which can lead to the improper decoding of the template. It is possible that the structure also plays a role in frame maintenance. Future studies can focus on measuring the rates of frameshifting in the presence of the phosphorothioate-substituted templates.

Conclusions of the thesis

The overall goal of my dissertation was to expand on the understanding of how mRNA structure impacts tRNA selection. For my research, I focused on understanding the effects of chemical damage of mRNA on tRNA selection, as well as elucidating a role for the structure of the phosphodiester backbone of mRNA during decoding. In addition to refining and redefining what is known about mRNA structure during decoding, these findings demonstrate that chemical damage of mRNA can stall ribosomes *in vivo* and elicit cellular responses. The studies performed in this thesis demonstrate that mRNA is more than just a passive template during

decoding, and I believe future studies will continue to demonstrate the important role mRNA structure plays throughout the various steps in translation.

To further understand the importance of mRNA structure during translation, we explored how both oxidative as well as alkylative damage alters the way in which nucleotides are decoded. Additionally, we explored the previously underappreciated role of the mRNA phosphodiester backbone during tRNA selection. We also provide the first evidence that the *trans*-translation ribosome rescue pathway in bacteria is responsible for rescuing ribosomes stalled by RNA damage. As the field progresses, this data will be integral to our understanding of how cells deal with structural alterations to mRNA.

Moving forward, there are still many questions remaining as to how organisms tolerate mRNA damage as well as how mRNA might be specifically modified to regulate cellular processes. Our studies support the idea that the preservation of mRNA structure is important to maintaining the speed and fidelity of decoding and elude to the possibility that mRNA structure can be intentionally regulated to modulate this process. I am confident that, over time, additional alterations to mRNA structure will identify further roles for mRNA in the regulation as well as the maintenance of translation.

REFERENCES

1. Zhang,C. and Jia,G. (2018) Reversible RNA Modification N1-methyladenosine (m1A) in mRNA and tRNA. *Genomics, Proteomics Bioinforma.*, **16**, 155–161.

2. You,C., Dai,X. and Wang,Y. (2017) Position-dependent effects of regioisomeric methylated adenine and guanine ribonucleosides on translation. *Nucleic Acids Res.*, **45**, 9059–9067.

3. Zhou,H., Kimsey,I.J., Nikolova,E.N., Sathyamoorthy,B., Grazioli,G., Mcsally,J., Bai,T., Wunderlich,C.H., Kreutz,C., Andricioaei,I., *et al.* (2016) m 1 A and m 1 G disrupt A-RNA structure through the intrinsic instability of Hoogsteen base pairs. *Nat. Publ. Gr.*, **23**, 803–810.

4. Zaher,H.S. and Green,R. (2009) Quality control by the ribosome following peptide bond formation. *Nature*, **457**, 161–166.

5. Pape,T., Wintermeyer,W. and Rodnina,M. V. (2000) Conformational switch in the decoding region of 16S rRNA during aminoacyl-tRNA selection on the ribosome. *Nat. Struct. Biol.*, **7**, 104–107.

6. Ramakrishnan,V., Carter,A.P., Clemons,W.M., Brodersen,D.E., Morgan-Warren,R.J. and Wimberly,B.T. (2000) Functional insights from the structure of the 30S ribosomal subunit and its interactions with antibiotics. *Nature*, **407**, 340–348.

7. Dominissini,D., Nachtergaele,S., Moshitch-moshkovitz,S., Peer,E., Kol,N., Ben-haim,M.S., Dai,Q., Segni,A. Di, Clark,W.C., Zheng,G., *et al.* (2016) The dynamic N 1 -methyladenosine methylome in eukaryotic messenger RNA. *Nature*, **530**, 441–446.

8. Li,X., Xiong,X., Wang,K., Wang,L., Shu,X., Ma,S. and Yi,C. (2016) Transcriptome-wide mapping reveals reversible and dynamic N 1 -methyladenosine methylome. *Nat. Publ. Gr.*, **12**, 311–316.

9. Safra,M., Sas-chen,A., Nir,R., Winkler,R., Nachshon,A., Bar-yaacov,D., Erlacher,M., Rossmanith,W., Stern-ginossar,N. and Schwartz,S. (2017) The m1A landscape on cytosolic and mitochondrial mRNA at single-base resolution. *Nat. Publ. Gr.*, **551**, 251–255.

10. Simms,C.L. and Zaher,H.S. (2016) Quality control of chemically damaged RNA. *Cell. Mol. Life Sci.*, **73**, 3639–3653.

11. Simms,C.L., Hudson,B.H., Mosior,J.W., Rangwala,A.S. and Zaher,H.S. (2014) An Active Role for the Ribosome in Determining the Fate of Oxidized mRNA. *Cell Rep.*, **9**, 1256–1264.

12. Beranek,D.T. (1990) Distribution of methyl and ethyl adducts following alkylation with monofunctional alkylating agents. *Mutat. Res.*, **231**, 11–30.

13. Wyatt,M.D. and Pittman,D.L. (2008) Methylating agents and DNA repair responses: methylated bases and sources of strand breaks. *Chem Res Toxicol*, **19**, 1580–1594.

14. Moore,S.D. and Sauer,R.T. (2005) Ribosome rescue: tmRNA tagging activity and capacity in Escherichia coli. *Mol. Microbiol.*, **58**, 456–466.

15. Ivanova,N., Pavlov,M.Y. and Ehrenberg,M. (2005) tmRNA-induced release of messenger

RNA from stalled ribosomes. *J. Mol. Biol.*, **350**, 897–905.

16. Ivanova,N., Pavlov,M.Y., Felden,B. and Ehrenberg,M. (2004) Ribosome rescue by tmRNA requires truncated mRNAs. *J. Mol. Biol.*, **338**, 33–41.

17. Richards,J., Mehta,P. and Karzai,A.W. (2006) RNase R degrades non-stop mRNAs selectively in an SmpB-tmRNA-dependent manner. **62**, 1700–1712.

18. Ge,Z., Mehta,P., Richards,J. and Karzai,A.W. (2010) Non-stop mRNA decay initiates at the ribosome. **78**, 1159–1170.

19. Simms,C.L., Thomas,E.N. and Zaher,H.S. (2017) Ribosome-based quality control of mRNA and nascent peptides. *Wiley Interdiscip. Rev. RNA*, **8**, 1–27.

20. Trewick,S.C., Henshaw,T.F., Hausinger,R.P., Lindahl,T. and Sedgwick,B. (2002) Oxidative demethylation by Escherichia coli AlkB directly reverts DNA base damage. *Nature*, **419**, 174–178.

21. Ougland,R., Zhang,C.M., Liiv,A., Johansen,R.F., Seeberg,E., Hou,Y.M., Remme,J. and Falnes,P. (2004) AlkB restores the biological function of mRNA and tRNA inactivated by chemical methylation. *Mol. Cell*, **16**, 107–116.

22. Jeggot,P. (1979) Isolation and Characterization of Escherichia coli K-12 Mutants Unable to Induce the Adaptive Response to Simple Alkylating Agents. **139**, 783–791.

23. Mccarthy,T. V and Lindahl,T. (1985) Methyl phosphotriesters in alkylated DNA are repaired by the Ada regulatory protein of E. coli. *Nucleic Acids Res.*, **13**, 2683–2698.

24. Sakumi,K. and Sekiguchi,M. (1989) Regulation of Expression of the ada Gene Controlling the Adaptive Response. *J. Mol. Biol.*

25. Uphoff,S., Lord,N.D., Okumus,B., Potvin-trottier,L., Sherratt,D.J. and Paulsson,J. (2016) Stochastic activation of a DNA damage response causes cell-to-cell mutation rate variation. **351**, 1094–1098.

26. Hofer,T., Badouard,C., Bajak,E., Ravanat,J.L., Mattsson,Å. and Cotgreave,I.A. (2005) Hydrogen peroxide causes greater oxidation in cellular RNA than in DNA. *Biol. Chem.*, **386**, 333–337.

27. Shen,Z., Wu,W. and Hazen,S.L. (2000) Activated Leukocytes Oxidatively Damage DNA , RNA , and the Nucleotide Pool through Halide-Dependent Formation of Hydroxyl Radical †. 10.1021/bi992809y.

28. Cheng,X., Kelso,C., Hornak,V., de los Santos,C., Grollman,A.P. and Simmerling,C. (2005) Dynamic behavior of DNA base pairs containing 8-oxoguanine. *J. Am. Chem. Soc.*, **127**, 13906–18.

29. Zaher,H.S. and Green,R. (2009) Fidelity at the Molecular Level: Lessons from Protein Synthesis. *Cell*, **136**, 746–762.

30. Gromadski,K.B. and Rodnina,M. V. (2004) Streptomycin interferes with conformational coupling between codon recognition and GTPase activation on the ribosome. *Nat. Struct. Mol. Biol.*, **11**, 316–322.

31. Demirci,H., Iv,F.M., Murphy,E., Gregory,S.T. and Albert,E. (2013) A structural basis for streptomycin-induced misreading of the genetic code. *Nat. Commun.*, 10.1038/ncomms2346.A.

32. Freudenthal,B.D., Beard,W.A. and Wilson,S.H. (2013) DNA polymerase minor groove interactions modulate mutagenic bypass of a templating 8-oxoguanine lesion. *Nucleic Acids Res.*, **41**, 1848–1858.

33. Vasquez-Del Carpio,R., Silverstein,T.D., Lone,S., Swan,M.K., Choudhury,J.R., Johnson,R.E., Prakash,S., Prakash,L. and Aggarwal,A.K. (2009) Structure of human DNA polymerase κ inserting dATP opposite an 8-OxoG DNA lesion. *PLoS One*, **4**.

34. Batra,V.K., Shock,D.D., Beard,W.A., McKenna,C.E. and Wilson,S.H. (2011) Binary complex crystal structure of DNA polymerase reveals multiple conformations of the templating 8-oxoguanine lesion. *Proc. Natl. Acad. Sci.*, **109**, 113–118.

35. Brieba,L.G., Eichman,B.F., Kokoska,R.J., Doublié,S., Kunkel,T.A. and Ellenberger,T. (2004) Structural basis for the dual coding potential of 8-oxoguanosine by a high-fidelity DNA polymerase. *EMBO J.*, **23**, 3452–3461.

36. Fan,Y., Wu,J., Ung,M.H., De Lay,N., Cheng,C. and Ling,J. (2015) Protein mistranslation protects bacteria against oxidative stress. *Nucleic Acids Res.*, **43**, 1740–1748.

37. Demeshkina,N., Jenner,L., Westhof,E., Yusupov,M. and Yusupova,G. (2012) A new understanding of the decoding principle on the ribosome. *Nature*, **484**, 256–259.

38. Selmer,M., Dunham,C.M., Murphy,F. V, Weixlbaumer,A., Petry,S., Kelley,A.C., Weir,J.R. and Ramakrishnan,V. (2006) Structure of the 70S ribosome complexed with mRNA and tRNA. *Science*, **313**, 1935–42.

39. Ortiz-meoz,R.F. and Green,R. (2011) Helix 69 Is Key for Uniformity during Substrate Selection on. **286**, 25604–25610.

40. Zaher,H.S. and Green,R. (2010) Kinetic basis for global loss of fidelity arising from mismatches in the P-site codon : anticodon helix. 10.1261/rna.2241810.aminoacylation.

Appendix I

Tables of Kinetics Data

Chapter 2 Rate and Endpoint Data

Table 1: m^1A Glu Rate and Endpoint Data

Glu Codon: GAA
m1AGlu Codon: $G^{m1}AA$

Codon	tRNA/RF	Treatment	Rate	Endpoint
Glu	Glu	NT	65.89	0.807
			49.22	0.8614
m1A	Glu	NT	0.1347	0.126
			0.1618	0.07675
m1A	Glu	Paromo	0.1624	0.1726
			0.243	0.04352
Glu	Lys	NT	0.01676	0.06504
			0.01988	0.06279
m1A	Lys	NT	0.04841	0.01304
			0.06531	0.01988
Glu	RF1	NT	0.001309	0.6147
			0.001525	0.9687
m1A	RF1	NT	0.1047	0.001309
			0.1099	0.001785
Glu	RF2	NT	0.003196	0.03785
			0.03537	0.01446
m1A	RF2	NT	0.3265	0.000638
			0.4124	0.00071

Chapter 3 Rate and Endpoint Data

Table 2: 8-oxoG Val Rate and Endpoint Data

Val Codon: GUU
8oxoVal Codon: ^{8oxo}GUU

Codon	tRNA	Treatment	Rate	Endpoint	Average Rate	Average Endpoint
8oxoG	Val	NT	0.0474	0.3011	0.04369	0.30825
			0.03998	0.3154		
8oxoG	Val	Strep	0.08455	0.5521	0.080465	0.56635
			0.07638	0.5806		
8oxoG	Val	Paromo	0.2025	0.609	0.19075	0.5931
			0.179	0.5772		
G	Ile	NT	0.08125	0.02796	0.049925	0.14523
			0.0186	0.2625		
G	Ile	Strep	0.08165	0.6934	0.07821	0.68285
			0.07477	0.6723		
G	Ile	Paromo	0.07731	0.6789	0.07268	0.67135
			0.06805	0.6638		
8oxoG	Ile	NT	0.0816	0.02899	0.081225	0.02782
			0.08085	0.02665		
8oxoG	Ile	Strep	0.01849	0.06192	0.01528	0.11976
			0.01207	0.1776		
8oxoG	Ile	Paromo	0.02389	0.08755	0.022375	0.113575
			0.02086	0.1396		
8oxoG	Phe	NT	0.01956	0.1015	0.018155	0.11265
			0.01675	0.1238		
8oxoG	Phe	Strep	0.3361	0.6393	0.29145	0.65565
			0.2468	0.672		
8oxoG	Phe	Paromo	0.2534	0.5937	0.2207	0.60375
			0.188	0.6138		
G	Phe	NT	0.1872	0.01531	0.18695	0.016395
			0.1867	0.01748		
G	Phe	Strep	0.1504	0.7181	0.12895	0.72225
			0.1075	0.7264		
G	Phe	Paromo	0.2108	0.6519	0.1871	0.6749
			0.1634	0.6979		
8oxoG	Leu	NT	0.07894	0.005643	0.072675	0.0063375
			0.06641	0.007032		
8oxoG	Leu	Strep	0.05692	0.01688	0.054465	0.016615
			0.05201	0.01635		

8oxoG	Leu	Paromo	0.1048	0.01161	0.080325	0.01422
			0.05585	0.01683		
G	Leu	NT	0.1318	0.004502	0.09455	0.0049815
			0.0573	0.005461		
G	Leu	Strep	0.02859	0.01089	0.026535	0.01099
			0.02448	0.01109		
G	Leu	Paromo	0.05557	0.01259	0.051935	0.01137
			0.0483	0.01015		
G	Val	NT	31.39	0.6868	28.95	0.729
			26.51	0.7712		
G	Val	Strep	26.77	0.8663	23.79	0.795
			20.81	0.7237		
G	Val	Paromo	31.76	0.925	28.56	0.82835
			25.36	0.7317		

Table 3: 8-oxoG Arg Rate and Endpoint Data

Arg: CGC
8oxoVal Codon: $C^{8oxo}GC$

Codon	tRNA	Treatment	Rate	Endpoint	Average Rate	Average Endpoint
8oxoG-Arg	Leu	NT	0.02064	0.3555	0.015645	0.47645
			0.01065	0.5974		
8oxoG-Arg	Leu	Strep	0.03287	0.7419	0.030825	0.6412
			0.02878	0.5405		
8oxoG-Arg	Leu	Paromo	0.08754	0.6805	0.074255	0.66565
			0.06097	0.6508		
8oxoG-Arg	His	NT	0.02932	0.009227	0.02801	0.010874
			0.0267	0.01252		
8oxoG-Arg	His	Strep	0.07271	0.02029	0.036867	0.073995
			0.001023	0.1277		
8oxoG-Arg	His	Paromo	0.03536	0.04542	0.0182	0.20316
			0.001039	0.3609		
8oxoG-Arg	Pro	NT	0.1513	0.001144	0.09327	0.002369
			0.03524	0.003593		
8oxoG-Arg	Pro	Strep	0.01943	0.003755	0.014225	0.004578
			0.00902	0.0054		
8oxoG-Arg	Pro	Paromo	0.07701	0.002805	0.04913	0.003337
			0.02125	0.003868		
8oxoG-Arg	Arg	NT	0.018	0.02483	0.009748	0.027685
			0.001495	0.03054		
8oxoG-Arg	Arg	Strep	0.03647	0.4865	0.022026	0.37025
			0.007582	0.254		
8oxoG-Arg	Arg	Paromo	0.08517	0.5697	0.04868	0.5221
			0.01219	0.4745		
G	Leu	NT	0.115	0.03705	0.073975	0.020229
			0.03295	0.003407		
G	Leu	Strep	0.03705	0.003785	0.020832	0.008468

			0.004614	0.01315		
G	Leu	Paromo	0.02586	0.07102	0.024835	0.04507
			0.02381	0.01912		
G	His	NT	0.0181	0.06442	0.010725	0.18076
			0.003349	0.2971		
G	His	Strep	0.2457	0.1624	0.1796	0.4935
			0.1135	0.8246		
G	His	Paromo	0.9127	0.5836	0.8262	0.58525
			0.7397	0.5869		
G	Pro	NT	0.138	0.000745	0.109185	0.001686
			0.08037	0.002626		
G	Pro	Strep	0.02478	0.01144	0.015234	0.039575
			0.005687	0.06771		
G	Pro	Paromo	0.02645	0.03292	0.024145	0.02519
			0.02184	0.01746		
G	Arg	NT	33.47	0.7557	22.365	0.6392
			11.26	0.5227		
G	Arg	Strep	44.39	0.8139	37.08	0.8226
			29.77	0.8313		
G	Arg	Paromo	46.59	0.8675	29.965	0.6293
			13.34	0.3911		

Table 4: 8-oxoG Arg Ribosomal Mutant Rate and Endpoint Data

8oxoVal Codon: $C^{8oxo}GC$

tRNA	Ribosome	Rate	Endpoint	Average Rate	Average Endpoint
Arg	WT	0.001625	0.3788	0.001171	0.22146
		0.0007169	0.06412		
	HA	0.00000044	0.07934	0.00028	0.07934
		0.00056	NA		
	EP	0.01313	0.3776	0.007773	0.25655
		0.002415	0.1355		
Leu	WT	0.01526	0.5514	0.014385	0.5796
		0.01351	0.6078		
	HA	0.0008105	0.4841	0.00159	0.4338
		0.002369	0.3835		
	EP	0.0706	0.6504	0.07353	0.6559
		0.07646	0.6614		

Appendix II

Specifications for Mass Spectrometry

Table 1: Specifications for Mass Spectrometry

	precursor mass	product ion	retention time	collision energy	extinction coefficient	EC Wavelength
A	268.1	136	1.92	18	15600	259
C	244.1	112	0.48	14	9000	271
G	284.2	152	2.4	16	13700	252
U	245.2	152.1	1	14	10000	262
m1A	282.2	150.1	0.9	16	14600	258
m6A	282	150	4.08	16	15567	265
m3C	258.2	126	0.8	8	7008	254
m7G	298.2	166	1.5	10	9056	260
m1G	298	166	4.623	4.143	12948	254
m6G	298	166	4.84	4.84	7100	280
8oxoG	300	168.1	2.956	2.956	7868	296